EXTREME CLIMATE EVENTS PREDICTION OVER WEST-AFRICA USING A COUPLED ATMOSPHERE-HYDROLOGY MODEL SYSTEM AND CLIMATE INDICES

BY

QUENUM GANDOME MAYEUL LEGER DAVY

(MET/15/5748)

SEPTEMBER, 2019

EXTREME CLIMATE EVENTS PREDICTION OVER WEST-AFRICA USING A COUPLED ATMOSPHERE-HYDROLOGY MODEL SYSTEM AND CLIMATE INDICES

QUENUM GANDOME MAYEUL LEGER DAVY
BSc, MSc/UAC
(MET/15/5748**)**

A Thesis in the Department of Meteorology and Climate Science, School of Earth and Mineral Science In Partnership with the West African Science Service Centre on Climate Change and Adapted Land Use (WASCAL) submitted to the School of Postgraduate Studies in partial fulfillment for the requirement of the degree of Doctor of Philosophy in Meteorology and Climate Science of The Federal University Of Technology, Akure (FUTA), Nigeria

September, 2019

DECLARATION

I declare that this is my own work and that it has not been submitted previously as dissertation or thesis elsewhere at any other university for the award of a degree. All citations and sources of information are clearly acknowledged by means of references.

Candidate's Name: QUENUM Gandome Mayeul L. D.

Signature:…… **Date**……

CERTIFICATION

This is to certify that this work was carried out by Mr. QUENUM Gandome Mayeul Leger Davy under my supervision and that to the best of my knowledge, it has not been submitted elsewhere for the award of a degree.

Major Supervisor's Name: Prof. P.G. Oguntunde

Signature: …… **Date**……

Co-supervisor's Name: Dr. N. A. B. Klutse

Signature: …… **Date**……

ACKNOWLEDGMENTS

I am very grateful to God, the almighty, maker of heaven and earth and that is in him I have had the strength and well-being that enabled me to complete this research.

I'm grateful to the German Ministry of Education and Research (BMBF), which fully sponsored this Ph.D work through the West African Science Service Centre for Climate Change and Adapted Land-use (WASCAL).

My sincere thanks to the executive director and the staff of WASCAL Headquater in Accra, Ghana, and the Director Prof. K.O. Ogunjobi and staff of WASCAL-GSP-WACS, FUTA, Nigeria for their support and encouragement throughout the period of the study at FUTA. My thanks are also addressing to the deputy Director Dr. V. O. Ajayi, the heard and staff of Meteorological Departement, FUTA, Nigeria for their cooperation.

I would like to express my sincere gratitude to Prof. P. G. Oguntunde for the supervision of this work, for all the guidance he provided along the way of this study. My thank to Prof. Dr. Harald Kunstmann by hosting me almost 15 months in his research group (Regional Climate and Hydrology) and offered all the facilities to me at the Institute of Meteorology and Climate Research Atmospheric Environmental Research (IMK-IFU), Campus Alpin, Garmisch-Partenkirchen.

My special thanks and gratitude to Dr. Joël Arnault for his candid supervision, advice, and support during my stay in Garmisch-Partenkirchen. He introduced and assisted me on HPC using, models installing, models calibration and simulations, and also provided to me some codes. You were more than a supervisor of my Ph.D work, but a brother and a friend.

I would like also express my gratitude to Dr. Patrick Laux, Dr. Zhenyu Zhang and Mr. Maurus Borne for their kind collaborations and advises. You are the bests.

I would be remiss if I did not send a special thanks and gratitude to my lovely sister Dr. Diarra Dieng for all her collaboration, encouragement and contributions for the achievement of my work.

I’m thanking Mr. Joël Atayi-Guèdègbé for his encouragement and support for the achievement of this Ph.D thesis.

I'm addressing a Warm thanks to Mrs. Agathe Dogue-Tossah, my mother-in-law for all her support, prayers, and hopes for the outcome of this study.

To Prof. Abel A. Afouda, I will never miss to thank you for having identified me and having included me to your research team since 2009, thanks for the confidence you have in me. See in this achievement the results of all your efforts.

To Prof. Emmanuel A. Lawin, see in this achievement the results of the seed that you put underground since 2010, thanks for everything I have learned and still learning from you.

I would like to thank Dr. Ilse Hamann and the German Climate Computing Center (DKRZ) for providing the computing facilities. I am also grateful to the Deutscher Akademischer Austauschdienst (DAAD) for the short grant it allocated for us. I am acknowledging the European Center for Medium-Range Weather Forecasts (ECMWF), for providing the operational analysis dataset and products. The TRMM data used in this study were acquired as part of the Tropical Rainfall Measuring Mission (TRMM), and the observational station data from Benin Agency of Meteorology.

A special thanks to my seniors and colleagues: Prof. Eric A. Alamou, Prof. Expedit W. Vissin, Drs. Japhet Kodja, Arsène Akognongbe, Fernand Avahouin, Romaric C. Odoulami, Ines Oloye, Charlène Gaba, Eliezer Biao for their encouragement and support for the completion of the present work.

My gratitude also goes to all my fellow WASCAL- GSP-WACS comrades, mainly: Naomi Kumi, Aïssatou Faye, Alima Dajuma, Windmanagda Sawadogo, Abdoulatif Bonkaney, Aboulaye Ballo.

Finally, I am happy to thank all my family and related members to have assisted me encouraged me and support me during these 43 months away, I would like to mention especially: Fr. Luc Quenum, Mrs. Yenoukounme Quenum-Zinzindohoue, Mr. Eric Quenum, Mrs. Flora Quenum-Fagnisse, Mr. Bruno Quenum, Mrs. Valentine Quenum-Laleye, Mrs. Irene Alapini-Quenum, Mrs. Hilda Quenum-Houedji, Fr. Magnus Quenum, and Fr. Philipe-Neri Quenum, Mr. Isaac Tossah, Mrs. Gertrude Kouye-Tossah, Mrs. Nadege Tossah-Hangnilo, Mrs. Tabitha Hangnilo.

I am full of appreciation and gratitude for a wide range of support, encouragement, and prayers from many people towards the completion of this Ph.D work.

DEDICATION

This work is dedicated to my wife, Tossah E. A. Manoella, and my sons Oderic and Yanis Quenum who endured my absence for the whole period of this study.

It is also dedicated in memory of Valentin S. Quenum, my late father who contributed a lot to whom I'm becoming today, may his soul rest in peace.

The great price of the dedication is in memory of Sokpoekpe M. Agnès, my late mother who saw the beginning of this work, encouraged me to have the strength to finish it, but who unfortunately will not be congratulated for this achievement, may her soul rest in peace.

Finally, this work is a thanking in memory of Tossah D. Nicolas, my late father-in-law for all the knowledge we shared together, may his soul rest in peace.

ABSTRACT

Rising temperature is one of the direct indicators of global climate change. To investigate how the rising global temperature will affect the spatial pattern of rainfall and consequent flood and drought in West Africa, precipitation and potential evapotranspiration variables from ten Global Climate Models (GCMs) under the RCP8.5 scenario were downscaled by the Rossby Centre regional atmospheric model (RCA4) from the Coordinated Regional Climate Downscaling Experiment (CORDEX) and analysed at four specific global warming levels (GWLs) (i.e., 1.5℃, 2.0℃, 2.5℃, and 3.0℃) above the pre-industrial level. This study utilized four indices: the standardized precipitation evapotranspiration index (SPEI), the precipitation concentration index (PCI), the precipitation concentration degree (PCD), and the precipitation concentration period (PCP) to explore the spatio-temporal variations in the characteristics of precipitation concentrations. Additionally, studying the impact of the four GWLs on consecutive dry days (CDD), consecutive wet days (CWD), and frequency of the intense rainfall events led to a better understanding of the spatiotemporal pattern of extreme precipitation. The onset of rainfall comes one month earlier in the Gulf of Guinea compared to the historical period, with increasing rainfall intensity in the whole study domain. To encourage adaptation to the various changes in climate in general, and particularly in respect of rainfall, the study proposes two adaptation methods that can be implemented at the local (country) level, as well as some mitigation and adaptation strategies at the regional level. More practically, to analyze flood events which became more frequent since 2000 in West Africa, this research improve on previous analysis by designing an experimental work using the coupled atmosphere-hydrology modeling system WRF-Hydro over Ouémé-river basin in Benin for the period 2008-2010. Such a coupled model allows exploring the contribution of

atmospheric components into the flood event, and its ability to simulate and predict accurate streamflow. The potential of WRF-Hydro to correctly simulating streamflow in the Ouémé-river basin is assessed by forcing the model with operational analysis dataset from the ECMWF. Atmospheric and land surface processes are resolved at a spatial resolution of 5 km. The additional surface and subsurface water flow routing are computed at a resolution 1:10. Key parameters of the hydrological module of WRF-Hydro were calibrated offline and tested online with the coupled WRF/WRF-Hydro. As a result, WRF-Hydro was able to simulate the discharge in Ouémé river on offline and fully-coupled modes with a Kling-Gupta Efficiency (KGE) of 0.70 and 0.76 respectively. In fully-coupled modes, the model captures the flood event that occurred in 2010 in the catchments of interest. The uncertainty of atmospheric modeling on coupled results is assessed with the stochastic kinetic-energy backscatter scheme (SKEBS) by generating an ensemble of 10 members for three rainy seasons. It shows that the coupled model performance in terms of KGE ranges form 0.14-0.79 and 0.13-0.75 at Savè and Bétérou respectively. This ability in realistically reproducing observed discharge in the Ouémé-river basin demonstrates the potential of the coupled WRF-Hydro modeling system for flood forecasting applications.

RÉSUMÉ

L'élévation de la température est l'un des indicateurs directs du changement climatique mondial. Pour étudier l'impact de la hausse de la température globale sur la configuration spatiale des précipitations, les inondations et la sécheresse qui sévissent en Afrique de l'Ouest, les variables de précipitations et d'évapotranspiration potentielles de dix modèles climatiques globaux (MCG) du scénario RCP8.5 ont été réduites en échelles avec le modèle atmosphérique regional du Centre Rossby (RCA4), disponible dans la base de l'Expérience de réduction d'échelle climatique coordonnée (CORDEX) et analysé à quatre niveaux de réchauffement planétaire (GWL) spécifiques (c.-à-d. 1,5 ℃; 2,0 ℃; 2,5 ℃ et 3,0 ℃) au-dessus du niveau pré-industriel. Cette étude a utilisé quatre indices: l'indice normalisé de précipitations et d'évapotranspiration (SPEI), l'indice de concentration de précipitation (PCI), le degré de concentration de précipitation (PCD) et la période de concentration de précipitation (PCP) pour explorer les variations spatio-temporelles des caractéristiques de la concentration des précipitations. De plus, l'étude de l'impact des quatre GWLs sur les jours secs consécutifs (CDD), les jours pluvieux consécutifs (CWD) et la fréquence des épisodes de précipitations intenses a permis de mieux comprendre le schéma spatio-temporel des précipitations extrêmes. Comme resultas, il et à retenir que le début des précipitations survient un mois plus tôt dans le golfe de Guinée par rapport à la période historique, avec une intensité croissante des précipitations dans l'ensemble du domaine d'étude. Pour encourager l'adaptation aux divers changements climatiques en général, et en particulier en ce qui concerne les précipitations, l'étude propose deux méthodes d'adaptation pouvant être mises en œuvre au niveau local (pays), ainsi que des stratégies d'atténuation et d'adaptation au niveau régional (Ouest Africain). Plus concrètement, afin d'analyser les inondations devenues plus fréquentes depuis 2000 en Afrique de

l'Ouest, cette étude améliore les analyses précédentes en concevant un travail expérimental utilisant le système de modélisation couplé hydrologie-atmosphère WRF-Hydro sur le bassin de l'Ouémé au Bénin sur la période 2008-2010. Un tel modèle couplé permet d'explorer la contribution des composants atmosphériques dans la crue et sa capacité à simuler et à prédire un débit précis. La potentialité du modèle WRF-Hydro à simuler correctement le débit dans le bassin de la rivière Ouémé à Savè est évalué en forçant le modèle avec un ensemble de données d'analyse opérationnelle du ECMWF. Les processus atmosphériques et de surface sont résolus à une résolution spatiale de 5 km. Le débit supplémentaire des écoulements d'eau de surface et souterraine est calculé à une résolution de 1:10. Les paramètres clés du module hydrologique WRF-Hydro ont été calibrés hors ligne (mode non-couplé) et testés en ligne (mode couplé) avec le couplage WRF/WRF-Hydro. WRF-Hydro a ainsi pu simuler le débit de la rivière Ouémé à Savè en mode déconnecté et entièrement couplé avec un rendement Kling-Gupta (KGE) de 0,70 et 0,76 respectivement. En mode totalement couplé, le modèle prend en compte les inondations survenues en 2010 dans les bassins versants étudiés. L'incertitude de la modélisation atmosphérique sur les résultats couplés est évaluée avec le schéma de rétrodiffusion d'énergie cinétique stochastique (SKEBS) en générant un ensemble de 10 membres pour trois saisons de pluie. Les results montrent que les performances du modèle couplé en termes de gammes de KGE sont respectivement de 0,14 à 0,79 et de 0,13 à 0,75 à Savè et à Bétérou. Cette capacité à reproduire de manière réaliste les débits observés dans le bassin de la rivière Ouémé démontre la potentialité du système de modélisation couplé WRF/WRF-Hydro pour les applications de prévision des crues.

TABLE OF CONTENTS

LIST OF TABLES

LIST OF FIGURES

LIST OF ACRONYMS

ACM	Asymmetric Convection Model
AEJ	African Easterly Jet
AEWs	African Easterly Waves
AR	Assessment Report
AWJ	African Westerly Jet
CAPE	Convective Available Potential Energy
CCI	Climate Change Initiative
CDD	Consecutive Dry Day
CHIRPS	Climate Hazards Group Infrared Precipitation With Station Data
COP	Conference Of Parties
CORDEX	Coordinated Regional Climate Downscaling Experiment
CRU	Climate Research Unit
CWD	Consecutive Wet Day
DHSVM	Distributed Hydrology Soil Vegetation Model
DG-Water	Direction General Of Water
ECMWF	European Centre For Medium-Range Weather Forecasts
ENSO	El Niño–Southern Oscillation
EOF	Empirical Orthogonal Function
ESA	European Space Agency
ESD	Empirical-Statistical Downscaling
GCM	Global Climate Model
GWL	Global Warming Level
HMS	Hydrologic Modeling System

HRLDAS	High Resolution Land Data Assimilation System Intertropical
HYMKE	Hydrological Model For Karst Environment
IPCC	Intergovernmental Panel on Climate Change
ITCZ	Intertropical Convergence Zone
IWRM	Integrated Water Resources Management
KGE	Kling-Gupta Efficiency
LSM	Land Surface Model
MCCs	Mesoscale Convective Complexes
MCSs	Mesoscale Convective Systems
MODIS	Moderate Resolution Imaging Spectroradiometer
NAMet	National Agency Of Meteorology
Noah-LSM	Noah Land Surface Model
NSE	Nash-Sutcliffe Efficiency
NWP	Numerical Weather Prediction
OCSs	Organized Convective Systems
PC	Principal Component
PCD	Precipitation Concentration Degree
PCI	Precipitation Concentration Index
PCP	Precipitation Concentration Period
PDSI	The Palmer Drought Severity Index
PET	Potential Evapotranspiration
RCA4	Rossby Centre Regional Atmospheric Model
RCM	Regional Circulation Model
RCMEAN	Regional Climate Model Mean
RCP	Representative Concentration Pathway

RRTM	Rapid Radiative Transfer Model
SHEDS	Shuttle Elevation Derivatives At Multiple Scales
SKEBS	Stochastic Kinetic-Energy Backscatter Scheme
SLs	Squall Line Systems
SM	Soil Moisture
SPEI	Standardized Precipitation Evapotranspiration Index
SPI	Standardized Precipitation Index
TEJ	Tropical Easterly Jet
TRMM	Tropical Rainfall Measuring Mission Data
UNEP	United Nations Environment Program
UNHCR	United Nations High Commissioner for Refugees
WAM	West African Monsoon
WAWJ	West African Westerly Jet
WOM	World Meteorological Organization
WPS	WRF Model Pre-Processing System
WRF	Weather Research And Forecasting Modeling System

CHAPTER ONE

INTRODUCTION

1.1 **Background of the Study**

Africa is one of the most vulnerable continents to climate change and climate variability, a situation aggravated by the interaction of 'multiple stresses', occurring at various levels, and low adaptive capacity (high confidence). In its 5th report, the Intergovernmental Panel on Climate Change (IPCC) stresses the increment of the number of extreme weather events for the 21st century due to climate change (IPCC, 2014). Tropical countries of West Africa are threatened particularly by climatic hazards, such as droughts, floods, high winds, the elevation of the sea level, etc. Among them, extreme meteorological events such as droughts and floods are the most important in terms of damages and impacts and represent an important limitation for the development of the poorest countries in West-Africa. In most of these developing countries, agriculture remains the main economic activity, and farming practices are mainly represented by agriculture, which depends strongly of rainfall (Rosegrant *et al.*, 2002).

Some studies referred to an investigation of these weather events. First of all, it turns out important to improve our understanding of droughts and floods. There is no standard definition about these extreme weather events, but for our understanding, drought could be defined as a series of years in which rainfall is significantly below average over an area. According to the dictionary Encarta, drought is a prolonged period of abnormally low rainfall, leading to a shortage of water. For Sivakumar *et al.* (2011) drought is defined as a normal, recurrent feature of climate characterized by a deficiency in precipitation over an extended period (usually a season or more), resulting in a water

shortage for some activities or some group. Dai (2011) and Kundzewicz (1997) are also closed to Sivakumar's *et al*., (2011) definition by explaining that drought is a recurrent and natural climatic event caused by below normal precipitation compared to the long-term average and extending over a long period of time. It is important not to confuse drought and aridity. For White *et al*. (1993), aridity should be defined as a permanent feature of drought in areas with low rainfall, then aridity represents the consequence of drought in a particular area. This deficiency of precipitation has an impact on both surface water and groundwater resources and leads to reduction in water supply and quality, reduced agricultural productivity, diminished hydro-electric power generation, disturbed riparian and wetland habitats, as well as reduced opportunities for certain recreational activities (Vicente-Serrano *et al*., 2012). The drought can then be characterized according to 4 types namely: Meteorological, hydrological, soil moisture and socio-economic droughts (e.g. Richard, 2002). This classification of drought is strongly linked to the time over which the water deficits accumulate (Gurrapu *et al*., 2014; Wilhite and Glantz, 1985). Therefore, timescales represent the basis of classification of drought into various types: 1-month timescale for meteorological drought, 3-6-month for an agricultural and 12-month timescale for hydrological droughts (Homdee *et al.*, 2016; Vicente-Serrano *et al*., 2010).

As oppose to drought, the flood can be defined as an event in which the volume of water expected and the flood crest is much above average. For the Encarta dictionary, the flood is an overflow of water that submerges land that is usually dry; whilst the glossary of meteorology defines the flood as the overflowing of the normal confines of a stream or other body of water, or the accumulation of water over areas that are not normally submerged. The main cause of floods (including fluvial floods, flash floods, urban floods, pluvial floods, etc.) are intense and/or long-lasting precipitation and are affected

by various characteristics of precipitation, such as its intensity, duration, amount, and timing. Therefore, floods result from abundant rainfall and have consequences such as loss of human life, damage to property, destruction of crops, loss of livestock, and deterioration of health conditions owing to waterborne diseases which both individuals and communities. Such consequences, affect directly social, economic, and environmental domains.

The drought that affected West African countries at the beginning of the 1970s, which peaked in the mid-1970s and lasted for several decades, causing millions of population displacement is known as one of the most undisputed and largest recent climate changes recognized by the climate research community (Dai *et al.*, 2004) and is well documented in terms of rainfall variability (Le Barbé *et al.*, 2002; Lebel and Ali, 2009; Paturel et al., 1998). To investigate on drought, some authors (e.g. : Kasei *et al.*, 2010) studied the temporal characteristics of meteorological droughts in the Volta basin, a semi-arid region in West Africa; their works analyzed drought intensity, areal extent and recurrence frequency using the standardized precipitation index (SPI). Kasei *et al.* (2010) found that during the period 1961-2005 there were five years within that period (1961, 1970, 1983, 1992 and 2001) where 75% of West Africa was under historical droughts. The criterion is that SPI was lower than -2 (case of extreme drought). According to Fontaine and Janicot, (1996) drought over all of West Africa is associated with the growth of positive SST anomalies in the Eastern Pacific and in the Indian Ocean, and negative SST anomalies in the Northern Atlantic and in the Gulf of Guinea. In contrast, drought limited to the Sahel corresponds mostly to a northward expansion of positive SST anomalies in the South Atlantic, and negative SST anomalies in the North Atlantic. Flooding overall West Africa is mainly associated with positive SST anomalies in the North Atlantic. L'Hôte *et al.* (2002) investigated on drought in West-

Africa on the period 1896-2000, they clearly found the drought events occurred in 1969 and 1970 over the Sahel area. Statistical results of this research also illustrate that the drought was not over at the end of 2000 in the whole West-Africa.

According to some authors, it is possible to identify a given threshold characteristic of drought (known as a peaks-under-threshold) or flood (a peaks-over-threshold). This definition was used by Petrow and Merz (2009) to provide a spatial pattern of high flow (flood) trend in Germany (Figure 1.1), and (Fiala *et al.*, 2010; Fleig *et al.*, 2006; Sung and Chung, 2014; Van De Giesen *et al.*, 2010) for a spatial trend of low flow (drought). Alternatively, meteorological indices such as the SPI, and Palmer Drought Severity Index (PDSI : Palmer, 1965) are used commonly to quantify hydrological drought (e.g.: Joetzjer *et al*., 2013 and Zhai *et al*., 2010 used the SPI , whilst Abatzoglou *et al*., 2014 used the PDSI). These meteorological approaches were also used by Garner *et al*., (2015), Teuling *et al*., (2013) and Trambauer *et al.*, (2014); they found numerous thresholds, which allow identifying extreme river flow events. A recent agreement that there is increasing of rainfall since the beginning of the 2000s was found by L'Hôte *et al.*, (2002) and Lebel *et al*., (2009), while Descroix *et al*., (2012) and Panthou *et al*., (2014) showed an intensification of the rainfall regime in the Sahelian region since the 2000s, characterized by a greater contribution of extreme precipitation to the annual total rainfall (Ezenwaji *et al*., 2017).

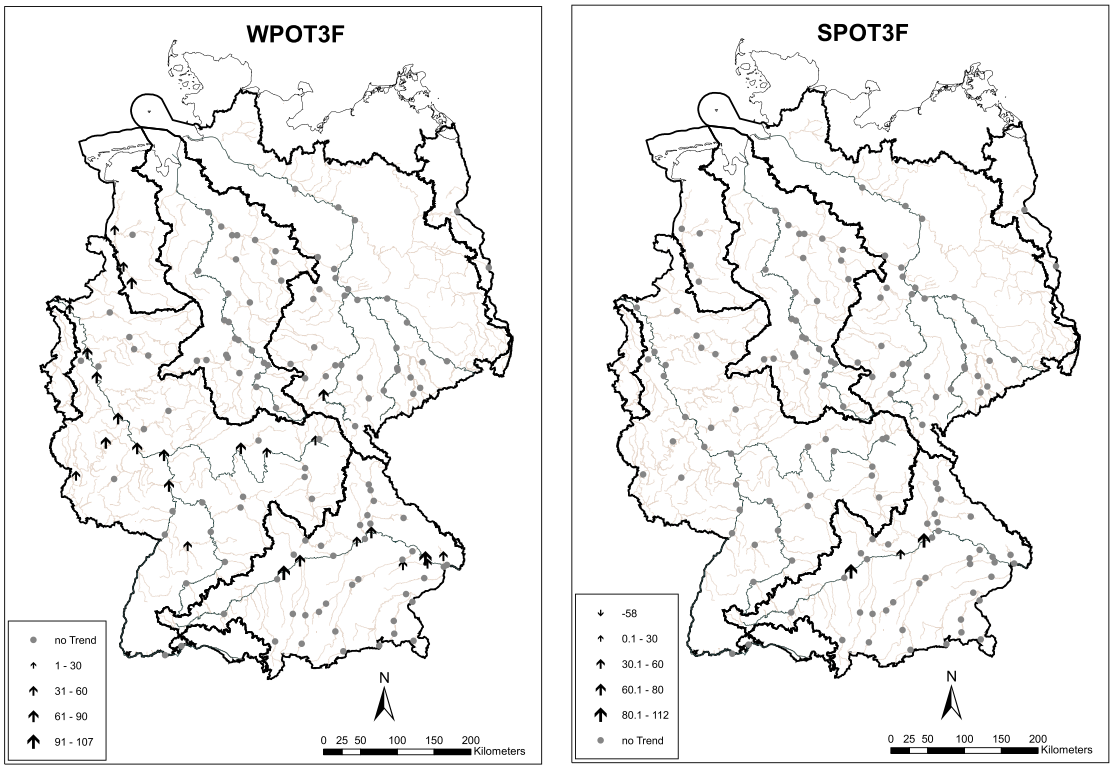

Figure 1.1 : Spatial distribution of trends in seasonal peak-over-threshold frequency – WPOT3F (winter, left map), SPOT3F (summer, right map) (upward arrows: significant increasing trend; downward arrows: significant decreasing trend; circles: no significant trend; size of arrows: relative change within 52 years; Mann–Kendall test, 2-sided option; 10% significance level). Source : Petrow and Merz (2009)

An investigation on the implication of the concentration and variability of rainfall on flood over Awka Urban Area (Nigeria) using the precipitation concentration index (PCI) by Ezenwaji *et al.* (2017) showed that the area is having reasonable floods with consequent pollution. Precipitation extremes are in close relation with flood events and droughts (Cancelliere *et al*., 2007; Jiang *et al*., 2013; Kundzewicz, 1997; Tsakiris and Vangelis, 2004 and Zhao *et al*., 2012). Therefore, the exploration of the spatial and temporal patterns of drought/ flood precipitation using SPEI and PCI indices respectively, and the analysis of both precipitation concentration and drought/flood classification trends across the study area using the t-test should contribute to a better understanding on the projection of future drought/flood episodes in West Africa.

As an illustration, many West African countries such as Benin, Burkina Faso, Cote d'Ivoire, Niger, Senegal, and Togo suffered from catastrophic floods with severe consequences as loss of life, property, and damage (Hounkpè *et al*., 2015). For example, Nouaceur *et al.*, (2013) studied seperatly the influences of climate change and the floods of 2003, 2005, 2007, 2008, 2009 and 2012 on the populations of the cities of Nouakchott (Mauritania) and Ouagadougou (Burkina Faso). But the research did not evaluate the impact of climate change on floods. Ouémé-river (in Benin) also in September-October 2010 experienced dramatic flooding, which affected 680,000 people, leading to 43 deaths (UNHCR, 2010). During this event, 55 out of 77 Benin municipalities including Cotonou were flooded. Similarly, in 2012 some southern and northern municipalities (Cotonou, Abomey-Calavi, Malanville, Karimama, etc.) were flooded. In an investigation on the impacts of dramatical floods over the southern part of Benin, Sossou-agbo (2013) showed that flood events that occurred in 2003, 2007, 2009 and 2010, have affected most the agroecological areas such as Zangnanado, Ouinhi, Bonou, Adjohoun, Dangbo, and Aguégué, whilst Godonou (2010) assessed the environmental

risks of the dramatical floods of 2010 at Dogbo, Lalo and Lokossa (Benin). In another study, Wallez (2010) studied the floods in Cotonou without involving climate variability. The spatial and temporal changes in runoff regime may increase flood vulnerability in a river basin. However, for operational reasons, hydrological models are ineffective in simulating this process (Delestre, 2011). Generally, this type of model uses Saint-Venant equations whose unknowns are the speed and the level of water. Afouda (1980) had conducted modeling of runoff through the equations of Saint-Venant in the 1980s in the city of Cotonou. However, his study solved these equations in one dimension, and the overall topography of the study area was not considered.

In this study, some climate indices were used to investigate probable present and future locations of extreme weather events over West-Africa. A narrow analysis of flood events in Ouémé-river basins was established. Therefore, the coupled atmospheric-hydrology modeling system WRF-Hydro was used to assess the West African extreme climate and provide a predicting tool for future floods, which can aid early warning policies to limit or avoid negative impacts of these extremes.

1.2 **Statement of the problem and research questions**

The anthropogenic influences on climate are progressively affecting the frequency and intensity of extreme climate events (extreme temperatures, extreme precipitation, droughts, flood, etc.) in some regions of the world (IPCC, 2012, 2014). Africa is one of the continents most exposed to the effect of climate. Some investigations led in Africa, especially in West-Africa illustrate its vulnerability to climate change. For instance, a joint study led by the United Nations Environment Program (UNEP) and some other programs explained that climate change could potentially have profound implications for food security and regional stability. The same study analyses the regional trends of

climate change in temperature, rainfall, droughts and flooding over the past four decades, and their implications for the availability of natural resources, livelihoods, migration, and conflict in 17 West African countries. The analysis has detected significant changes in regional climatic conditions, including an overall rise in mean seasonal temperature from 1970 to 2006 of approximately 1 °C, with a greater increase of between 1.5°C to 2°C observed in eastern Chad and northern Mali and Mauritania. It has been noticed that the frequency of floods and the area covered by flooding have increased in some parts of West-Africa over the past three decades especially southern Burkina Faso, western Niger and northern Nigeria experiencing more than ten floods events.

It is known that flood and drought impact on both individuals and communities, and have social, economic, and environmental consequences. Their consequences, both negative and positive, vary greatly depending on their location, duration, intensity and frequency. Among the negative consequences for individuals we have, loss of human life, damage to property, destruction of crops, loss of livestock, and deterioration of heath conditions owing to waterborne diseases. As communities get damaged, people are forced to leave their homes and normal life is disrupted. Some economic activities may come to a standstill as well. Particularly, the flood can traumatize victims and their families for long periods of time, and lead to psychological impacts. Knowing the spatial and temporal extent of the extreme event will help reduce the impacts of its consequences. A reliable flood forecasting system and drought warning over West Africa will also help adequate implementation management systems. With this, decision makers can take actions for addressing the disaster risk management. This study tasks to understand and implement the rainfall-run complexity and provide a reliable flood

forecasting and drought warning system over selected West African cities through extreme events study. The following questions were addressed:

i. Does climate change affect hydrometeorological parameters such as precipitation, temperature and discharge over West Africa?
ii. What will be the trend of flood and drought events in future climate?
iii. Is WRF-Hydro capable of improving precipitation, flood and drought forecasting?

1.3 **Aim and objectives**

The aim of the study is to use a regional climate model to improve our understanding of rainfall producing systems and predicts flood and drought in some cities in West Africa.

The specific objectives are to:

1. investigate extreme climate events and establish their trend according to projected Global Warming Levels (GWLs) using climate indices;
2. calibrate and validate hydro-atmospheric dynamic model over the study area;
3. simulate flood and drought characteristics under historical periods; and
4. perform seasonal forecasting of rainfall and discharge using reforecast dataset.

1.4 **Innovation**

The study innovates by investigating the spatial distribution of potential extreme climate events over West-Africa both for present and future periods for various global warming levels. It is an extension and adding values to some studies over the same region (e.g.: Diasso and Abiodun, 2015; Oguntunde *et al*., 2017). It is also the third times that the coupled atmospheric-hydrology modeling system WRF-Hydro is used over West-Africa after the one of Arnault *et al*., (2016) and Naabil *et al*. (2017). But in the present case,

it is the first times it is implemented for flood prediction on a basin over the region. Finally, focusing on the period 2008-2010, the study establishes WRF-Hydro as reliable flood forecasting model.

1.5 **Structure of the thesis**

This thesis is organized into five chapters. Chapter one provides the general introduction, the statement of the problem leading to the present study and some research questions which can derive from it. This chapter also details the objectives of the work and the innovation for the scientific community. Chapter two presents the literature relevant to the research areas. It discusses the West African climate system, defines extreme climate events (Flood and drought), exposed methods for their investigation. Chapter three enumerates the methodology used in the study. It presents the study area, the data used and methods adopted for investigation on flood and drought events. Chapter four presents and discusses the results obtained during these researches. It discusses the spatial repartition of potential flood and drought area, enhances the flood predictability skill with WRF-Hydro model. The last chapter (Chapter five) is dedicated to the conclusion, the limits and perspectives for future researches related to the same field.

CHAPTER TWO

LITERATURE REVIEW

Drought and subsequent floods have been experienced in West Africa over the last few decades especially since 2002, altering the annual rainfall cycles (Tschakert *et al.*, 2010). This chapter illustrates different methods used to study these weather events.

2.1 **West African climate systems**

The West African climate is dominated by the monsoon which is a large-scale circulation characterized by seasonal changes in wind direction mainly caused by the continent-maritime temperature contrast (Afiesimama *et al*., 2006). The climate system of West Africa is mainly influenced by two major air mass systems at low-level; the south-west maritime air called the monsoon and the north-east continental air. The dry season is mainly influenced by the north-east trade winds known as Harmattan from Sahara desert and the wet season is mainly influenced by the southern monsoon, with the changing position of the Inter-tropical discontinuity (ITD). During the rainy season from June to September (West African Monsoon period, Klutse *et al.*, 2015) in the West Africa Sahel, the ITCZ is associated with a very large convective available potential energy (CAPE) and also horizontal moisture flux through the available abundant water vapor. These conditions with the inherent conditional instability generate deep convection, which constitutes the major rain-producing systems in that region (Omotosho, 1985).

The West African Monsoon (WAM) circulation provides West African countries with more than 75% of their annual rainfall (Omotosho, 1985); it is the primary rainfall-producing systems during summer months (Abiodun *et al*., 2008a). However, other

rainfall-producing systems known in West Africa include the African Easterly Jet (AEJ), Tropical Easterly Jet (TEJ) (Cook, 1999; Grist *et al*., 2001; Nicholson and Grist, 2001), and the African Easterly Waves (AEWs) (Diedhiou *et al*., 2001; Druyan and Fulakeza, 2000; Thorncroft and Hodges, 2000). Several types of precipitation systems cause rainfall over West Africa. Mainly those systems are: mesoscale convective systems (MCSs), monsoon rains. The MCSs comprise squall line systems (SLs; e.g., Aspliden *et al.*, 1976; Chong and Hauser, 1988; Eldridge, 1957; Fink and Reiner, 2003 and Roux, 1987), organized convective systems (OCSs; Mathon *et al*., 2002), and mesoscale convective complexes (MCCs; Laing *et al.*, 2008). Such convection systems are frequently initiated by AEWs, south of the AEJ. Reed *et al*., (1988) have estimated that about 50% of the June-September rainfall in West Africa occurs under the influence of AEWs. Two other low-level westerly jets are involved in the processes, the African Westerly Jet (AWJ) over the continent and the West African Westerly Jet (WAWJ) over the Atlantic (Grodsky *et al*., 2003; Nicholson, 2013 and Pu and Cook, 2010).

The annual rainfall over different zones is relatively constant but decreases from south to north away from the equator (Eltahir and Gong, 1995). Figure 2.1 shows that West Africa can be classified into four major climatic zones:

- Guinean zone: the annual average rainfall varies between 900-1500 mm, and could be more in some places,

- Sudanese zone: with annual average rainfall between 400-900 mm,
- Sahelian zone: average annual rainfall in the range of 150-400 mm,
- Saharan zone: mostly less than 150 mm of rainfall per year.

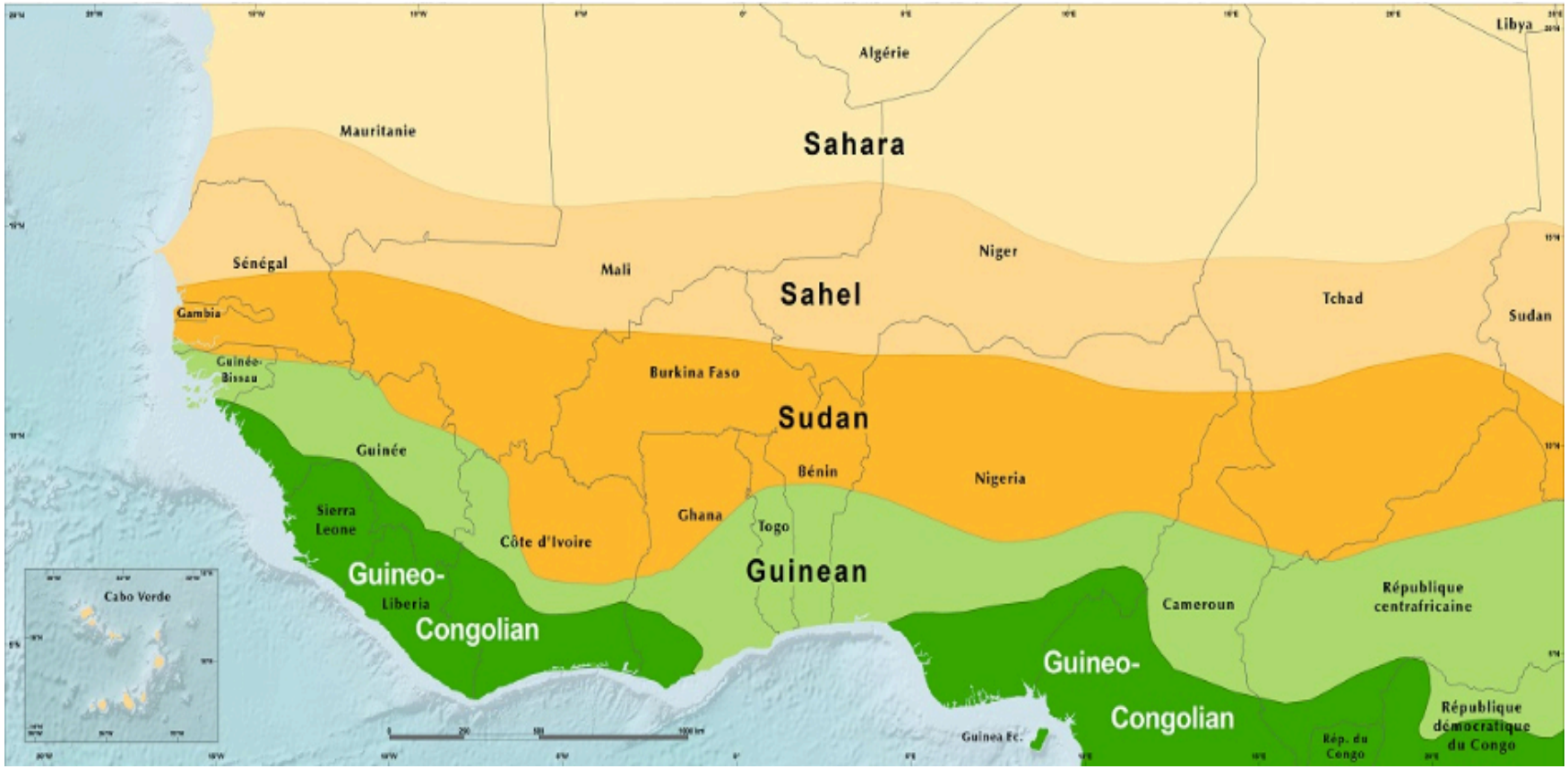

Figure 2.1: Different climatic zones in West- Africa (Source: https://eros.usgs.gov/westafrica/node/147 accessed on 26 January 2019)

2.2 **Flood and drought events**

Floods and droughts are extreme hydroclimatic events (Shelton, 2009). They are recurrent events in the world with characteristics of frequency, magnitude, duration and timing. However, there are no universal definitions of these characteristics to allow objective identification of a flood or drought event (Mishra and Singh, 2010). Hydrological extremes are caused by meteorological anomalies (i.e. severe deviations from climatic or average weather conditions; Tallaksen and Stahl, 2014), the effects of which are moderated by river basin properties. Commonly, flood and drought events are defined as the highest or lowest flow in a given year; and an extreme event is typically defined as a value occurring above or below a threshold value near the upper or lower ends of the range of observed values (Seneviratne *et al*., 2012). Flood events usually follow high-intensity precipitation events, series of precipitation events; but contrary to flood, drought events are associated with a prolonged period of low or no precipitation (meteorological drought) and/or an air temperature anomaly (Loon *et al.*, 2012; Loon and Lanen, 2012; Teuling *et al.*, 2013). But the characteristics of meteorological anomalies leading to flood and drought vary spatiotemporally.

2.2.1 Characterization of drought and flood events using climate indices

Climate indices among many others that are frequently used for forecasting, monitoring and planning drought and flood events are Palmer Drought Severity Index (PDSI), Standardized Precipitation Index (SPI), and The Standardized Potential Evapotranspiration Index (SPEI).

2.2.1.1 The Palmer Drought Severity Index (PDSI)

The PDSI, based on a soil water balance equation represents one of the first climate indices used in literature to demonstrate success at quantifying the severity of droughts across different climates (Palmer, 1965). It is also the most prominent index of meteorological drought indices used in the world (Mishra and Singh, 2010). Figure 2.2 shows the monitoring of the drought events in California based on the computation of PDSI. But Burke *et al*. (2006) showed that it does not perform well everywhere; for instance, in regions where there are extremes in the variability of rainfall or run-off, such as in Australia and South Africa. To avoid this randomly analysis, the Self-calibrating PDSI (SC-PDSI) is developed. The SC-PDSI automatically calibrates the behavior of the index at any location by replacing empirical constants in the index computation with dynamically calculated values. This SC-PDSI were tested and validated by Burke *et al.* (2006) over 761 sites within the U.S. states of Nebraska, Kansas, Colorado, Wyoming, Montana, North Dakota, and South Dakota, and showed spatially a comparable result to PDSI. Some other studies (Gobena and Gan, 2013; Schrier *et al.*, 2006; Sousa *et al*., 2011) also demonstrated that the SC-PDSI can improve upon the PDSI significantly and is more appropriate for comparing the drought severity of diverse climates.

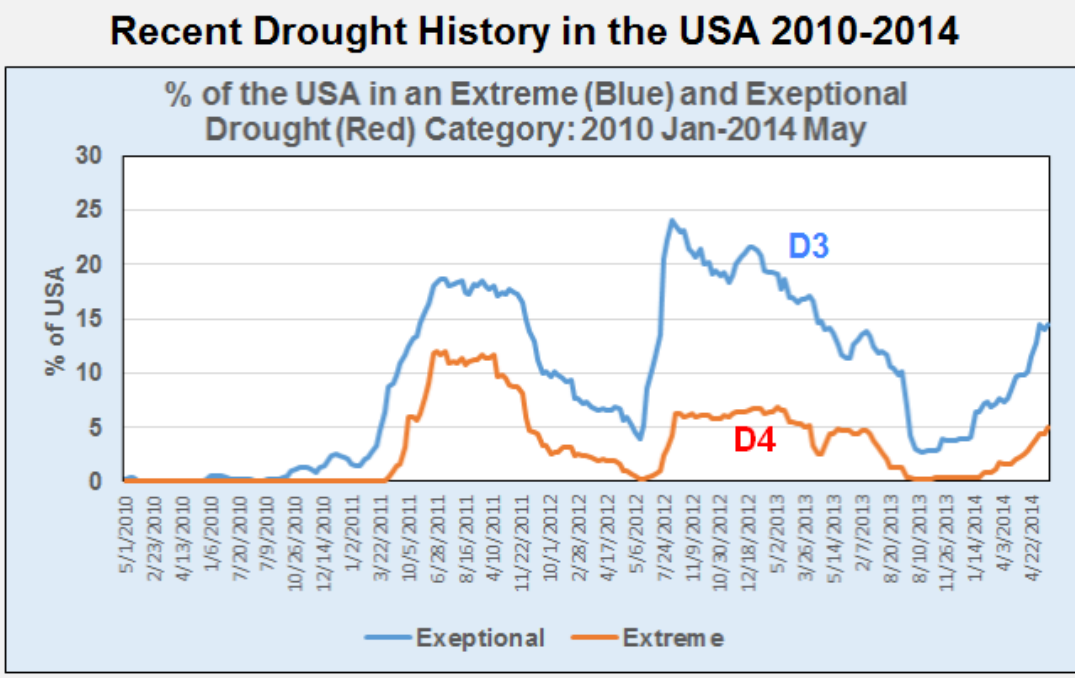

Drought Category	Description	Palmer Drought Index	CPC Soil Moisture %	USGS Weekly Streamflow %	Precipitation Index SPI
DO	Abnormally Dry	-1 to -1.9	21-30	21-30	-0.5 to -0.7
D1	Moderate Drought	-2 to -2.9	11-20	11-20	-0.8 to -1.2
D2	Severe Drought	-3 to -3.9	6-10	6-10	-1.3 to -1.5
D3	Extreme Drought	-4 to -4.9	3 - 5	3 - 5	-1.6 to -1.9
D4	Exceptional Drought	-5 or <	0 - 2	0 - 2	- 2 or <

Figure 2.2: Monitoring of the timing of the extreme and exceptional drought events in California (USA). Source: *United States Department of Agriculture -United States (USDA-US), 2014*

2.2.1.2 Standardized Precipitation Index (SPI)

In order to improve information gotten from PDSI which provides only a spatial overview of drought, the SPI based on a precipitation probabilistic using Gamma distribution approach was proposed by McKee *et al.* (2012) to investigate on particular drought and anomalously wet periods. They also classified the weather events in types since particular systems and regions can respond to drought conditions at very different time scales. This index has been increasingly used during the two last decades because of its solid theoretical development, robustness, and versatility in drought analyses (Redmond, 2002). In term of hydrological evaluation, the advantages of the SPI have been showed with various studies (Fiori *et al.* 2014; Lorenzo-lacruz *et al*., 2010; Vicente-Serrano and López-Moreno, 2005; Vicente-Serrano *et al.*, 2012). In addition, Vicente-Serrano *et al.*, (2005) have also illustrated variation in the response of agricultural, and ecological variables (Ji and Peters, 2003; Pasho *et al*., 2011; Vicente-serrano, 2007) to different time scales of the SPI.

The computation of SPI requires long term data on precipitation to determine the probability distribution function which is then transformed to a normal distribution with mean zero and standard deviation of one (Kumar *et al*., 2009). The major assumption in the SPI computation is that the precipitation and other meteorological factors are taking as stationary with no temporal trends (Vicente-Serrano *et al*., 2010). However, the variable temperature plays an important role in the moisture availability and various empirical studies have shown that an increase in temperature affects the severity and duration of droughts (Rebeteza *et al*., 2006). Thus, the computed values of the index indicated in standard deviations, when the value is positive means the index is greater than median precipitation and negative values expressing less than median precipitation (Edwards and McKee, 1997). McKee et al. (1993) proposed ranges for the SPI

corresponding to different severity levels of drought (Table 2.1). SPI has been recommended by the World Meteorological Organization (WMO) for drought monitoring (Wilhite, 2012). Szinell *et al.* (1998) used the SPI to analysis drought event in Hungary, they found that the SPI with time scale 2-3 is more relevant for agricultural drought (when the soil moisture is insufficient and results in the lack of crop growth and production) whilst 5-24 months relates to hydrological drought (refers to shortages of water resources, when for example; groundwater, reservoir, or stream levels are significantly reduced).

Table 2.1: Classification of SPI and SPEI values. Source: McKee *et al*. (2012)

SPI value	Moisture level
+2.0 and greater	Extremely wet
+1.5 to 1.99	Very wet
+1 to 1.49	Moderately wet
-0.99 to 0.99	Near normal
-1.49 to -1.0	Moderately dry
-1.99 to -1.5	Severely dry
Less to -2.0	Extremely dry

2.2.1.3 The Standardized Potential Evapotranspiration Index (SPEI)

Some region are primarily dry and moisture deficient, i.e. the difference between annual precipitation and potential evapotranspiration (PET) is less than zero (Hogg and Hurdle, 1995). SPI does not consider other variables that can influence droughts, such as temperature, evapotranspiration, wind speed and soil water holding capacity. In a context of global warming where temperature is expected to increase (Dai, 2011) raised the concern that the contribution of temperature to evapotranspiration might play an important role in drought impacts on ecology and mortality (Allen *et al*., 2011; Barber *et al.*, 2000) and water resources. Therefore, using a drought index based on precipitation data alone may not be sufficient to monitor spatiotemporally the droughts. To address this, Vicente-Serrano *et al.* (2010) developed the Standardized Precipitation Evapotranspiration Index (SPEI) which is similar to SPI, because based on the same calculation procedure with difference that it is incorporating estimates of moisture losses to the atmosphere due to evapotranspiration. The SPEI combines the sensitivity of PDSI to changes in evaporation demand with the simplicity of calculation and the multi-temporal nature of the SPI (Čadro *et al.* 2017). It is computed at various temporal scales based on the non-exceedance probability of precipitation and potential evapotranspiration (PRE-PET) differences Vicente-Serrano *et al.* (2010) and is capable of depicting the multi-temporal nature of drought. When take account the climate water balance (CWB) defined as the difference between precipitation and potential evapotranspiration (PRE-PET), the index has ability to capture the effects of global warming on drought occurrence. There is a slight differences when compare the performance of the SPI and the SPEI indices, but the SPEI was the drought index that best captured the responses of the assessed variables to drought in summer, the season in which more drought-related impacts are recorded and in which drought monitoring is

critical (Vicente-Serrano *et al*. 2012). Oguntunde *et al.* (2017) used this index over West Africa, and shown that the historical (1970-2013) pattern of drought is consistent with previous studies over the Volta River Basin, while Diasso and Abiodun, (2015) grouped about 60 % of spatial-temporal variability of SPEI over West Africa in four groups : east Sahel, west Sahel, Guinea coast and Savanna.

2.2.2 Characterization of drought and flood using climate simulation

Several regions in the world are impacted by hydrological extremes, i.e. drought and flood events, with important consequences for countries' economy. There is serious preoccupation about future hydrological extremes due to climate change or climate variability. In the aim to address this issue, some authors proposed to capture realistically the location of the extremes and how and why the change is or will be observed on a specific period, also propose appropriate policies to reduce the negative impacts of hydrological extremes. It is obvious that when the hydrological drought occurs water abstraction and irrigation are significantly impacted (Kumar *et al.*, 2016); whilst during flood events, protection measures such as levees, alter the frequency, magnitude and spatial distribution of the events (Baldassarre *et al*., 2009; Blöschl *et al*., 2013; Heine and Pinter, 2011). To earlier warning about these weather extremes (Di Baldassarre *et al.*, 2013; Sivapalan *et al*., 2011) developed adaptation measures which underpinning integrated water resources management (IWRM). Precipitation playing an important role in the characterization of hydrological extremes. García-Valdecasas *et al.* (2017) used the Weather Research and Forecasting (WRF) model to dynamically downscaling high-resolution precipitations in aim to evaluate the dry and wet area in Spain. They compared the spatiotemporal variabilities of agricultural and hydrological droughts using SPI and SPEI methods with the high estimated variables from WRF outputs, on the one hand with the observational (monthly precipitation and temperature

databases of Spain, MOPREDAS and MOTEDAS) and on the other hand with the European Centre for Medium-Range Weather Forecasts Interim Re-Analysis (ERA-Interim) data sets. Chawla *et al*. (2018), Maussion *et al.* (2011) and Ngailo *et al*. (2018), provided rainfall estimates with WRF at fine grid spacing to monitor flood events. WRF model was also used by Flesch and Reuter, (2012) to investigate two flooding events in Alberta, Canada. They found that there was little sensitivity to topography in the precipitation outside the mountain areas. Yukiko *et al*. (2010) simulated daily discharge from a high-resolution general circulation model (GCM) to investigate on future projections of extremes, and found an increase of frequency of floods and droughts in some specific areas. They concluded that changes in flood and drought are not explained simply by changes in annual precipitation, heavy precipitation, or differences between precipitation and evapotranspiration. Milly *et al*. (2002) investigated changes in flood extremes using monthly river discharge data for both gauge observations and GCM simulations, and noticed increasing of the risk of great floods.

2.3 **Effects of El Niño and La Nina on African rainfall**

The El Niño-Southern Oscillation (ENSO) cycle is a scientific term that describes the fluctuations in temperature between the ocean and atmosphere in the east-central Equatorial Pacific (approximately between the International Date Line and 120 degrees West). El Niño and La Niña are opposite phases of what is known as the ENSO cycle. La Niña is sometimes referred to as the cold phase of ENSO and El Niño as the warm phase of ENSO (Figure 2.3).

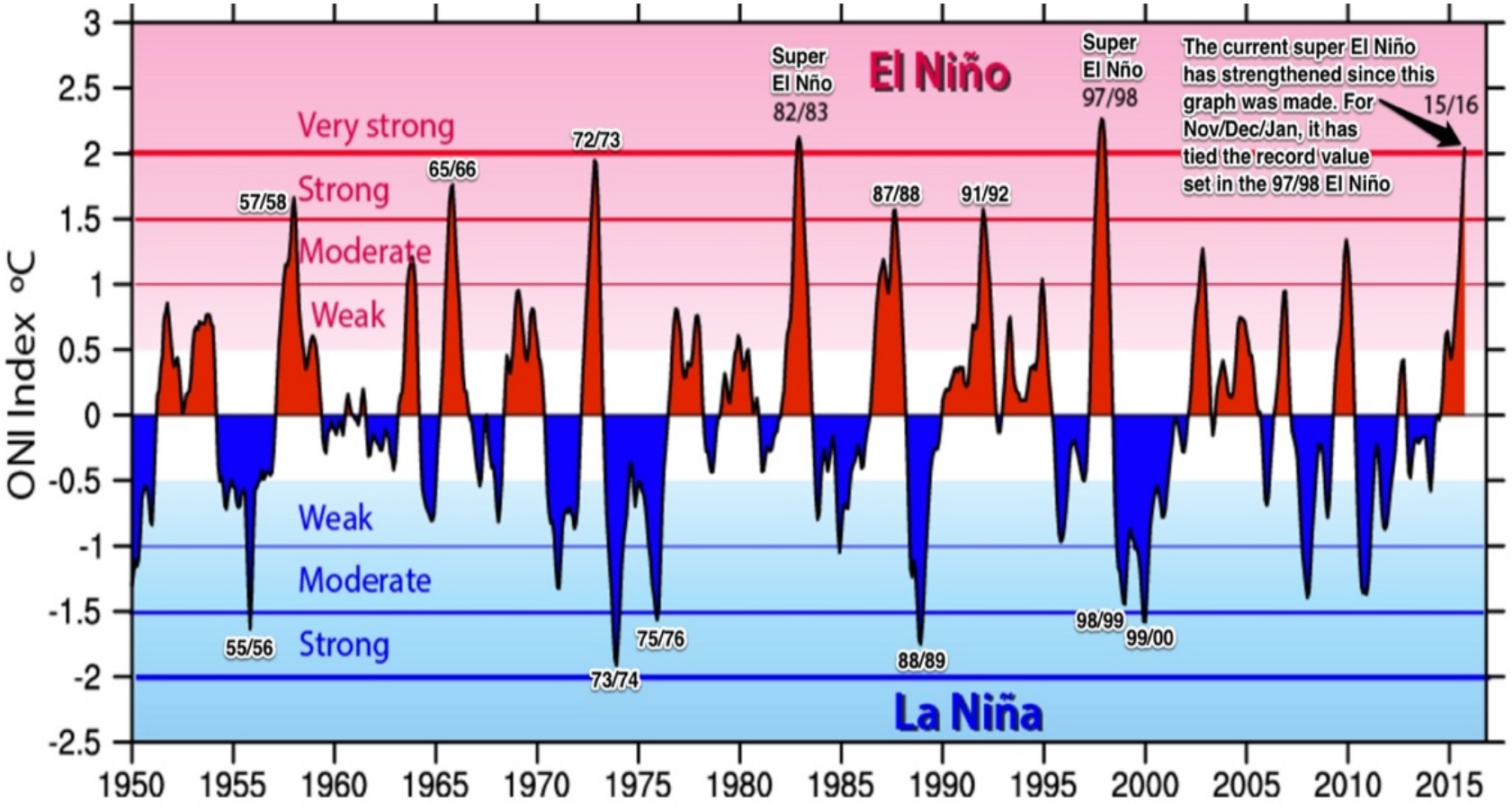

Figure 2.3: The Oceanic Niño Index shows warm El Niño (red) and cold La Niña (blue) phases of abnormal sea surface temperatures in the east-central tropical Pacific Ocean. (Source: Kevin Trenberth/National Center for Atmospheric Research, 2016)

It has long been recognized that the Pacific El Niño has a close association with rainfall variability in many parts of Africa. Geographically specific studies indicated a tendency for droughts in southern Africa during El Niño events (Heerden et al., 1988; Lindesay, 1988) and above-normal rainfall in much of equatorial eastern Africa (e.g. Beaufort et al., 1997). As El Niño, La Niña is a general association between wet conditions continentally and cold temperatures in the Atlantic and Indian Oceans, and dry conditions in association with warm sea-surface temperatures (SSTs) in these oceans. La Niña appears to have the greatest influence on rainfall in southern Africa and wet episodes tend to occur throughout the subcontinent during the first few months of the post-La Niña year (Nicholson and Selato, 2000). Klutse *et al*. (2015) using GCMs (CAM3 and HadAM3) found that the both models give reasonable simulations of significant relationship between the regional rainfall and SST over the Nino 3.4 region and show that ENSO strongly drives the climate of Southern Africa.

Over West Africa, El Niño events tend to result in enhanced north-easterlies/reduced monsoon flow, coupled to weakened upper easterlies, and hence dry conditions over West Africa close to the surface position of the ITCZ in July–September, as well as January–March. The combination of ENSO and Atlantic SST anomalies are found to give rise to complex wind flow changes in the near-equatorial Atlantic. In addition to large-scale SST-forced atmospheric dynamics, a few regional atmospheric signals are found to explain residual parts of rainfall variance. For instance, a strengthening of the African Easterly Jet (AEJ), or northerly wind anomalies across the Sahara, are shown to be related to drought conditions in the Sahel (July–September) and the Gulf of Guinea area (January–March), once the remote effect of SST anomalies is removed (Camberlin *et al*., 2001).

2.4 **Representative Concentration Pathways (RCPs)**

In the aim to investigate and understand future climates, scientists refer to climate scenarios to provide a plausible explanation of how the future may evolve with respect to a number of variables including socioeconomic change, technological change, energy and land-use, and emissions of greenhouse gasses and air pollutants (Van Vuuren *et al.*, 2011). For this issue, there are many factors that researchers have to take account when predicting how future global warming will contribute to climate change. Among the factors, future greenhouse gas emissions is a key variable. So for research of various groups be comparable or/and complementary, a standard set of scenarios should be retained to ensure that starting conditions, historical data, and projections are employed consistently across the various branches of climate science. So, for the Intergovernmental Panel on Climate Change (IPCC) meeting in 2007, four (04) RCP radiative forcing levels were retained (Moss *et al.*, 2008). The four RCPs, namely RCP2.6, RCP4.5, RCP6, and RCP8.5, are labeled after a possible range of radiative forcing values till the year 2100 (2.6, 4.5, 6.0, and 8.5 W/m^2, respectively). But for the preparation of the Fifth Assessment Report (AR5) of the Intergovernmental Panel on Climate Change (IPCC) meeting in 2014, researchers thought about the development of a new approach the create a standard and usable climate change scenarios for research. Table 2.2, has been proposed for projections of global warming for the Mid- and late-21st century (2046–2065 and 2081–2100, respectively). For these projections, they suggested that temperature projections can be compared to a reference period of 1850–1900 or 1980–99 by adding 0.61 or 0.11 °C, respectively. Across all RCPs, global mean temperature is projected to rise by 0.3 to 4.8 °C by the late-21st century, whilst the global mean sea level rises by 0.26 to 0.82 m.

Table 2.2: Global warming (°C) and sea level (m) increase projections according to AR5 (Source: https://en.wikipedia.org/wiki/Representative_Concentration_Pathway).

	Description	Global warming (°C) increase		Global sea level (m) increase	
	Rising radiative forcing pathway	2046-2065	2081-2100	2046-2065	2081-2100
Scenario		Mean and likely range	Mean and likely range	Mean and likely range	Mean and likely range
RCP2.6	(~490 ppm CO_2 eq) by 2100	0.4 to 1.6	0.3 to 1.7	0.17 to 0.32	0.26 to 0.55
RCP4.5	(~650 ppm CO_2 eq) by 2100	0.9 to 2.0	1.1 to 2.6	0.19 to 0.33	0.32 to 0.63
RCP6	(~850 ppm CO_2 eq) by 2100	0.8 to 1.8	1.4 to 3.1	0.18 to 0.32	0.33 to 0.63
RCP8.5	(~1370 ppm CO_2 eq) by 2100	1.4 to 2.6	2.6 to 4.8	0.22 to 0.38	0.45 to 0.82

Stemming from the Paris Agreement in 2015 at COP21 (Rogelj *et al*., 2016) inviting for keeping global temperature increase below 2ºC, and even possible engaged this temperature increase to 1.5ºC. Recently, Déqué *et al.* (2017) suggested a classification of the global warming for all the RCPs and for Global warming levels (GWLs) form 1.5ºC to 4ºC. Based on *Déqué et al*. (2017) suggestion, several studies (Abiodun, 2018; Klutse *et al.*, 2018; Kumi and Abiodun, 2018; Maúre *et al.*, 2018; Nikulin *et al*., 2018) were done to assess the impact of each GWL on various fields. Figure 2.4 is showing the emission of atmospheric concentration of carbon dioxide CO_2 (parts per million) under the four scenarios, while Figure 2.5 is referred to the Projected global surface temperature change under different emissions scenarios. This Figure 2.5 is a chart showing forecast temperature change under the best (RCP2.6) and worst (RCP8.5) scenarios.

From Figure 2.5, if we assumed that by 2020 that the emission reached its peak and then reduced to zero this century (i.e. the assumption of RCP2.6), the global temperature could be stabilized at around 1°C above levels in the late 1900s. The IPCC says it is unlikely (<33% probability) that the rise will exceed 2°C. On the other hand, if we carry on as if there is no problem without even a slowdown in emissions growth until late in the 21st century (i.e. RPC8.5), the forecast outcome is not pretty. Temperatures are forecast to continue increasing and by 2100 and reach around 4°C higher than late 20th century levels.

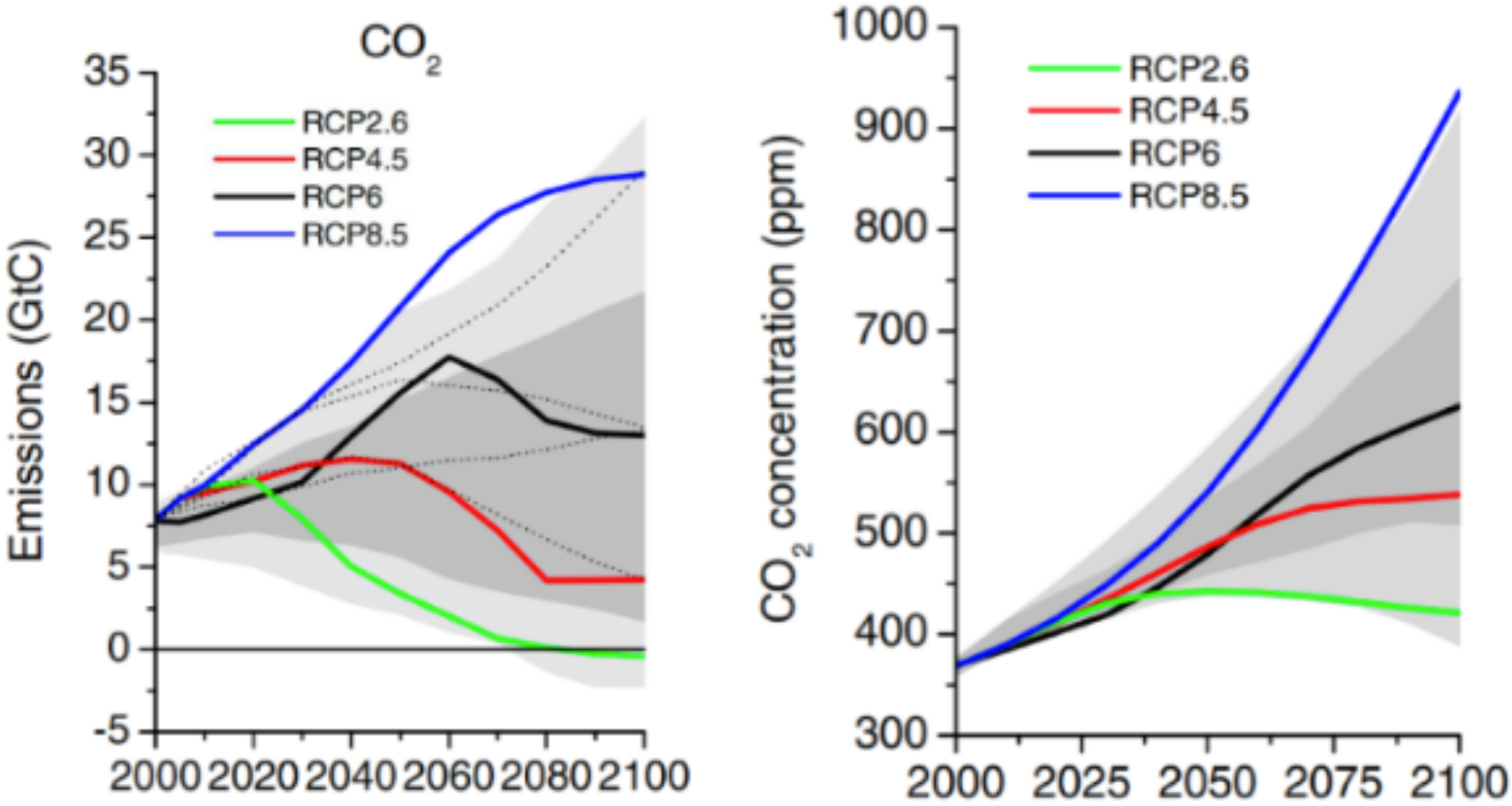

Figure 2.4: Global carbon dioxide (CO_2) emissions and Atmospheric concentration of CO_2

(Source: Van Vuuren et al., 2011)

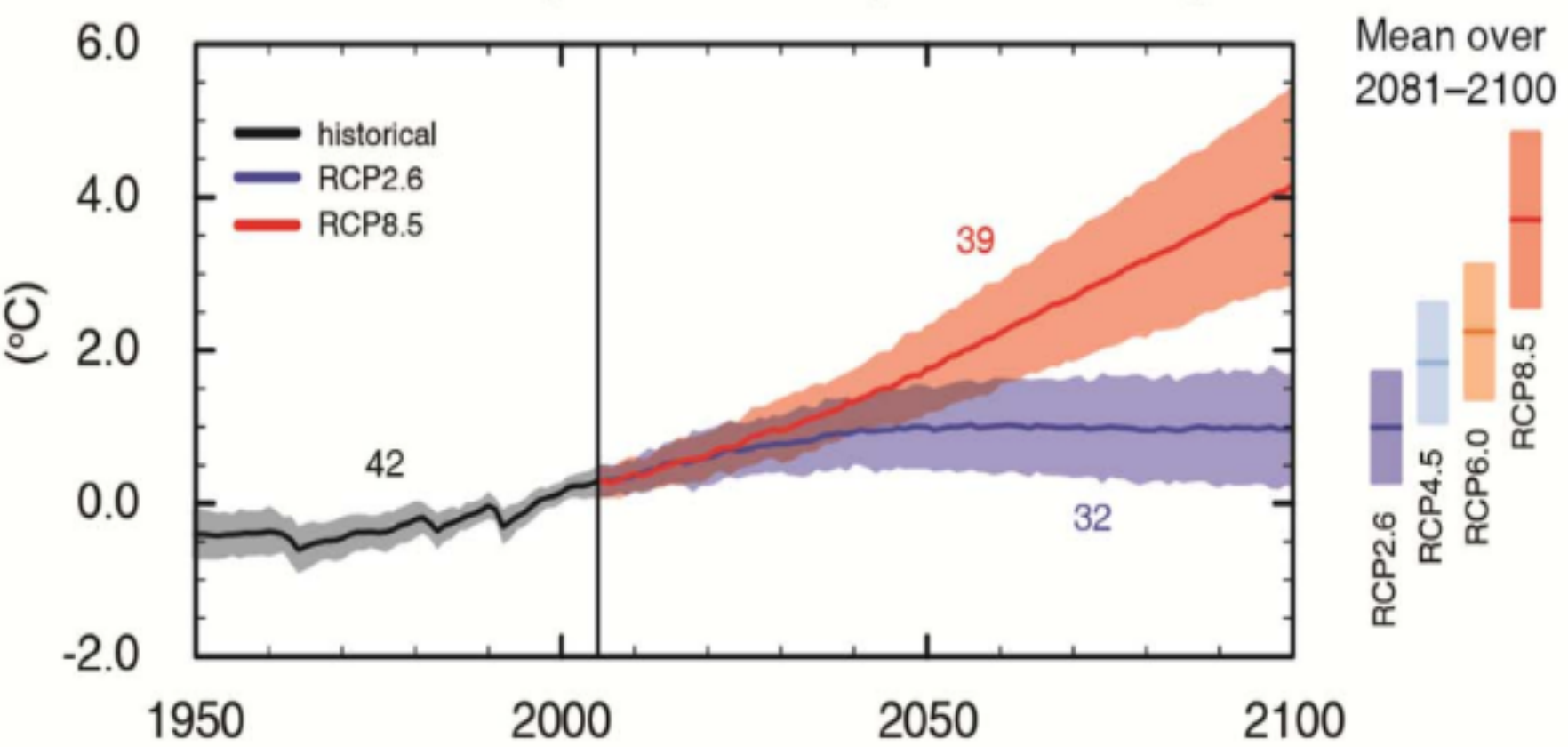

Figure 2.5 : Projection of global surface temperature change under different emissions scenarios.

(Source: IPCC Working Group I Assessment Report, Summary for Policy Makers, 2013)

2.5 **Global and Regional Climate Models**

Prediction means obtaining projected data of an area over a period of time. There are two main ways in prediction: (i) statistical method where historical data is set to detect significant past variability, to provide a basis for predicting future changes; and (ii) physically-based model approach to simulate past climate processes and predict the future climate. According to Garner *et al*. (2015), the second approach requires an in-depth understanding of the physical processes driving the climate and changes within an area. For that, it is important to study the dynamics of the future climate using climate models. There are two types of climate models: Global Climate Models (GCMs) and Regional Climate Models (RCMs).

GCMs have coarse resolutions; and are designed to simulate earth's climate over the entire planet, but are limited when they come to describing local details due to heavy computational demands. For that challenge, GCM's output may be downscaled using RCMs or empirical-statistical downscaling (ESD) methods. For instance, there is a broad agreement in the literature that the atmosphere will warm, and accordingly its water-holding capacity will increase; in turn, this will drive a change in the type and frequency of precipitation extremes and increase evaporation (Stocker *et al*., 2013); investigation of this example could be done for the whole earth planet using GCM and locally details (with a much finer grid) should be driven by the RCM or ESD from GCM's results. RCMs can add details such as the influence of lakes, sea breeze, mountain ranges, and sharper weather fronts. Diallo *et al*. (2012), Giorgi (2014) and Laprise *et al*. (2013) have demonstrated that downscaling GCM output with RCM could potentially improve spatial and temporal information, especially for detailed impact assessments at the regional level. The Coordinated Regional Downscaling Experiment (CORDEX) downscaled multiple GCMs over fourteen domains such as Europe, Asia

(East, Central, South), South-East Asia, Africa, Middle East North Africa, America (North, Central, South), Australasia, Antarctica, Arctic, and Mediterranean. Many works used this CORDEX dataset to investigate on drought events (Diasso and Abiodun, 2015; Maúre *et al*., 2018; Meque and Abiodun, 2015, Oguntunde *et al*., 2017), on the characteristics of West African precipitation (Klutse *et al*., 2015; Nikulin *et al*., 2012), on the impacts of different levels of global warming in some specific domains (Abiodun *et al*., 2018; Déqué *et al.*, 2017; Klutse *et al*., 2018; Kumi and Abiodun, 2018; Mba *et al*., 2018; Nikulin *et al*., 2018).

The scale at which GCMs and downscaled RCMs simulate the global water cycle processes is too coarse for catchment-scale modeling (Maraun *et al*., 2010). Therefore, GCMs or RCMs outputs are often used to drive offline hydrological models, and thus simulate catchment moisture stores and runoff at smaller spatial scales (Duan and Mei, 2014). However, not all of the hydrological models are equally suitable to represent floods or droughts (Tallaksen and Stahl, 2014, and Van Loon *et al*., 2012). Therefore, Wilby and Dessai (2010) suggests that climate model outputs should be evaluated for a specific hydrological application, while Huijgevoort *et al*. (2014) advise an a priori selection of GCM–hydrological model combinations.

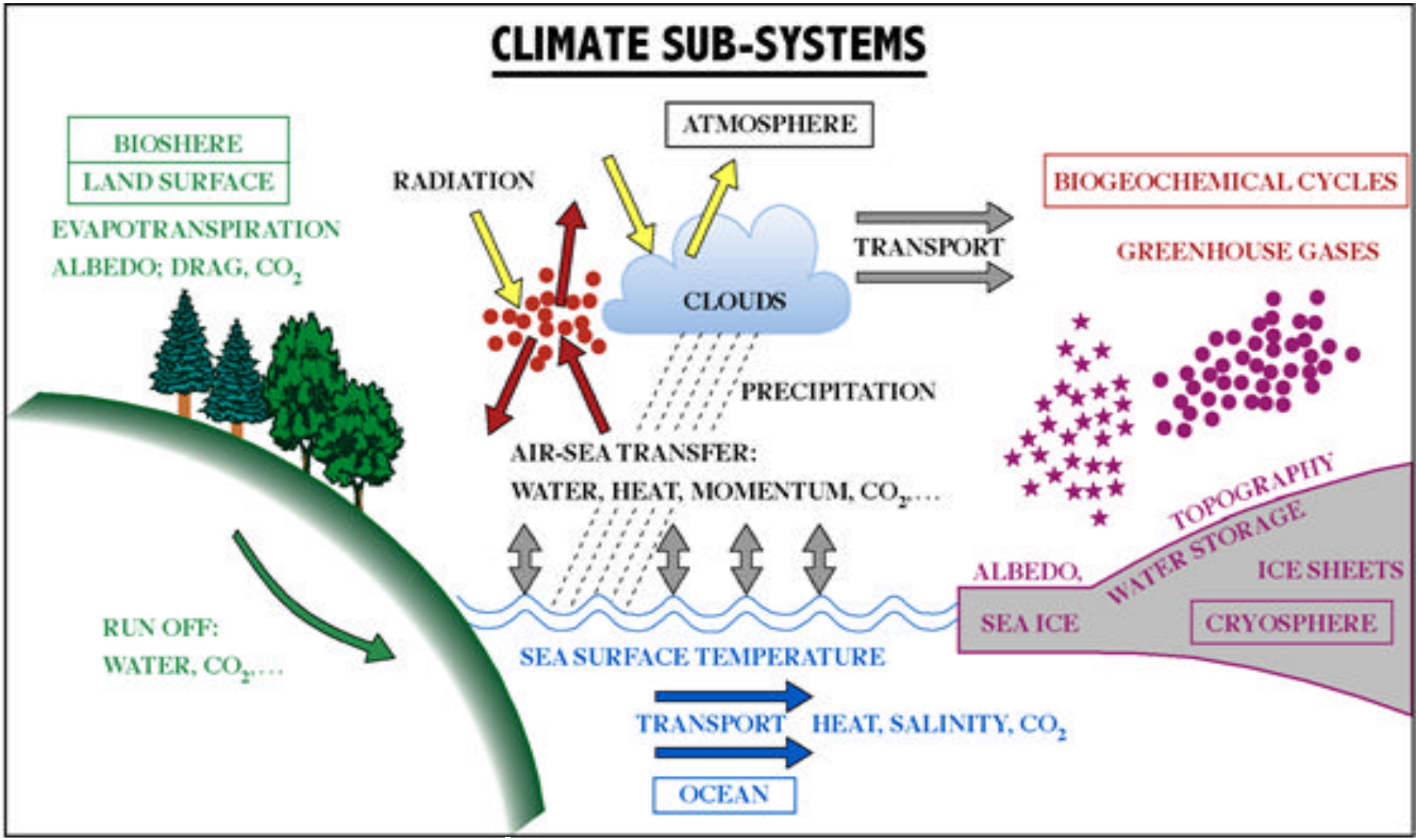

Figure 2.6: Components of a dynamical climate model (Source: Hasselmann, 1990).

2.6 **Coupled atmospheric models and hydrological models**

2.6.1 Weather Research and Forecasting (WRF) Model parametrization

The WRF model is a non-hydrostatic, mesoscale numerical weather prediction, and atmospheric simulation system, and is suitable to simulate a wide range of scales (i.e. from thousands of kilometers to a few meters). It gives several physics options for the parametrization of the subgrid-scale physical processes, for instance, convection, microphysics, radiation, or the planetary boundary layer (Wagner *et al*., 2016), and makes it appropriate for a broad range of applications such as forecasting research, Real-time Numerical Weather Prediction (NWP), Regional climate research, Couple model applications, etc. Besides, it disposes options of land surface models (LSMs) which compute heat and moisture fluxes over the surface and is used as a lower boundary for atmospheric models. The behaviors of the WRF model depend directly to how well it represents atmospheric processes, which is related to the choice of suitable parametrization schemes with respect to the research question of the study. The performance of any physics scheme depends largely on the main feature of atmospheric processes in the domain of interest, the model resolution and the appropriate choice of parameterization for the particular problem (Klein *et al*., 2015). The choice of parameterization schemes influences strongly the outcome of the model simulations. These schemes are summarized into the categories of the land surface, atmosphere interaction, water-atmosphere interaction, planetary boundary layer and turbulence, convection, microphysics and radiation (Stensrud *et al.*, 2009). Details of these parameterizations are available e.g., in Skamarock *et al*. (2007).

2.6.2 WRF-Hydro modeling system

In this study, the WRF hydrological modeling extension package (WRF-Hydro V.3.0; (Gochis *et al.*, 2015) is explored. WRF-Hydro has been established to facilitate improved representation of terrestrial hydrologic processes related to the spatial redistribution of surface, subsurface and channel waters across the land surface and to facilitate coupling of hydrologic models with atmospheric models (Gochis *et al*., 2015). The underlying land surface model upon which the hydrological model is built is made up of a fully distributed, 3-dimensional, variably-saturated surface and sub-surface flow model previously referred to as 'Noah-distributed'. The conceptual architecture for WRF-Hydro is shown in Figure 2.7 where WRF-Hydro exists as a coupling architecture (blue box: to an atmospheric model) or "middleware" layer between weather and climate models and terrestrial hydrologic models and land data assimilation systems. WRF-Hydro can also operate in a standalone mode ("uncoupled" or "offline") like a traditional land surface hydrologic modeling system (Gochis *et al*., 2015). The principle model physics options in WRF-Hydro include:

- 1-dimensional (vertical) land surface parameterization
- surface overland flow
- saturated subsurface flow
- channel routing
- reservoir routing
- conceptual/empirical baseflow

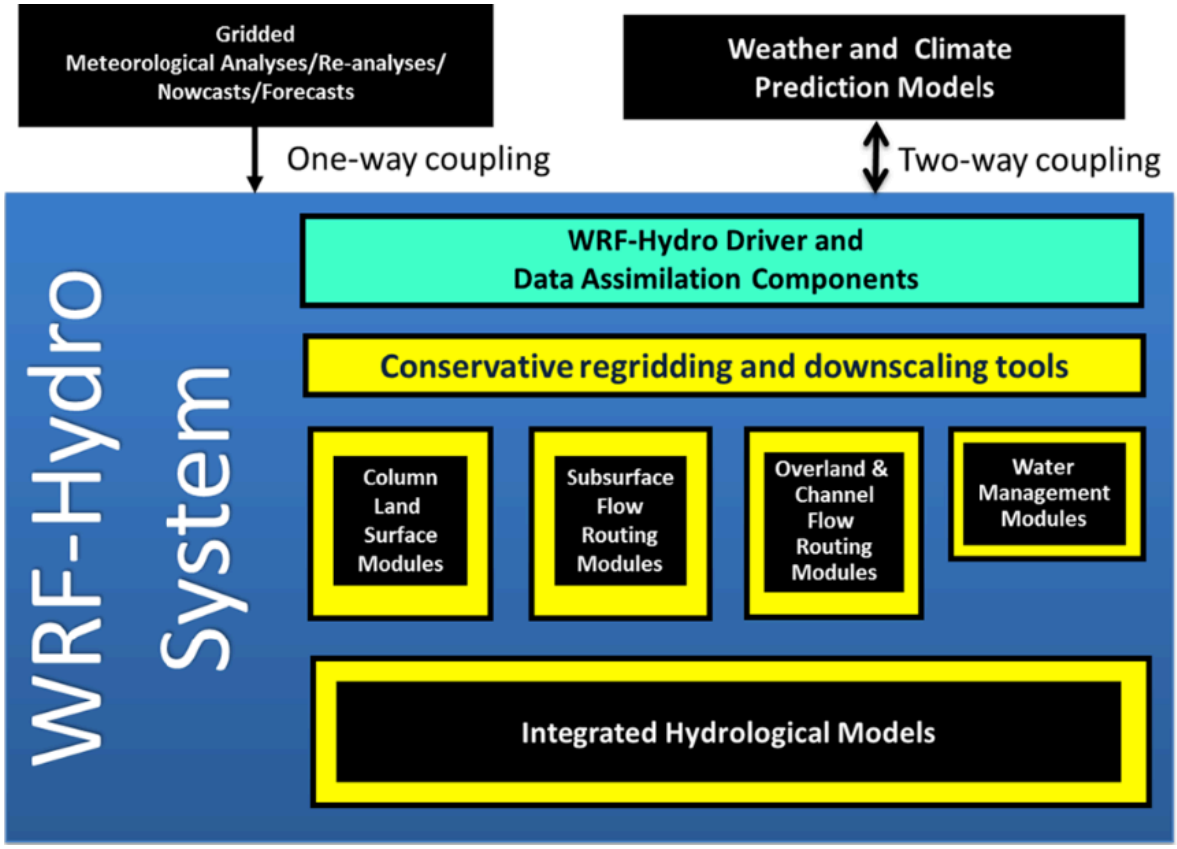

Figure 2.7 : Conceptual Schematic WRF-Hydro architecture showing, various categories of model components (Source: Gochis et al., 2015)

The details of the routing processes are available in Gochis *et al.* (2015). A brief statement of some processes are provided below.

First the 1-dimensional (1D) column land surface model calculates the vertical fluxes of energy (sensible and latent heat, net radiation) and moisture (canopy interception, infiltration, infiltration-excess, deep percolation) and soil thermal and moisture states. Infiltration excess, ponded water depth and soil moisture are subsequently disaggregated from the 1D LSM grid, typically of 1–4 km spatial resolution, to a high-resolution, typically 30–100 m, routing grid using a time-step weighted method (Gochis and Chen, 2003) and are passed to the subsurface and overland flow terrain-routing modules. Other land cover and soil type classification datasets can be used with WRF-Hydro but users are responsible for mapping those categories back to the same categories as used in the USGS or MODIS land cover and STATSGO soil type datasets. The WRF model pre-processing system (WPS) also provides a fairly comprehensive database of land surface data that can be used to set up the Noah and Noah-MP land surface models. It is possible to use other land cover and soils datasets.

The subsurface lateral flow in WRF-Hydro is calculated prior to the routing of overland flow to allow exfiltration from fully saturated grid cells to be added to the infiltration excess calculated from the LSM. The current existing method used to calculate the lateral flow of saturated soil moisture is that of Wigmosta and Lettenmaier (1999) and Wigmosta *et al*. (1994) implemented in the Distributed Hydrology Soil Vegetation Model (DHSVM). It calculated a quasi-3D flow, which includes the effects of topography, saturated soil depth, and depth-varying saturated hydraulic conductivity values. Hydraulic gradients are approximated as the slope of the water table between adjacent grid cells in either the steepest descent or in both x- and y-directions. The flux of water from one cell to its down-gradient neighbor on each time-step is approximated

as a steady-state solution. WRF-Hydro specifies the water table depth according the depth of the top of the saturated soil layer that is nearest to the surface. By default in the model, a minimum of four soil layers are used in a 2-meter soil column. The depth of each column can be adapted according to each field.

Overland flow is represented using a fully-unsteady, explicit, finite-difference, diffusive wave formulation with either a two dimensional or a steepest descent approach. The continuity equation for an overland flood wave is combined with the diffusive wave formulation (the diffusive wave formulation accounts for backwater effects hence allowing flow on adverse slopes) of the momentum equation (Kerandi, 2017).

Channel routing along the river network defined by grid cells is being simulated by application of St. Venant's equation, which provides solution to conservation of mass and momentum equations, to single direction shallow water wave flows. If there is a reservoir along river, model also applies reservoir routing.

WRF-Hydro uses precipitation, temperature, wind (u and v), humidity and incoming short, long wave radiation as forcing dataset. In addition to these data, hydrologic base layers like high resolution topography, flow direction, stream network, stream order, basin boundaries are needed to use in land and channel routing modules (Önen, 2013). The high-resolution domain is generated by processing topographic data in Geographic Information System (GIS) environment (ArcGIS in particular). Within the model algorithm, excess precipitation calculated by water and energy balance, soil moisture and hydraulic conductivity are downscaled from the low scale of the LSM to the high-resolution by grid disaggregation technique (Gochis *et al*., 2015) and are used in routing modules to perform surface, sub-surface and channel routing processes.

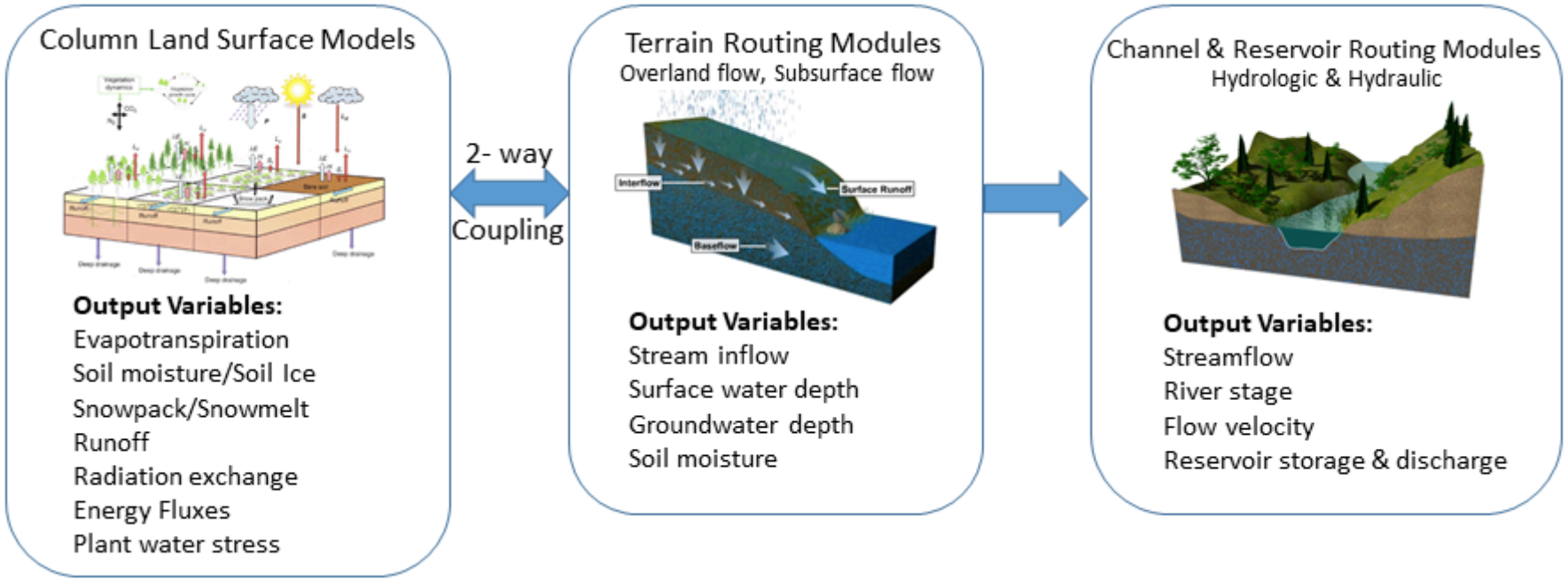

Figure 2.8: Conceptual diagram of WRF-Hydro physics components and relative outputs (Source: Gochis *et al*., 2015)

2.6.3 Coupling models atmospheric-hydrologic model WRF/WRF-Hydro

The accuracy of flood forecasts depends strongly on the skill of quantitative precipitation forecasts and their spatial distribution (Cloke and Pappenberger, 2009; Shih *et al.*, 2014; Younis *et al.*, 2008). Most modern hydrological models can use precipitation input from various sources: rain gauges, radar, remote sensing or simulated precipitation from numerical weather models. Operational global weather forecast centers routinely provide over the Eastern Mediterranean region relatively coarse precipitation forecasts with resolutions of 16–27 km (Givati *et al.*, 2016). These forecasts cannot typically resolve the necessary details of complex, intense precipitation structures that are forced by mesoscale orography, land-surface heterogeneities, and land-water contrasts (Fiori *et al*., 2014). To overcome this, Givati *et al*. (2012) used the Weather Research and Forecast (WRF) model to provide high-resolution precipitation forecasts of 1.3 - 4 km horizontal resolution; and found that WRF model was able to provide precipitation forecast both in terms of quantity and in spatial distribution. Givati *et al*. (2012) used the output from the WRF model to run Hydrological Model for Karst Environment (HYMKE) for the upper Jordan River basin; for over Ayalon basin case Givati and Sapir (2014) preferred HEC-HMS hydrological model.

Similar experiments were set in different areas and the authors found that rainfall estimates from the WRF model underestimated the magnitude of the heavy precipitation events in comparison with rain gauges, and so the surface runoff hydrograph determined from WRF-derived precipitation was also underestimated (Ratnayake *et al*., 2010; Yucel and Keskin, 2011).

Several studies (Bouilloud *et al*., 2010; Chen and Dudhia, 2001; Jasper *et al*., 2002; Marty *et al.*, 2013; Moreno *et al*., 2013; Seuffert *et al*., 2002; Wang et al., 2012; and

Zabel and Mauser, 2013) have shown the advantages of using coupled atmospheric-land surface models for temperature and precipitation in different areas and for different seasons. Wagner *et al*. (2016) studied simulations with a fully coupled atmospheric-hydrological model (WRF-HMS) and uncoupled model for several meteorological variables and found a better performance for the fully coupled model. Senatore *et al.* (2015) compared a one-way forced implementation of the WRF-Hydro system to a fully 2-way coupled instance of WRF/WRF-Hydro in order to evaluate the impact of 2-way coupling on simulated precipitation and stream flow. They found that the two setups performed well for the precipitation but the correlation from the two-way coupled WRF/WRF-Hydro simulation was higher than the one-way WRF model both compared with the observed data and statistical criteria. Based on the finding of Senatore *et al*. (2015), Givati *et al*., (2016) tried to assess the accuracy of operational hydrologic forecasts when using different sources (rain gauge data, offline simulated precipitation from the WRF model (WRF one way) and online simulated precipitation from the fully-coupled atmosphere-land-hydrology WRF/WRF-hydro model (WRF two way)) of precipitation data as input including one-way versus two-way coupled modeling systems. To assess the advantages and limitations of one-way versus two-way coupled modeling systems for flood prediction over Ayalon basin (Israel), Givati *et al*. (2016) used both hydrological model Hydrological Engineering Center-Hydrological Modeling System (HEC-HMS) and the Weather Research and Forecasting Hydro modeling system (WRF-Hydro). The models were forced by observed, interpolated precipitation from rain-gauges within Ayalon basin, and with modeled precipitation from the WRF atmospheric model. They used the two-way coupled WRF/WRF-Hydro modeling system to improve both the precipitation and hydrological simulations as compared to the one-way WRF simulations. They found that, the use of two-way atmospheric-hydrological coupling has the potential to improve precipitation and, therefore,

hydrological forecasts for early flood warning applications. Kerandi *et al*. (2018) applied the fully coupled WRF/WRF-Hydro to improve understanding of the hydrometeorological conditions of the Tana River basin of Kenya by investigating on the joint atmospheric-terrestrial water balances of the coupled model. They concluded that the coupled WRF/WRF-Hydro slightly reduces precipitation, evapotranspiration, and the soil water storage but increases runoff over Tana River basin. Arnault *et al*. (2016) applied for the first time the model WRF-Hydro over a basin in West-Africa. They assessed the influence of the runoff–infiltration partitioning and resolved overland flow on land–atmosphere feedbacks, and shown that resolved overland flow increases infiltration and evapotranspiration at the beginning of the wet season when soils are still dry whilst precipitation is relatively sensitive to runoff–infiltration partitioning. They also illustrated that WRF-Hydro was able to reproduce daily streamflow in the Sissili river's with a reasonable performance. Naabil *et al.* (2017) in a work about water resource management in Ghana, explored the potentiality of WRF-Hydro in a fully coupled mode with WRF to assess water resources, in Tono basin. Another work led by Arnault *et al*. (2018) in central Europe, used WRF-Hydro to investigate on the sensitivity of precipitation to the uncertainty in the representation of terrestrial water flow. Their work demonstrated that the uncertainty of terrestrial water flow increases the normalized ensemble spread of daily precipitation where topography is moderate, surface flux spatial variability is high, and the weather regime is dominated by local processes.

CHAPTER THREE

MATERIALS AND METHODS

3.1 Study domain

The study area lies in West Africa, which is located between latitudes 0°N and 20°N and longitudes 20°W and 20°E (Figure 3.1). This region is bordered in the South by the Gulf of Guinea, in the north by Mauritania, Mali, and Niger; the Cameroon highlands form the eastern boundary, while the Atlantic Ocean forms the western limit. The annual mean temperature is about 18℃, but in the Sahel, maximum temperatures can reach above 40°C. Rainfall patterns over this region are mostly affected by ocean currents and local features, such as topography. In terms of climatic zones, West Africa can be divided into three different regions. The first region covers the Sahel and is characterized as a semi-arid zone ranging from western Senegal to eastern Sudan, between 12°N and 20°N. The second region is the Sudano-Sahelian zone, while the last and the third comprises the Gulf of Guinea, which is characterized by a bimodal mode driven by the Intertropical discontinuity (ITD). At the Gulf of Guinea, precipitation is abundant year-round without a clear marked dry season (in August). At higher latitudes, precipitation decreases and is limited to a wet season of decreasing duration. Therefore, along the south-north gradient of decreasing rainfall, countries around latitude 5ºN record a mean annual rainfall of 1,600 mm; those around 12ºN 700 mm within a 5-month rainy season; and 18ºN and up less than165 mm annually in a short 2.5-month rainy season (Figure 3.2).

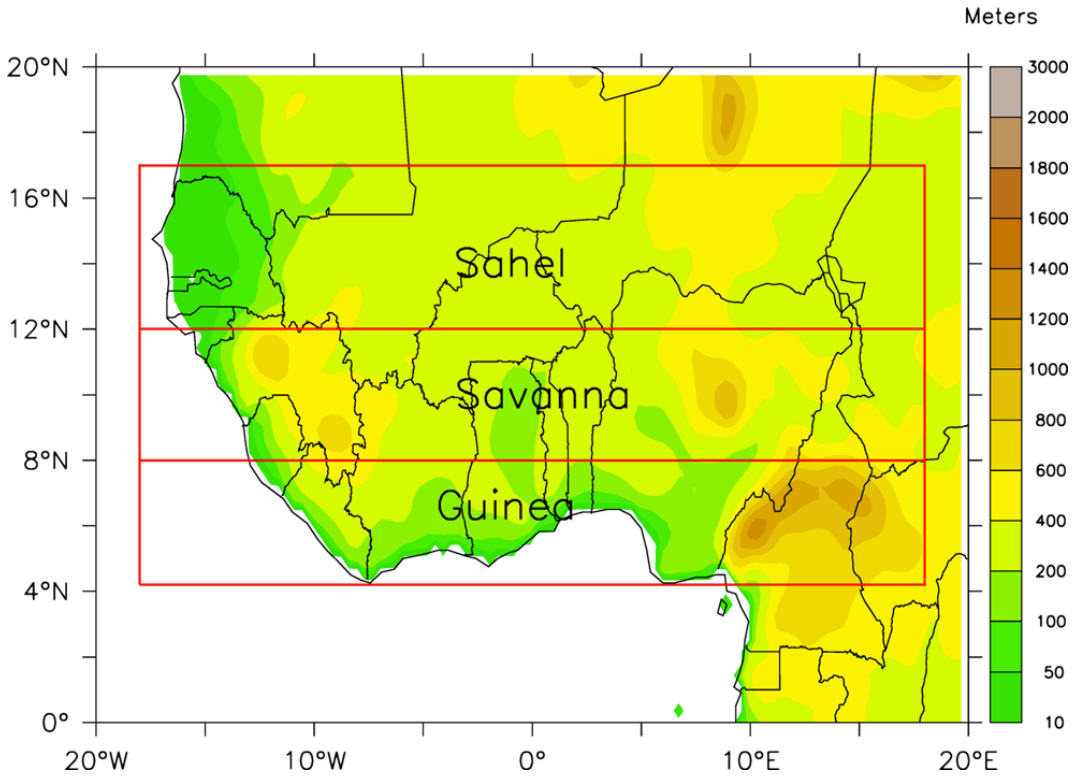

Figure 3.1: Study domain showing the West African topography and the area of focus, which comprises the Gulf of Guinea (Guinea), the Savanna, and the Sahel zones. Source: Diasso and Abiodun, 2015.

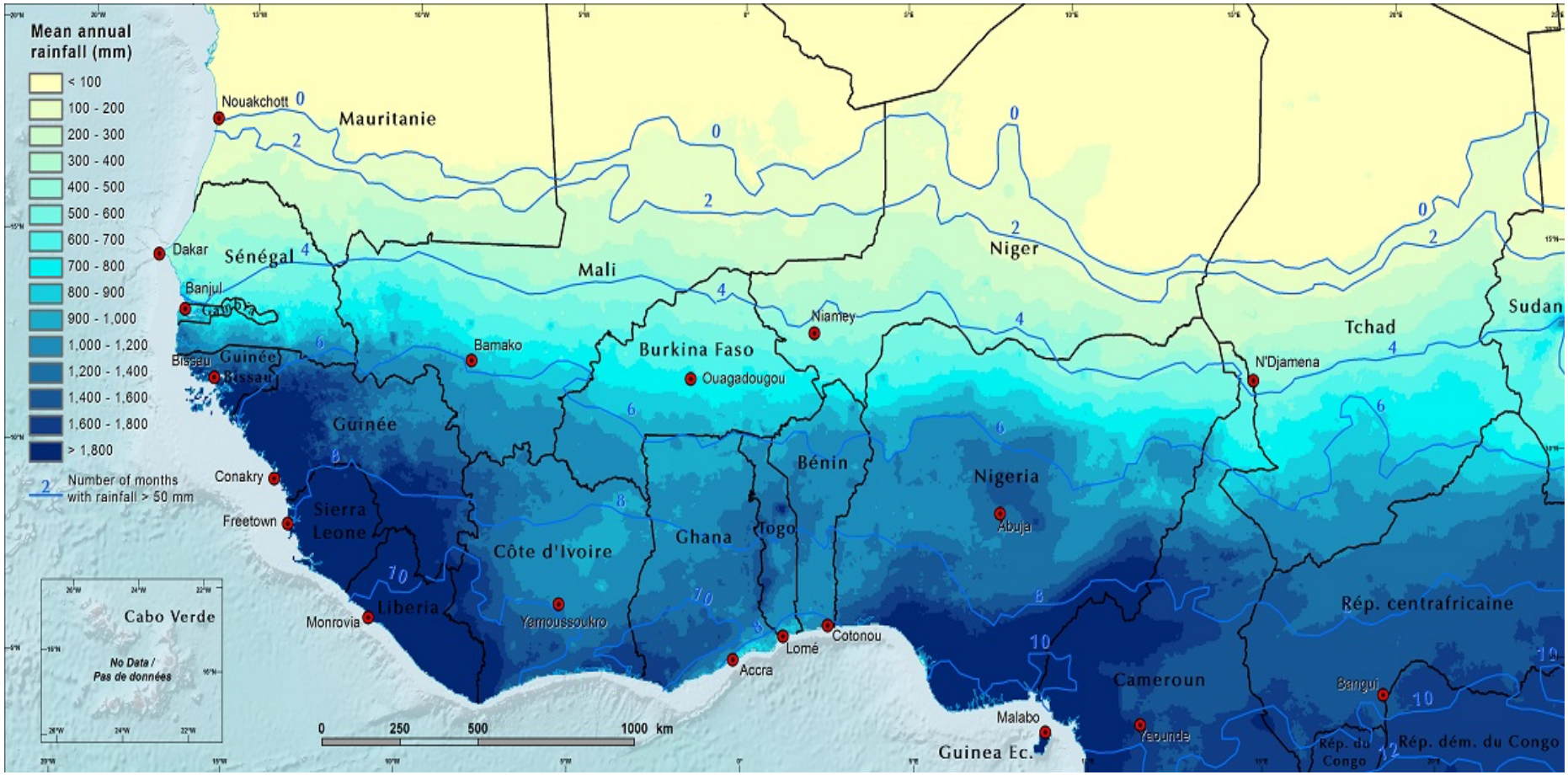

Figure 3.2: Mean annual rainfall 1981–2014, with number of months of 50 mm or more of rainfall.

Source : https://eros.usgs.gov/westafrica/node/157

To experimentally evaluate the ability of the atmosphere-hydrology modeling system in West-Africa, the study domain is narrowed to Figure 3.3 which represent the simulated domain located between latitudes 0°N and 18°N and longitude 7°W and 12°E. Within this domain, the study focused on Ouémé-river located in the Benin Republic.

Benin is located in the inter-tropical zone (between 06°10′N and 12°25′N), that has a wet and dry tropical climate (Hounkpè *et al*., 2015) contains the interested rivers (Savè and Bétérou) on which the study is focused on. The Ouémé catchment at Savè (resp. Bétérou: inner-catchment to Savè) outlet covers an area of 24.800 km^2 (resp. 10.475 km^2). It is located between 7º58-10º12N and 1º35-3º05E, and represent 47.2% of the whole Ouémé-river (Le Barbé *et al*., 1993).

The seasons of Benin correspond to the periods of dominance of the wet tropical continental air masses. The seasonal distribution of rainfall follows the direction of the ITD and varies almost proportionally with distance from the coast. Therefore, Bétérou has a unimodal precipitation diet (May to October), whilst the southern part of Savè catchment has a transitional diet (April and October, with a short dryness in August). The averages of annual rainfall between 1960 – 2007 are 1205 mm at the Bétérou rainfall station and 1098 mm at Savè. The dynamics of the river is characterized by a high discharge during the rainy season. The average of the maximum flow between May and September over the period 1960-2007 is in order of 470 m^3/s at Bétérou and 880 m^3/s at Savè outlet. From November to May almost all the rivers dry up and the averages of low flows are about 5m^3/s at Savè, and 2m^3/s at Bétérou. The annual mean temperature range is between 24ºC and 33ºC.

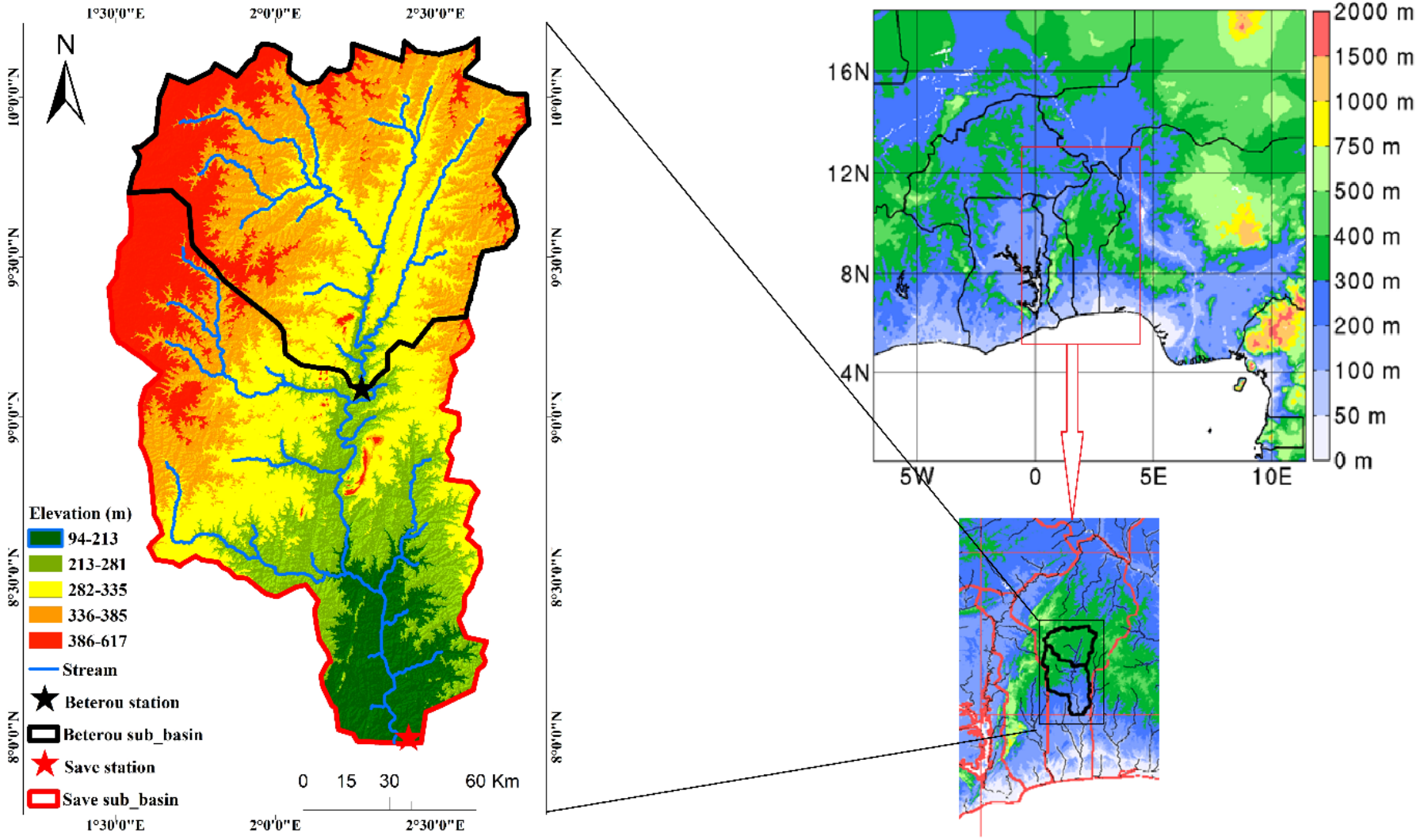

Figure 3.3: WRF and WRF/WRF-Hydro simulated domain, and studied catchments (Savè and Bétérou)

3.2 Study datasets

For the present study, rainfall and potential evapotranspiration data from Coordinated Regional Climate Downscaling Experiment (CORDEX) are used to identify the present and potential future drought and flooding areas in West Africa. This CORDEX evaluation is compared to the satellite data CRU used as observed data. The observational dataset is used in the present study to evaluate the capability of WRF in simulating climate variables.

3.2.1 Regional climate model dataset

To investigate how the rising global temperature will affect the spatial pattern of rainfall in West Africa, and also its impact on the extreme climate events, the study used the precipitation and potential evapotranspiration (PET) variables from ten Global Climate Models (GCMs) under the RCP8.5 scenario were driven by the Rossby Centre regional atmospheric model (RCA4) from CORDEX and analysed at some specific global warming levels (GWLs) above the pre-industrial level. Data from CORDEX are driven by RCA4 at daily and monthly timesteps. The simulated dataset used was collected from the coordinated regional climate downscaling experiment (CORDEX) (Nikulin *et al.*, 2012), and has a horizontal resolution of 0.44°×0.44°. The period of 1971-2000 was extracted from the simulated dataset as the historical period, while the period of 2006-2100 was used for projections. This study focuses specifically on the GWLs of 1.5℃, 2.0℃, 2.5℃, and 3.0℃ above the pre-industrial levels and under the RCP8.5 scenario. The 30-year projection according to each GWL can be found in Table 3.1.

Table 3.1: Recapitulative of the selected years for the ten GCMs drove by RCA4 model according to each global warming level (Nikulin et al., 2018)

	RCP85				
RCM	**GCM**	**1.5ºC**	**2.0ºC**	**2.5ºC**	**3.0ºC**
RCA4	**CanESM2**	1999-2028	2012-2041	2024-2053	2034-2063
	CNRM-CM5	2015-2044	2029-2058	2041-2070	2052-2081
	CSIRO-Mk3	2018-2047	2030-2059	2040-2069	2050-2079
	EC-EARTH	2005-2034	2021-2050	2034-2063	2047-2076
	GFDL-ESM2M	2020-2049	2037-2066	2052-2081	2066-2095
	HadGEM2-ES	2010-2039	2023-2052	2033-2062	2042-2071
	IPSL-CM5A-MR	2002-2031	2016-2045	2027-2056	2036-2065
	MIROC5	2019-2048	2034-2063	2047-2076	2058-2087
	MPI-ESM-LR	2004-2033	2021-2050	2034-2063	2059-2088
	NorESM1-M	2019-2048	2034-2063	2047-2076	2059-2088

3.2.2 Observational datasets

This section presents the various datasets that are used to assess the climate data trend, and also those used for calibration, evaluation, and validation of the simulation results used in the study. The rainfall, discharge, and temperature data were obtained from the national agency of meteorology of Benin. Precipitation, temperature and soil moisture were also obtained from satellite or gridded datasets.

3.2.2.1 Observed station data

The rainfall station data is collected over 34 stations over the whole Ouémé-basin, the temperature is from 4 synoptical stations (Cotonou, Bohicon, Savè, and Parakou), and the discharge data from the outlets (Bonou, Bétérou, Ahlan, Atchérigbé, Savè) of the basin. The dataset are collected from Benin's National Agency of Meteorology (NAMet) and the General Directorate of Water (GD-Water) on the period 2000-2015. A particular focus is on the year 2010, known as the year when Ouémé-river experienced a devastating flooding. Hounkpè *et al.*, (2015) showed that the maximum values of discharge recorded during period 1989-2009 is less than 1400 m^3/s at Savè, and 650 m^3/s at Bétérou; and Avahounlin *et al.*, (2013) who showed that the peaks of discharge at Savè (resp. Bétérou) are 914.31 (resp. 472.89), 1066.75 (resp. 561.8), and 1196.93 (resp. 640.35) m^3/s respectively for 5-, 10-, and 20-year return period.

3.2.2.2 Gridded observed dataset

The evaluation of the model WRF-Hydro namely is performed with two dataset, the satellite estimates of Tropical Rainfall Measuring Mission (TRMM, 3B42 v7 derived daily at 0.25° horizontal resolution, 1998-2015; Huffman *et al.*, 2007), and the Climate Hazards Group Infrared Precipitation with Stations (CHIRPS; chirps- v2.0 at 0.05°

horizontal resolution; 1981-near present; Funk *et al.*, 2015). The TRMM (prepared and distributed by the NASA GES DISC) is used to evaluate both temporally and spatially the model over the WRF-Hydro domain. This 3-hourly (beginning at 00Z and ending 21Z; unit: mm) dataset which spatially covered the latitude 50°S-50°N and all longitude, is interpolated to hourly data over the selected WRF-Hydro domain. The CHIRPS, one of the recent global dataset, also spatially cover the latitude 50°S-50°N and longitude 180ºE-180ºW. It is also a satellite product based on in-situ station data with three timesteps (daily, pentad and monthly), the daily is the one used by this study. It is designed as a suitable alternative for data sparse regions that depend on convective rainfall Kerandi, (2017). The gridded climate research unit (CRU v3.23, monthly at 0.5° horizontal resolution, 1901-2014; Harris *et al.*, 2014) provided by the University of East Anglia and prepared based on the archive of monthly mean precipitation and temperature provided by more than 4000 weather stations distributed all over the world.

3.2.2.3 Gridded soil moisture data

Soil moisture content dataset from the Climate Change Initiative of the European Space Agency (ESA-CCI-SM; available at https://www.esa-soilmoisture-cci.org/) has become a well-established dataset within the scientific climate community, with a long temporal coverage (1978-2016). It merges the soil moisture data from multiple active and passive microwave sensors are used for the surface soil water content validation. It has a 0.25° spatial resolution and a daily temporal resolution. The long temporal coverage is an essential prerequisite for robust trend assessments and the investigation of soil moisture drivers of hydrological process.

3.3 Methods

Prior climate indices are applied to identify some particular areas impacted by climate change and variability. The second aspect of the work is to investigate based on experimental work with an atmosphere-hydrology modelling system over specific basins.

3.3.1 Climate indices

This section presents some climate index methods used in the present work such as : the Standardized precipitation evapotranspiration index (SPEI), the precipitation concentration index (PCI); the precipitation concentration degree (PCD), precipitation concentration period (PCP), the consecutive dry day (CDD), the consecutive wet day (CWD), and frequency of intense rainfall events.

3.3.1.1 Standardized precipitation evapotranspiration index (SPEI)

SPEI is an index computed based on the non-exceedance probability of the climate water balance which is the differences between precipitation (PRE) and potential evapotranspiration (PET) described by the Equation (3.1), adjusted using a three-parameter log-logistic distribution which accounts for common negative values (Vicente-Serrano et al., 2010). The SPEI uses a three-parameter distribution to capture the deficit values since it is most likely that in arid and semi-arid areas the moisture deficit can be negative. For two-parameter distributions as used in case of Standardized precipitation index (SPI), the variable x has a lower boundary of zero ($0 > x < \infty$) meaning that x can only take positive values while for the three-parameter distributions used in SPEI, x can take values in the range ($\gamma > x < \infty$) implying that x can also take negative values; γ is the parameter of origin of the distribution (Vicente-Serrano et al.,

2010). The SPEI is obtained by normalizing the water balance into the Log-logistic probability distribution. The difference (Di) between PRE and PET for the month (i).

$$D_i = PRE_i - PET_i \tag{3.1}$$

The calculated D values are aggregated at different time scales as follows:

$$D_n^k = \sum_{i=0}^{k-1} PRE_{n-1} - PET_{n-1} \tag{3.2}$$

With k the timescale (months) of the aggregation and n is the particular month for which the climate water balance is computed.

The probability density function of a Log-logistic distribution is given as:

$$f(x) = \frac{\beta}{\alpha}\left(\frac{x-\gamma}{\alpha}\right)^{\beta-1}\left(1+\left(\frac{x-\gamma}{\alpha}\right)^{\beta}\right)^{-2} \tag{3.3}$$

Where α, β and γ are respectively scale, shape and origin parameters for $\gamma > D < \infty$. The probability distribution function for the D series is then given as:

$$f(x) = \left[1+\left(\frac{\alpha}{x}-\gamma\right)^{\beta}\right]^{-1} \tag{3.4}$$

With f(x) the SPEI can be obtained as the standardized values of F(x) according to the method of Abramowitz and Stegun, (1965):

$$\text{Where SPEI} = W - \frac{C_0+C_1W+C_2W^2}{1+d_1W+d_2W^2+d_3W^3} \tag{3.5}$$

$$\text{and } W = \sqrt{-2\ln(P)} \text{ for } P \leq 0.5 \tag{3.6}$$

P is the probability of exceeding a determined D_i value and is given as $P = 1 - f(x)$ whilst the constants are:

$C_0 = 2.515517$, $C_1 = 0.802853$, $C_2 = 0.010328$, $d_1 = 1.432788$, $d_2 = 0.189269$,

$d_3 = 0.001308$

The computation of the SPEI is done over each grid point for each dataset. The SPEIs have been spelt for 1-month, 3-month, 6-month and 12-month.

3.3.1.2 Empirical Orthogonal Function (EOF)

EOF technique aims at finding a new set of variables that captures most of the observed variance from data through a linear combination of the original variables. This method splits the temporal variance of data into orthogonal patterns called empirical eigenvectors. This approach has been widely used to identify the patterns of drought at global (Dai, 2011) or European scales (Brázdil et al., 2009; Ionita et al., 2012). The EOFs were calculated on standardized anomalies of seasonal SPEI series.

3.3.1.3 Calculation of precipitation concentration index (PCI)

The PCI, which was developed by Oliver (1980), modified by De Luis *et al.* (2011) and also used by Shi *et al.* (2015), was used as an indicator of rainfall concentration for annual and seasonal scales (wet and dry seasons). In this study, the PCI was tested to identify future trends in respect of the spatial distribution of rainfall. According to Oliver (1980), PCI values of less than 10 represent a uniform precipitation distribution (i.e., a low precipitation concentration), values between 11 and 15 denote a moderate precipitation concentration, values from 16 to 20 denote an irregular distribution, and values above 20 represent a strong irregularity of precipitation distribution (i.e., a high precipitation concentration). The following equations were used on each grid point to calculate the PCIs:

$$PCI_{annual} = \frac{\sum_{i=1}^{12} P_i^2}{\left(\sum_{i=1}^{12} P_i\right)^2} \times 100 \quad (3.7)$$

$$PCI_{wet} = \frac{\sum_{i=1}^{nw} P_i^2}{\left(\sum_{i=1}^{nw} P_i\right)^2} \times \frac{100*nw}{12} \quad (3.8)$$

$$PCI_{dry} = \frac{\sum_{i=1}^{nd} P_i^2}{\left(\sum_{i=1}^{nd} P_i\right)^2} \times \frac{100*nd}{12} \quad (3.9)$$

Equation (3.7) was used for annual PCI, while Equations (3.8) and (3.9) were utilised for seasonal scales (respectively rainy and dry seasons); nw and nd represent, respectively, the number of rainy and dry season months, and P = precipitation of the i^{th} month. In order to investigate changes in the PCI, a 30-year period was considered both for historical and future periods. Table 3.1 shows the projection periods used for each GWL; the historical 30-year period is 1971-2000.

3.3.1.4 Computation of precipitation concentration degree (PCD) and precipitation concentration period (PCP)

The PCD and PCP were proposed by Zhang and Qian (2003) to measure the distribution of rainfall and the peak of its concentration date. The basic principle is based on the vector of daily or monthly total precipitation. The assumption can be made that at a time scale (daily, 5-day, weekly, decade or monthly) total precipitation is a vector quantity with both magnitude and direction and can be illustrated as a circle (360°). According to Li *et al.* (2011) and Zhang and Qian (2003), the indices were calculated as follows:

$$\theta_j = \left(360° * \frac{j}{n}\right) \quad (3.10)$$

$$R_i = \sum r_{ij}$$

$$R_{xi} = \sum_{j=1}^{N} r_{ij} * \sin\theta_j \quad (3.11)$$

$$R_{yi} = \sum_{j=1}^{N} r_{ij} * \cos\theta_j \quad (3.12)$$

$$PCD_i = \frac{\sqrt{R_{xi}{}^2 + R_{yi}{}^2}}{R_i} \quad (3.13)$$

Where i is the year (e.g., for the historical period i = 1971, 1972, …, 2000), j represents the time scale (**daily**, 5-day, weekly, decade or **monthly**) of that year, R_i is the amount of rainfall of a year, r_{ij} is the precipitation of the j^{th}time scale in the i^{th} year, n is the number of time scales per year (e.g., daily: for a non-leap year, n = 365, while in a leap year, n = 366)

$$\alpha_i = \tan^{-1}\left(\frac{R_{xi}}{R_{yi}}\right) \quad (3.14)$$

$$D_i = \begin{cases} \alpha_i & (R_{yi} > 0, R_{xi} \geq 0) \\ \alpha_i + 360º & (R_{yi} > 0, R_{xi} < 0) \\ \alpha_i + 180º & (R_{xi} < 0) \end{cases} \quad (3.15)$$

$$PCP_i = D_i * \left(\frac{n}{360°}\right)$$

(3.16)

3.3.2 Experimental assessment with the coupled model WRF/WRF-Hydro

3.3.2.1 Model configurations and parametrization

The configuration of a model depends on the geographical location and the purpose of the study. This involves to design the correct model domains at the WRF preprocessing stage (e.g., identifying the resolution both horizontal and vertical, the parameterizations, etc.) Kerandi (2017). The model domain details for the WRF over West Africa, which are also common in the case of the fully coupled WRF/WRF-Hydro are explained. The specific details of the calibration of the WRF-Hydro in offline mode is also discussed.

3.3.2.1.1 Weather Research and Forecasting (WRF) and WRF/WRF-Hydro model setups over West-Africa

The Weather Research and Forecasting (WRF) version 3.7.1 (Arnault *et al*., 2016) is utilized both for WRF-only and fully-coupled WRF/WRF-Hydro modeling over the research area. In the following, the fully coupled WRF/WRF-Hydro is referred as WRF-H. It is a non-hydrostatic, mesoscale Numerical Weather Prediction (NWP) and atmospheric simulation system. Table 3.2 shows the different physics schemes and experimental details. The setup uses one domain at 5-km spatial resolution covering the area 7ºW-12ºE, 0º-18ºN and 400x400 grid points, with 30s as numerical simulation time step. The vertical structure of the domain consists of 50 levels, from the surface up to a 10 hPa pressure top. The option of land use categories "Moderate Resolution Imaging Spectroradiometer (MODIS, 20 classes; Friedl *et al.*, 2002)" is selected. The Noah LSM model (Chen and Dudhia, 2001) is used as the column land surface physics model.

For purposes of hydrometeorological simulations with WRF-H, the WRF domain is additionally coupled with routing processes at 500 m resolution with 4000 × 4000 grid points in east-west and north-south directions. The fully coupled mode simulations are performed for 3 years, from January 2008 to December 2010, with January-February 2008 as spin-up period. The driving data is the operational analysis dataset from European Centre for Medium-Range Weather Forecasts (ECMWF) which provides the initial and lateral boundary conditions. Both WRF-H and WRF-only components of the coupled modeling system share the same physics parameterizations (Table 3.2).

Table 3.2: Experimental details of the atmosphere model, WRF-only and WRF-H

Subject	Option	Reference
Driving data	Operational analysis	ECMWF
Horizontal resolution	5 km	
Horizontal grid	400×400	
Integration time step	30 s	
Projection resolution	Mercator	
Vertical discretization	50 layers	
Output interval	24h for WRF, 30 days for WRF/WRF-Hydro	
Simulation period	1st January 2008 – 31st December 2010	
Pression top	10 hPa	
Microphysics scheme	Single Moment 5, WSM5	Dudhia, and Chen, 2004
Longwave radiation	Rapid Radiative Transfer Model (RRTM)	Mlawer *et al.*, 1997
Shortwave radiation	Dudhia	Dudhia, 1989
Planetary boundary lager	Asymmetric Convection Model (ACM2)	Pleim, 2007
Land use	MODIS	Friedl *et al.*, 2002
Land surface scheme	Noah LSM	Chen and Dudhia, 2001

3.3.2.1.2 Calibration of Weather Research and Forecasting-Hydro in offline mode

The calibration constitutes in hydrology, one of the first stage through a model should be evaluated over the specific region of study before be applied for any validation or to be used for hydrological investigations. Thus, this section focuses on the forcing data, the procedure of the optimization of the selected parameters in uncoupled (offline mode) WRF-Hydro.

Specification of meteorological forcing data

Modern land surface hydrology models (e.g: WRF-Hydro), require meteorological forcing data to simulate land-atmosphere exchanges and terrestrial hydrologic processes when uncoupled to atmospheric modeling systems (Gochis *et al.*, 2018). The available optional forcing data are : High- Resolution Land Data Assimilation System (HRLDAS) hourly, hourly with specified precipitation and minute format input files, WRF model output and WRF model output with specified precipitation, the idealized and idealized with specified precipitation (Gochis *et al.*, 2018 for more details).

Since the investigation is on the potential of WRF-Hydro (model coupled with WRF) for flood forecasting, the available WRF precipitation at the highest spatio-temporal resolution is used to force the uncoupled WRF-Hydro model. Therefore, the hourly output of WRF at 5-km spatial resolution are used as meteorological forcing data which contain necessary variables such as incoming shortwave radiation (W/m^2), incoming longwave radiation (W/m^2) Specific humidity (kg/kg), air temperature (K), surface pressure (Pa), u and v components of near surface wind (m/s), and liquid water precipitation rate (mm/s). The meteorological forcing data needed by the Noah LSM (land surface hydrological modeling system) are prepared as hourly gridded data. The

Noah LSM static data (topography, land cover, soil type) are too coarse for a WRF-Hydro application. Additional datasets from the Shuttle Elevation Derivatives at Multiple Scales (HydroSHEDS) data base (Lehner *et al.*, 2008 , e.g. high-resolution topography and channel network) are considered to accurately route water across the landscape through overland, subsurface or channel flow.

Parameters selected for the calibration

The uncoupled WRF-Hydro model consists of a variety of parameters (e.g. Kerandi *et al.*, 2018), which usually require calibration. Since the aim of the research is to evaluate the performance of WRF-Hydro to simulate discharge, and therefore analyze its predicting skills about floods, the calibration is performed based on discharge at the Savè catchment outlet. The WRF model is run over the domain displayed in Figure 3.2.a in order to generate atmospheric input data for the uncoupled WRF-Hydro calibration. To reduce the computation cost for the calibration in offline mode, the simulation domain (Figure 3.2.a) is reduced to the subdomain shown in Figure 3.2.b. This inner-domain (0.5ºW - 4.5ºE, and 0º-13ºN, 100x150 grid points) contains the research area (Ouémé-river basin), where floods are frequently recorded.

For calibrating the model WRF-Hydro 3.0, we focus on selected sensitive parameters highlighted in previous works (Kerandi *et al.*, 2017; I. Yucel *et al.*, 2015), such as REFKDT, SLOPE, RETDEPRTFAC, OVROUGHRTFAC, and MannN. Applying a stepwise approach, following previous WRF-Hydro studies (Arnault *et al.*, 2016; Givati *et al.*, 2016; Senatore *et al.*, 2015; Yucel *et al.*, 2015), we first focus on the parameters controlling the total water volume, namely infiltration factor (REFKDT) and surface retention depth (RETDEPRT). It is noted that REFKDT is a tunable parameter that significantly impacts surface infiltration and hence the partitioning of total runoff into

surface and subsurface runoff; increasing REFKDT decreases surface runoff. Since there is not a historical range to estimate these parameters over the interested domain, the study tasks to calculate them from 0.1 to 10 with 0.1 increments. The second step of the calibration is to evaluate the coefficient governing deep drainage (SLOPE); the same method used in case of REFKDT and RETDEPRTFAC for selecting the optimum value is applied, by testing values from 0.1 to 1.0 with 0.1 as increment. The adjustment of the roughness parameter, which controls the overland flow is performed from the default value to the optimum one.

Sensitivity tests are additionally done on the surface and channel roughness parameter (MannN), which controls the shape of the hydrograph. The three efficiency criteria Nash-Sutcliffe Efficiency (NSE), Kling–Gupta efficiency (KGE), and Correlation coefficient (Corr) are used to evaluate the model performance within the calibration process.

$$Corr = \frac{n(\sum xy)-(\sum x)(\sum y)}{\sqrt{[n\sum x^2-(\sum x)^2][n\sum y^2-(\sum y)^2]}} \quad (3.17)$$

Where x is the observations and the y the simulations.

The Nash-Sutcliffe efficiency (NSE) is a normalized statistic that determine the relative magnitude of the residual variance (called "noise") compared to the measured data variance (observed) (Nash and Sutcliffe, 1970). The NSE indicates how well the plot of observed versus simulated data fits the line y=x. The computation formula for NSE is showed by the equation (3.18):

$$NSE = 1 - \left[\frac{\sum_{i=1}^{n}({Y_i}^{obs}-{Y_i}^{sim})^2}{\sum_{i=1}^{n}({Y_i}^{obs}-{Y_i}^{mean})^2}\right] \quad (3.18)$$

Where Y_i^{obs} is the ith observation for the constituent being evaluated, Y_i^{sim} is the ith simulated value for the constituent being evaluated, Y_i^{mean} is the mean of observed data for the constituent being evaluated, and n is the total number of observations (Moriasi *et al.*, 2007). Values between 0.0 and 1.0 are generally viewed as acceptable levels of performance. The NSE = 1 indicates perfect correspondence between simulations and observations; NSE = 0 indicates that the model simulations have the same explanatory power as the mean of the observations, whereas values ≤ 0.0 indicate that the mean of observed time series is a better predictor that the simulated time series and this is an unacceptable performance.

The Kling-Gupta Efficiency (KGE) addresses several shortcomings in NSE and is increasingly used for model calibration and evaluation. Its computation formula is shown by the equation (3.19):

$$KGE = 1 - \sqrt{(r-1)^2 + \left(\frac{\sigma_{sim}}{\sigma_{obs}} - 1\right)^2 + \left(\frac{\mu_{sim}}{\mu_{obs}} - 1\right)^2} \quad (3.19)$$

Where r is the linear correlation between observations and simulations, σ_{obs} is the standard deviation in observations, σ_{sim} the standard deviation in simulations, μ_{sim} the simulation mean, and $\mu_{obs}$the observation mean. Like NSE, KGE = 1 indicates perfect agreement between simulations and observations.

In order to harmonize the uncoupled and coupled setups, the uncoupled simulations use the same time step as the WRF-only and WRF-H simulations (30s). The calibration of the model is performed using hourly dataset input, and the focus is on the performance skill in reproducing daily discharge in the sub-catchments. One year calibration is considered as sufficient to evaluate the basic parameter sensitivities (e.g. Senatore *et al.*, 2015). WRF-Hydro is therefore calibrated on P_1 (2008) and validated on P_2 (2009-

2010), where P_1 and P_2 are the shared periods containing into the whole study period named P (2008-2010).

3.3.3 Evaluation of model uncertainty with the stochastic kinetic energy backscatter scheme

The Stochastic Kinetic Energy Backscatter scheme (SKEBS; Berner *et al.*, 2015; Berner *et al.*, 2009; Shutts, 2005), which primarily acts on the dynamical tendencies at the lateral boundaries, is activated into WRF-H for the fully-coupled simulation (WRF-H-SKEBS). The SKEBS technique provides several advantages over perturbation techniques that only perturb the initial state. The method aims to represent model uncertainties associated with scale interactions that take place in the real atmosphere but are absent in a truncated numerical model (Leutbecher *et al*., 2017). SKEBS perturbs the model fields by adding random, amplitude perturbations (noise) to the horizontal wind and potential temperature tendency equations at the lateral boundaries for each time step (Judt and Chen, 2016). An ensemble of 10 members using the WRF-H-SKEBS model is generated for each rain season of the period P (2008-2010).

CHAPTER 4

RESULTS AND DISCUSSION

In this chapter, the research findings relative to the exposure of West Africa to the extreme climate events are presented. In the first part, some potential drought and flooding areas in West Africa for the present day and future projection are identified, and the second part evaluates the skill of the regional climate model WRF-Hydro to be used as a flood forecasting model.

4.1 Projection of Dry and wet areas in West Africa under global warming

4.1.1 Selection of simulation models

Figures 4.1 and 4.2 show the ability of RCA4's models to reproduce the historical precipitation and Potential-Evapotranspiration (PET) in respect to the observed CRU. The efficient criterium on which the examination is based is the Kling-Gupta efficiency (KGE), this KGE value reached up to 0.85 for precipitation (PRE), and 0.9 for the potential evapotranspiration (PET). Figure 4.1 illustrates that the precipitation variable of the ten GCMs driven by RCA4 misjudged the Southern and Northern parts of Africa compared to CRU, but they all agree at a good correlation between latitude 20ºS and 20ºN. In contrary as observed in Figure 4.1, Figure 4.2 shows that the models reproduced well the PET of CRU dataset in the Southern and Northern part of Africa.

According to the potential GWLs classification computed by Déqué *et al.*, (2017), all the ten selected models have not shown the GWLs 2.0℃, 2.5℃, and 3.0℃ in scenario RCP 4.5's case, but did it for scenario RCP 8.5. Therefore, for consistency and plausible analysis, the scenario RCP8.5 is retained for this part of the study. Thus, Table 4.1 which represents the classification of the projection periods of global warming levels in respect

to the pre-industrial period, and results from Figures 4.1 and 4.2 led to select all the ten GCMs driven by RCA4 for the scenario RCP8.5. Additionally, it is noticed that the models reproduced well both precipitation and potential evapotranspiration (PET) over the study area (0-20ºN and 20ºE-20ºW). Precipitation and PET variables are then used to perform the assessment of historical and projected dry and wet areas thru SPEI.

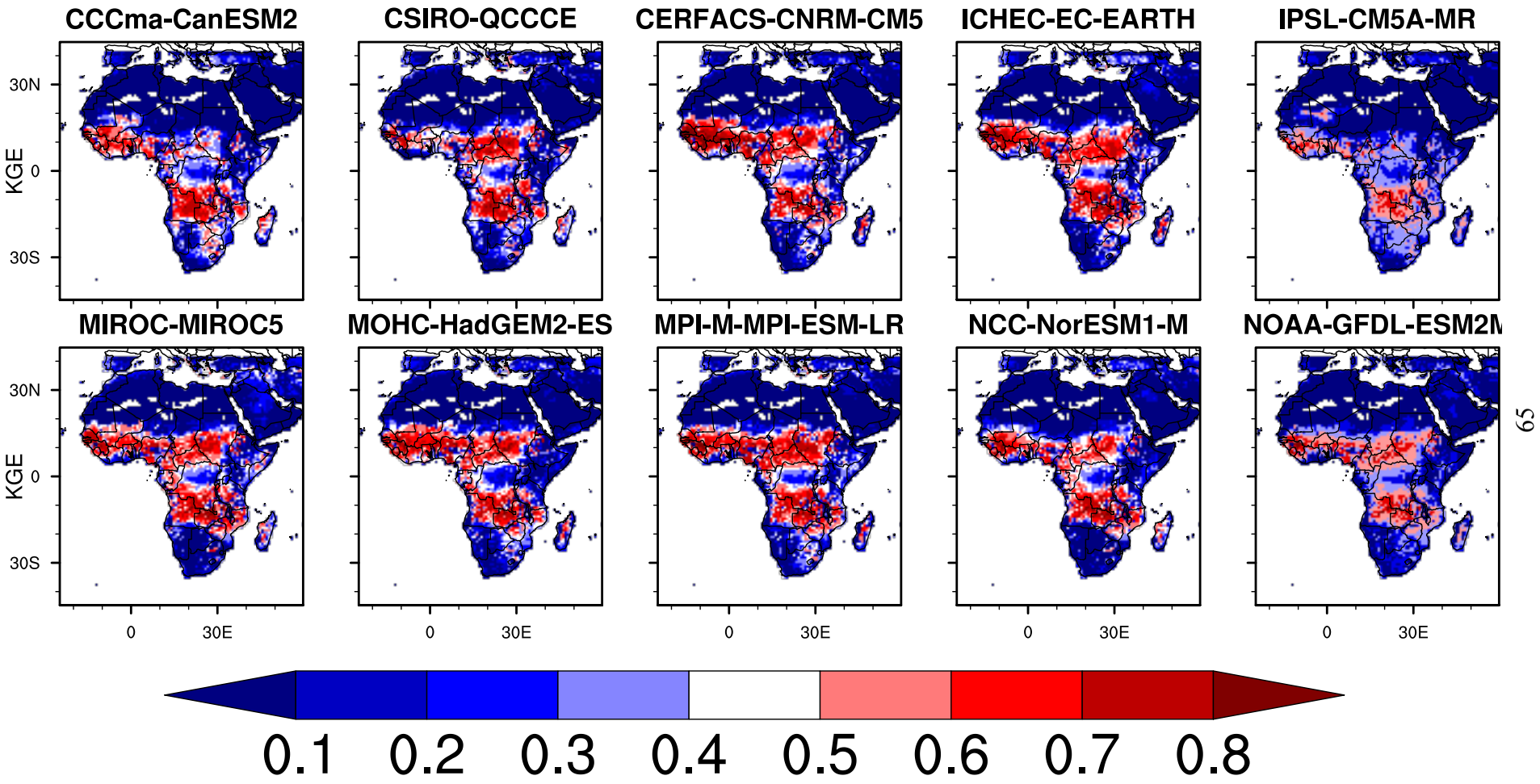

Figure 4.1: Correlation of precipitation between CRU and CORDEX-RCA4 model over Africa with the Kling-Gupta efficiency as statistic criterium.

Table 4.1: Recapitulative of the selected years of RCA4 models from CORDEX according to the Global warming levels

	RCP8.5				
RCM	**GCM**	**1.5**℃	**2.0**℃	**2.5**℃	**3.0**℃
RCA4	**CanESM2**	1999-2028	2012-2041	2024-2053	2034-2063
	CNRM-CM5	2015-2044	2029-2058	2041-2070	2052-2081
	CSIRO-Mk3	2018-2047	2030-2059	2040-2069	2050-2079
	EC-EARTH-r12	2005-2034	2021-2050	2034-2063	2047-2076
	GFDL-ESM2M	2020-2049	2037-2066	2052-2081	2066-2095
	HadGEM2-ES	2010-2039	2023-2052	2033-2062	2042-2071
	IPSL-CM5A-MR	2002-2031	2016-2045	2027-2056	2036-2065
	MIROC5	2019-2048	2034-2063	2047-2076	2058-2087
	MPI-ESM-LR	2004-2033	2021-2050	2034-2063	2059-2088
	NorESM1-M	2019-2048	2034-2063	2047-2076	2059-2088

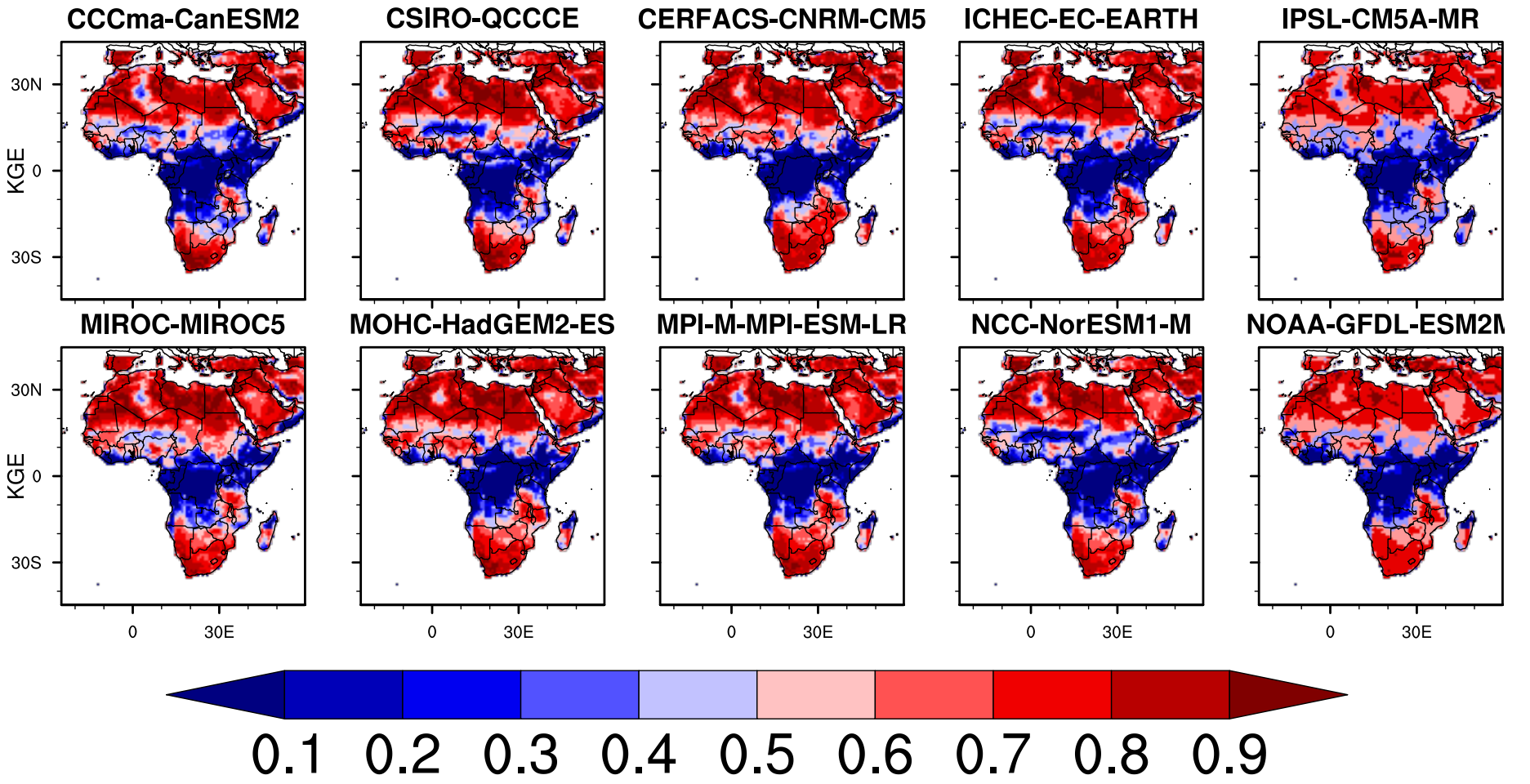

Figure 4.2: Correlation of Potential Evapotranspiration (PET) between CRU and CORDEX-RCA4 model over Africa with the Kling-Gupta efficiency as statistic criterium.

4.1.2 Climate models evaluation under historical period

4.1.2.1 Evaluation of the climate variables

The ensemble-mean of models (RCMEAN) simulate suitably over the West Africa, the moisture variables such as precipitation (PRE), the potential evapotranspiration (PET), and the climate water balance (CWB = PRE-PET) with a very good and significant (99% of confidence level) correlation ($r \geq 0.88$) in respect to the observed CRU. The precipitation is well reproduced in regard to the observed CRU. It was able to capture the spatial gradient of precipitation over the study area, with maxima well located (maximum around the Gulf of Guinea and minimum in the Sahel) with some scattering location of the maximum of rainfall in southern of Nigeria, Guinea-Conakry and Liberia; and the South-western part of Cameroon. In terms of amount, the ensemble globally fairly overestimate the precipitation except the South-eastern part of the study domain. This evaluation of the ensemble-mean confirm the results from Figure 4.1 where the East part of the coordinate 0-20ºN and 20ºE-20ºW is fairly reproduced. The PET is also well captured with low bias range between ± 50 mm month^{-1}, it also highlights the results of Figure 4.2 in regard to the performance of the KGE which evaluated the reproductivity skill of each model of the ensemble RCMEAN. The ensemble here is significantly correlated ($r = 0.95$). The Gulf of Guinea and Savanna are the ones well reproduced when over the Sahel the RCMEAN underestimate the observed. From the assessment of the climate water balance (CWB) (Figure 4.3 g-i), it can be seen a very important water deficit (negative bias) in the Savanna and Sahel, which is due to the underestimation of precipitation, whilst in the Gulf of Guinea, there is a surplus of water with particularly highest values recorded around countries as Liberia, Sierra-Leone, and southern Nigeria, when both the observed and the RCMEAN are considered. The deficit presented by CRU is the highest in the Sahel, bringing out a

drier condition over this area. The bias of the CWB presents globally the Gulf of Guinea and the Savanna as the deficit water areas except for Liberia, Sierra-Leone, and Togo, and Sahel/Sahara as surplus water area.

The inconsistency of the climate water balance assessment between the simulated models and observed can be assigned to various factors. For instance, the wet (positive values) bias over Western part of the study area indicate that the convective parameterization schemes at 0.44º horizontal resolution in RCA4 model may be too active in producing precipitation over this area (Abiodun *et al.*, 2018) , while the dry (negative values) bias over the Eastern part of the study area suggest that the convective parameterization schemes are not fully resolved over the Eastern area, producing less moisture available for inland rainfall. It can also be due to the density of the weather stations available over the area (both Eastern and Western) for the observed data estimation. The method of the calculation of PET also may be a factor. Abiodun *et al.* (2018) evaluated the uncertainty of PET estimation with Hargreaves method and Penman method and found that its uncertainty contributes also to the discrepancy of the climate water balance.

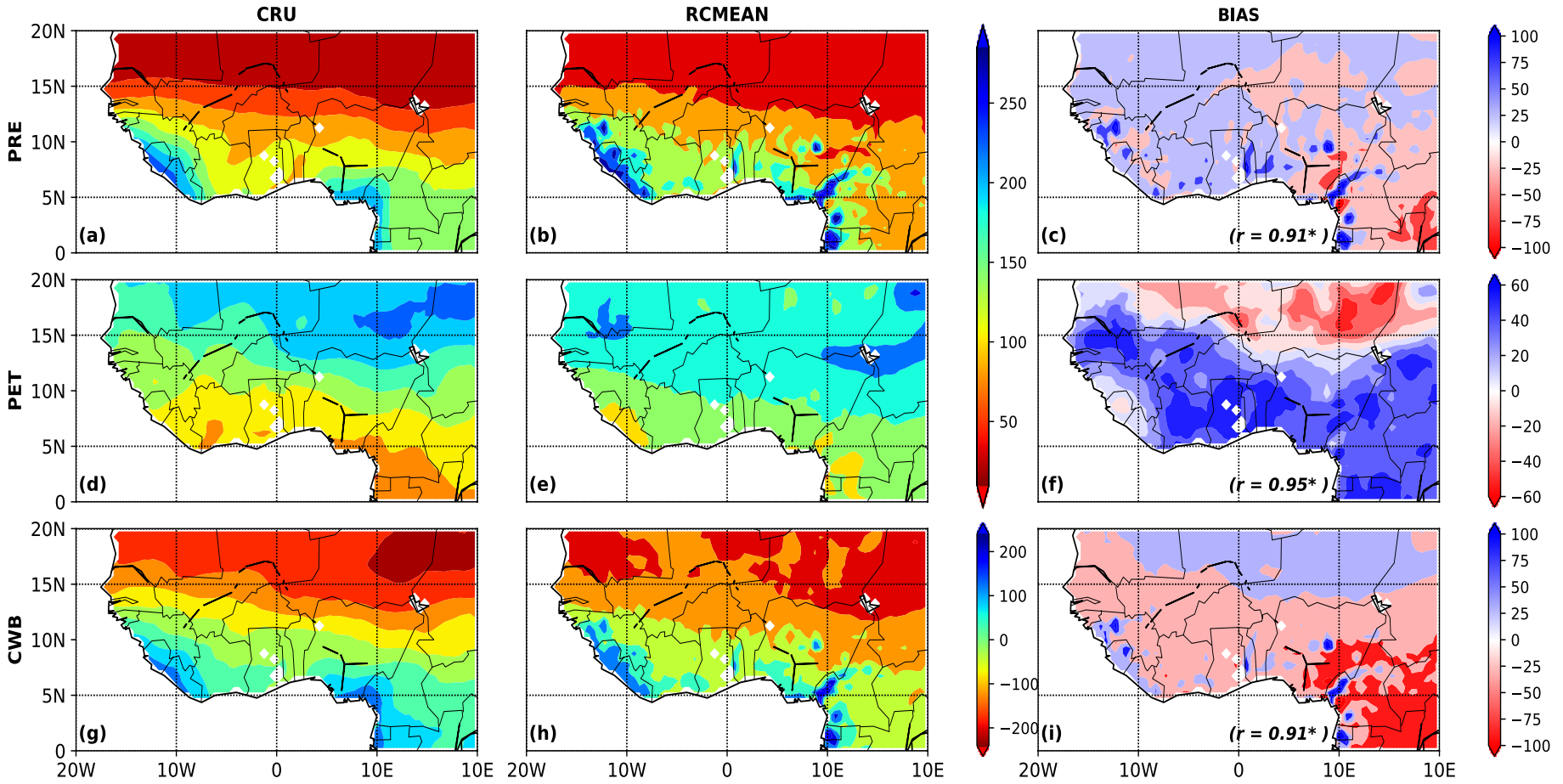

Figure 4.3 : Spatial distribution of climate variables for CORDEX RCA4 models ensemble (RCMEAN) and CRU over West Africa. The climate variables are: precipitation (PRE, mm month^{-1}), the potential evapotranspiration (PET, mm month^{-1}), and the climate water balance (CWB = PRE-PET, mm month^{-1}). r is the correlation between the observed CRU and RCMEAN, and the bias is the difference between them (bias: RCMEAN-CRU). the asterisk (*) explain the correlation which is statistically significant at 99% of confidence level.

An investigation on the dynamic of rainfall (gradient form Gulf-of-Guinea to the Sahel) is provided with the Figure 4.4. It shows that the RCMEAN have a good agreement to simulate the annual cycle of each sub-zone (the Gulf of Guinea, Savanna, and the Sahel) with respect to the observed CRU. The annual cycle of precipitation lies within the model ensemble spread in all the sub-zones, and the average of the ensemble closely follows the observed curve. At the Gulf of Guinea, both RCMEAN (model ensemble mean) and observed show the bimodal rainy seasons, whilst the Savanna and the Sahel have illustrated a monomodal regime with a dry season (winter dry) and a single rainy season (summer wet). These observations reflect the seasonal fluctuations (oscillation) of the Inter Tropical Discontinuity (ITD) over West Africa. The average of the precipitation value over the Gulf of Guinea and Savanna is increasing from the second part of May to up to a peak (180 mm month^{-1} for the Gulf of Guinea and 230 mm month^{-1} for the Savanna) in August when the ITCZ reached its northernmost position (second quasi-stable position) about 10ºN. The average value of precipitation in the Sahel recorded also its peak in August and increasing later in July than the other areas. The driest period is about October to March at the Gulf of Guinea, and October to May for the Savanna, where during those periods the PET increase and reach its maximum value. It can also be noticed that during the rainy season the PET value dropped to its minimum value. The observed does not lie within the model but follows the model's curve and underestimate the simulations over the Gulf of Guinea and Savanna. The Sahel is dry for the whole year because of negative value CWB for the period studied. The PET value falls within the models and follows the curve of simulations.

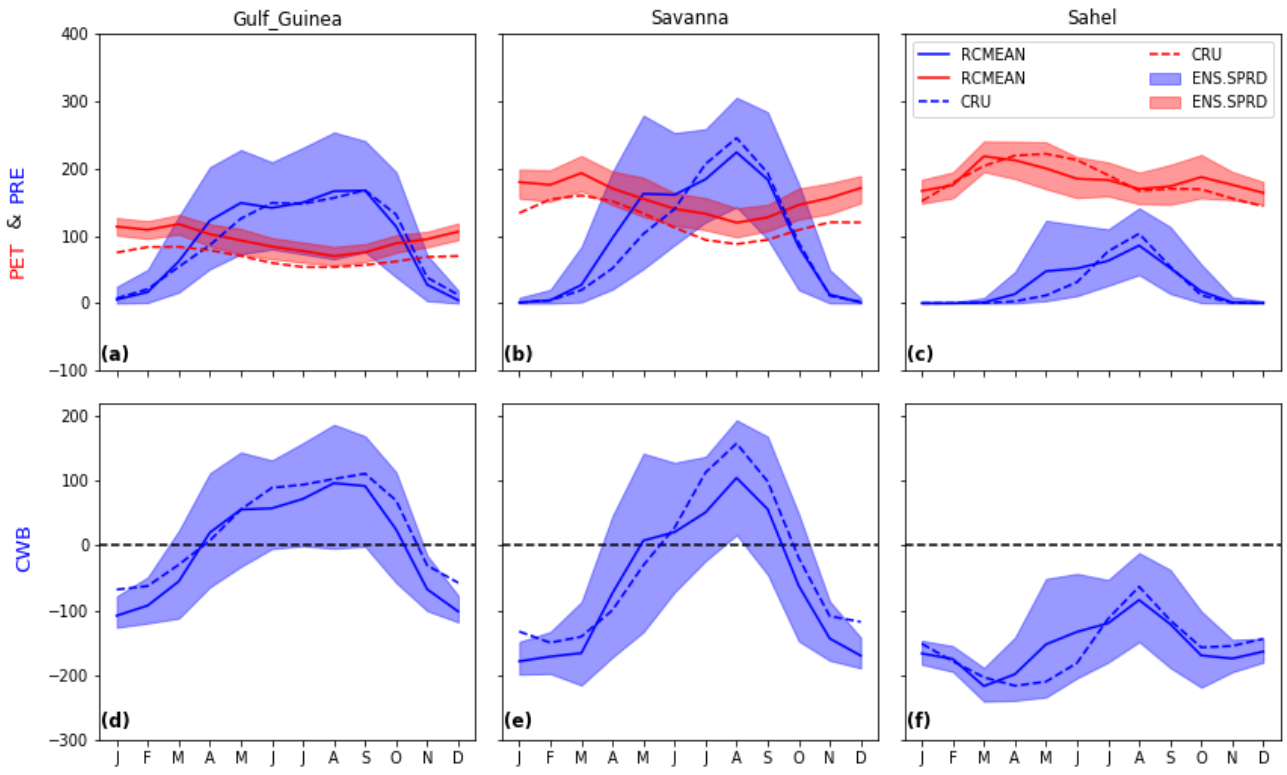

Figure 4.4: The annual cycle of the climate variables (precipitation (PRE : mm month^{-1}), potential evapotranspiration (PET : mm month^{-1}), and the climate water balance (CWB = PRE-PET, mm month^{-1})) over the three main zones of the study area (Gulf-of-Guinea, Savanna and Sahel). RCMEAN represents the ensemble mean (solid line) of simulated model, ENS.SPRD is the spread of CORDEX-RCA4 simulations. The dashed line presents the CRU variable.

4.1.2.2 Spatial variability of the Standardized Precipitation Evapotranspiration Index (SPEI)

According to the positive correlation of the models in respect to observed (Figure 4.3 and Figure 4.4), the evaluation of the spatial pattern to detect potential drought and flooding areas is performed using the SPEI for various scales in aim to focus on different types of drought. The SPEI1 is used to characterize the meteorological drought, whilst the couple (SPEI3, SPEI6) and (SPEI9, SPEI12) are used to assess agricultural and hydrological droughts respectively. Figure 4.5 shows that the models' ensemble-mean reproduce oppositely (with significant negative correlation) fairly well the patterns. This opposite performance may be due to various factors. It can be derived from the temporal gridded average for each model, and the ensemble mean. However, it has to be kept in mind that on a grid, the SPEI has either negative or positive values and its averaging could be responsible to the misjudgment for both model ensemble-mean and observed mean. It can also be mentioned based on Figure 4.5 that more the SPEI scale increase, the more the model improve its reproducibility with the observed pattern. It can also be due to a potential large discrepancy among the simulated patterns.

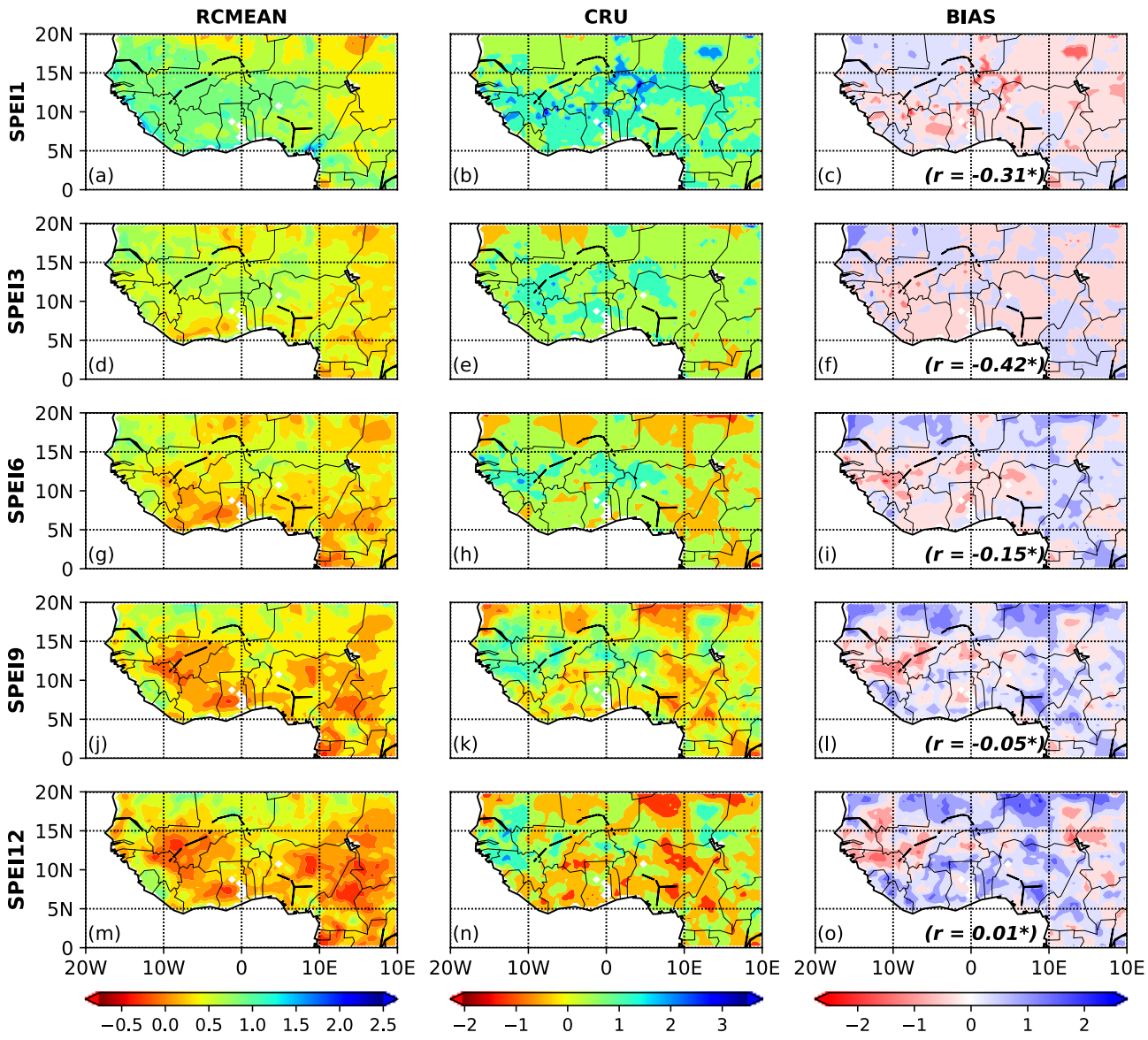

Figure 4.5: Standardized Precipitation Evapotranspiration Index (SPEI) over West Africa for historical period for various drought types (SPEI1: meteorological drought, SPEI3 and SPEI6 : agricultural drought, SPEI9 and SPEI12: hydrological drought). RCMEAN is the ensemble-mean of CORDEX-RCA4 models, CRU is the observed dataset, and BIAS = RCMEAN-CRU is the difference between the model ensemble mean and the observed

4.1.2.3 Assessment of the extreme dry events

To figure out this misrepresentation, the computation of the magnitude of drought frequency is undertaken. Figure 4.6 shows the frequency of extreme drought (SPEI < -2) in West Africa for the historical period both for the observed (CRU) and the model ensemble-mean (RCMEAN). The performance of the model in simulating drought intensity and frequency over the study area depends on the scale of which the SPEI is computed. The model significantly reproduces well the extreme drought for each type of drought with positive correlation. The agreement of the model decrease when the scale of the SPEI increase, which means that the RCMEAN captures well the meteorological and agricultural extreme droughts than the hydrological extreme drought. However, the ensemble-mean at the scale of meteorological and agricultural droughts overestimate the frequency of extreme drought events up to 2 events per decade at the north-western part and the Gulf of Guinea. The model illustrates that countries such as Senegal and Chad underestimate the meteorological extreme drought up to 2 events per decade with respect to the observed. The underestimation of the frequency of extreme drought lies to the Gulf of Guinea both for agricultural and hydrological drought events. Nevertheless, the models do capture well the magnitude of hydrological extreme drought over Nigeria, Benin, South of Ghana, Northern part of Niger. According to the model, the increasing of the frequency in extreme drought affect agriculture over the Gulf of Guinea, the Sahel and the Eastern part of the study area including Chad and the north of Nigeria. Conversely, the model shows decreasing frequency of agricultural extreme drought in Niger, Ghana, Cote d'Ivoire Guinea, and Cameroon.

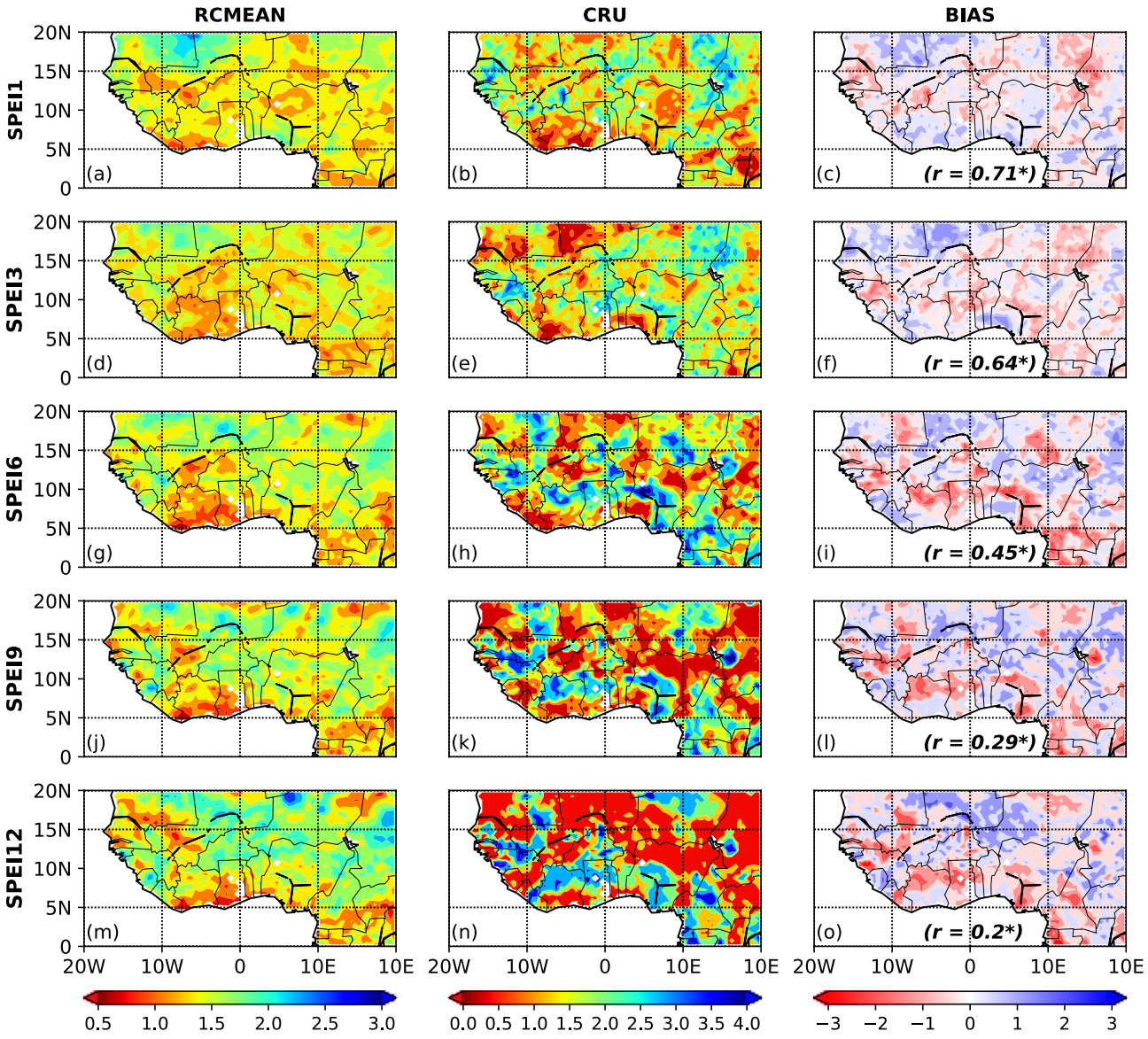

Figure 4.6: The frequency of the extreme dry over West Africa for various drought types (SPEI1: meteorological drought, SPEI3 and SPEI6 : agricultural drought, SPEI9 and SPEI12: hydrological drought). RCMEAN is the ensemble-mean of CORDEX-RCA4 models, CRU is the observed dataset, and BIAS = RCMEAN-CRU is the difference between the model ensemble mean and the observed.

4.1.2.4 Assessment of the severe dry events

Figure 4.7 illustrates the variability of severe drought (-2 < SPEI < -1.5) in West Africa both for the simulations and the observed CRU. The model shows that the frequency of severe drought is from 4 to 8 events per decade, while the observed frequency is between 2 to 12 events per decade. Globally at the scale of meteorological drought, there is an overestimation of the frequency of severe drought except for countries as Mauritania, Mali, and Cameroon which present an underestimation about 2 events per decade in response to the CRU frequency. The correlation is significantly important (r = 0.82). The correlation decrease with the increasing of the scale of the SPEI. However, they are all significantly correlated in the reproduction of the spatial pattern. The model at agricultural scale underestimates the severe drought over Chad, northern Nigeria, southern of Benin, Niger, and Mauritania up to 4 events per decade. But there is a particularity in the estimation of the severe drought with a 3-month lag; globally the model is close to the observed with a slight overestimation up to 2 events per decade. The model fails to reproduce the hydrological severe drought well. Despite having a good sign, the model widely underestimates the frequency of severe drought in Niger, Mali, Mauritania Nigeria, Chad, Benin, south of Ghana and Cote d'Ivoire. The highest value for this underestimation is over north-eastern part of Nigeria (a part of Lake Chad) and Mauritania, and northern of Chad where the model evaluates the magnitude of the hydrological severe drought about 7 events per decade against 12 events per decade for the observed. The model for all types of severe drought, overestimates the magnitude over Senegal, Mauritania, eastern of Mali, and the northern part of Niger, Cote d'Ivoire, and Ghana up to 4 events per decade.

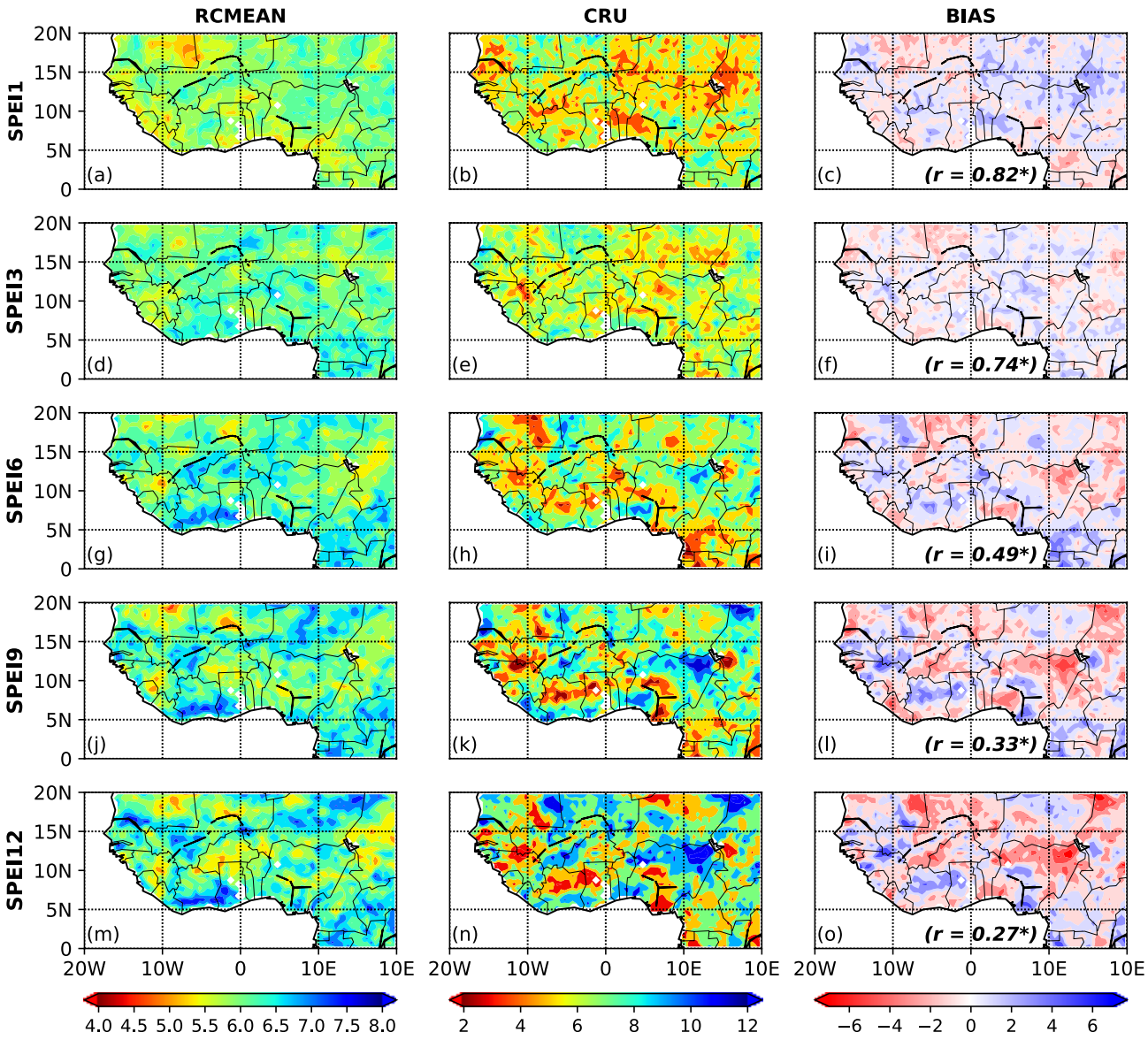

Figure 4.7: The frequency of the severe dry over West Africa for various drought types (SPEI1: meteorological drought, SPEI3 and SPEI6 : agricultural drought, SPEI9 and SPEI12: hydrological drought). RCMEAN is the ensemble-mean of CORDEX-RCA4 models, CRU is the observed dataset, and BIAS = RCMEAN-CRU is the difference between the model ensemble mean and the observed.

4.1.2.5 Assessment of the extreme wet events

The assessment of the model in inspecting the extreme and severe wet conditions respectively on Figure 4.8 and Figure 4.9 shows a significant negative correlation with respect to the observed CRU. This negative correlation is related globally to an opposite finding of the events by the model and the observed. When the model is showing a high value of the frequency of the event, the observed illustrates a low value for the same event, vice-versa (for instance when the model is showing a very high frequency of the extreme wet condition over the Sahel, the observed is giving for the same area low value in the case of hydrological drought index). By comparison of Figures 4.6 and 4.8 which are evaluating the extremely dry and wet areas respectively, the observed explains at the same grid two different information. It is showing in the Sahel that there is extremely dry when in the same Sahel there is also extremely wet, the same analysis is valid for the case of severe dry or wet areas investigation. Many factors could explain this fact. But one of them could be that the model explains the events on the same area for a different period, and because of the spatial average on time, the spatial pattern is carrying out different results for the same area. To find out the causes of this fact, further investigations are needed.

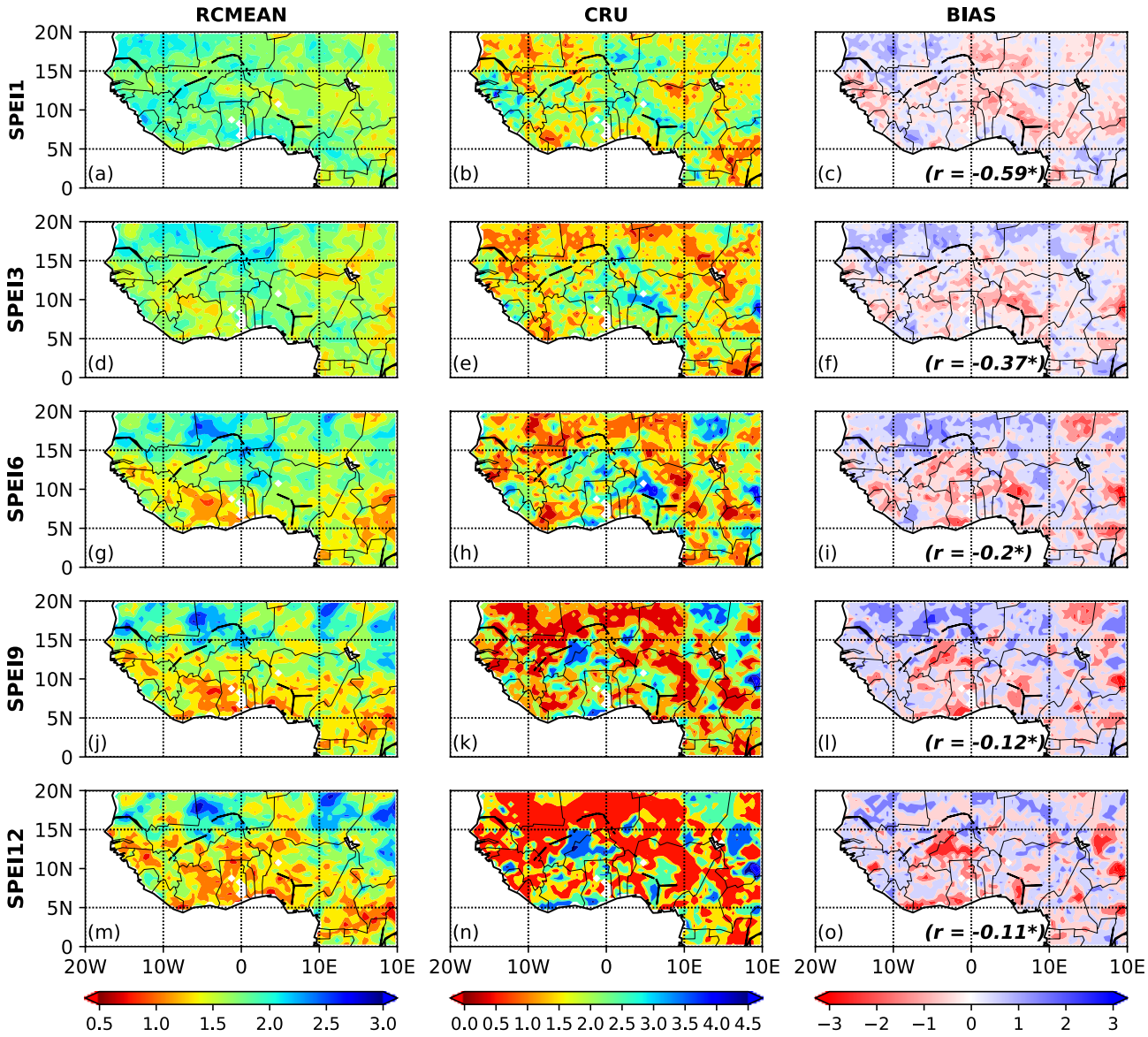

Figure 4.8 : The frequency of extreme wet over West Africa for various drought types (SPEI1: meteorological drought, SPEI3 and SPEI6 : agricultural drought, SPEI9 and SPEI12: hydrological drought). RCMEAN is the ensemble-mean of CORDEX-RCA4 models, CRU is the observed dataset, and BIAS = RCMEAN-CRU is the difference between the model ensemble mean and the observed.

Nevertheless, the analysis of the ensemble-mean of the model can be done. Here, at meteorological scale, the model finds about 2 events per decade over Mauritania, Guinea, Sierra-Leone, southern of Nigeria, Benin and Ghana. At agricultural and hydrological scales, the Sahel has the highest frequency of extreme wet event values with some peaks over Mali, northern of Niger, eastern of Chad about 2.5 events per decade and 3 events per decade for agricultural and hydrological scales respectively, while the Savanna and the Gulf of Guinea recorded fewer events. The RCMEAN at meteorological scale evaluates the frequency of severe wet events between 6 and 8 events per decade and seems to have a fair agreement with the observed except some particular points. Over the south of Niger, the agricultural severe wet events will increase compared to the meteorological scale. This increasing of the severe wet events is important under the hydrological scale, where countries as Niger, Burkina-Faso, northern of Benin, Togo and Ghana have up to 9 events per decade, the north of Mali, eastern of Niger, and Chad have less severe wet events at this stage. The extreme wet events assessment, farther investigations in the periods on which each event are recorded will lead to a better understanding of the negative correlation between the model and the observed dataset.

4.1.2.6 Assessment of the severe wet events

Globally, West Africa is characterized during 1971-2000 by various drought episodes, which have been revealed with the SPEI at different scales. The model shows that for all characterization of drought types, there are more extreme drought events in the Sahel than the Savanna and Gulf of Guinea, whilst the severe drought frequency is higher in the Gulf of Guinea than Savanna and Sahel, particularly for agricultural and hydrological drought events. The observed also follows globally the same analysis in terms of the trend but explain conversely in terms of magnitude. The extreme and severe

droughts are covering about 3% and 8% per decade of the study area respectively, and have been shown by both the model and the observed. The spatial pattern evaluation could hide the temporal estimation of these events. Therefore, an assessment with the empirical orthogonal function (EOF) and principal component (PC) analysis is driven with the aim to investigate both temporal variability and potential frequency on which the event replicates itself in the historical period.

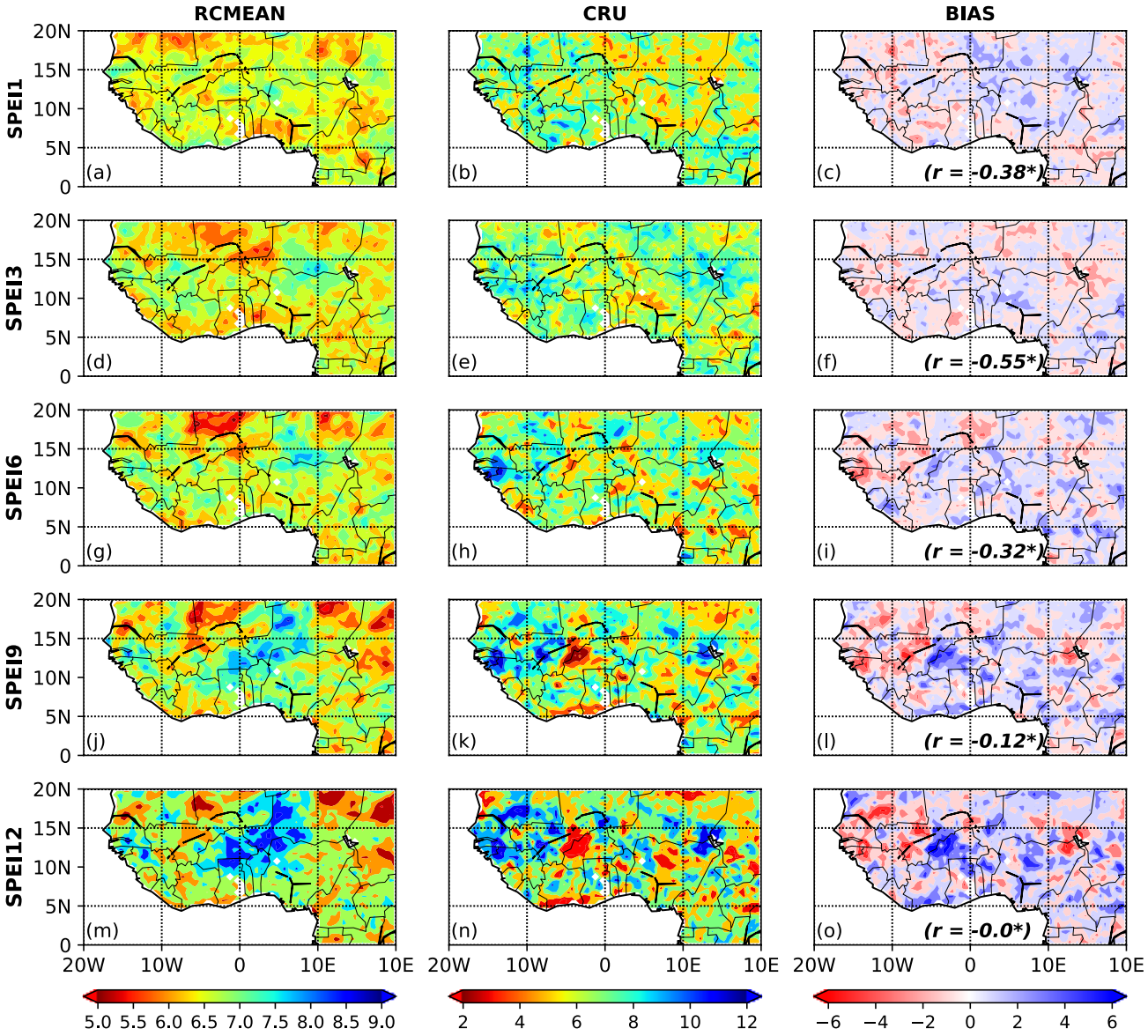

Figure 4.9: The frequency of severe wet over West Africa for various drought types (SPEI1: meteorological drought, SPEI3 and SPEI6 : agricultural drought, SPEI9 and SPEI12: hydrological drought). RCMEAN is the ensemble-mean of CORDEX-RCA4 models, CRU is the observed dataset, and BIAS = RCMEAN-CRU is the difference between the model ensemble mean and the observed.

4.1.3 Assessment of the spatial-temporal variability of the dry index with the Empirical Orthogonal Function (EOF)

The spatial patterns of the three leading EOFs do not differ essentially too much from one season to another. Therefore, we decided only to exemplify in Figure 4.10 the loading patterns of the first three leading EOFs of SPEI6 during the historical period considered to evaluate the extreme and severe dry/wet conditions.

The spatial correlation coefficients of EOF1 accounts for 32% of the variance in Figure 4.10 (panel a: extreme dry), have positive loadings with the highest values recorded around Savanna and Sahel areas, close to countries or part of countries like Northern of Benin-Togo-Ghana-Ivory-Coast, Burkina-Faso, also a part of Niger-Nigeria-Mali-Chad. This fact points out the high variabilities of the extreme and severity dry in West-Africa. The distribution of the spatial coefficients of EOF2 with a negative correlation at the center-western and south-coastal is trying to explore details at this area of the domain; the positive value obtained at the north-eastern is in the direction to reinforcing the analysis in EOF1. The spatial coefficients observed at EOF3 focus on the western part in case of severity-dry, and eastern part for the extreme-dry. Figure 4.10c and Figure 4.10d which represent the analysis of the wet condition based on the SPEI values follow the same interpretation like in the case of Figure 4.10a and Figure 4.10b. The wettest areas were located at the eastern of the study area and into the Sahel. We need to mention that the judgment of wet or dry is based on SPEI computation and classification, which is also in function of the climate water balance CWB = PRE-PET (where PRE: precipitation and PET: Potential evapotranspiration). When we have a supplement, potential flash-flood could be recorded; not necessary but it could happen. The analysis of EOF1 in case of wet condition showed that the Sahel and the eastern part of the Gulf-Guinea could be the most impacted by the wet condition. The EOF2 and EOF3 enhance

the analyses of the location of wet areas; they explained the existence of a gradient Gulf-of-Guinea-Savanna-Sahel, and also another gradient South-Western -North-Eastern (Figure 4.10d). The frequency and identification of roughly right dates of when all these climate extremes happened could be useful for better understanding of dry and wet phenomena. This is done through the interpretation of the principal component (PC).

The analysis of the three first PCs showed that Northern of Benin-Togo-Ghana-Ivory-Coast, Burkina-Faso, part of Niger-Nigeria-Mali-Chad and all the northern boundary of the study area experienced extreme-dry from 1971-1974; in additional from 1987-1989, a part of Mali-Burkina-Faso-Ghana-Ivory-Coast recorded extreme-dry. The severe-dry was registered in general from 1977-1980, 1989,1994 and 1995 roughly over West-Africa but some specific part illustrated themselves by some pick; like Nigeria in 1972 and 1973, also the whole Gulf of Guinea and the west-northern (Mauritania and Senegal) in 1998-2000. In the other side (Figure 4.10c and Figure 4.10d) 1978, 1979, 1987, 1988, 1994, 1995 recorded relatively an extreme-wet state; the Sahel was wetter in 1987 and 1988 as well as Liberia and Sierra-Leone. The Western part of West-Africa recorded severity-wet during the period 1981-1985; whilst in Savanna, it was in 1995, and 1996.

a: *Extreme dry*

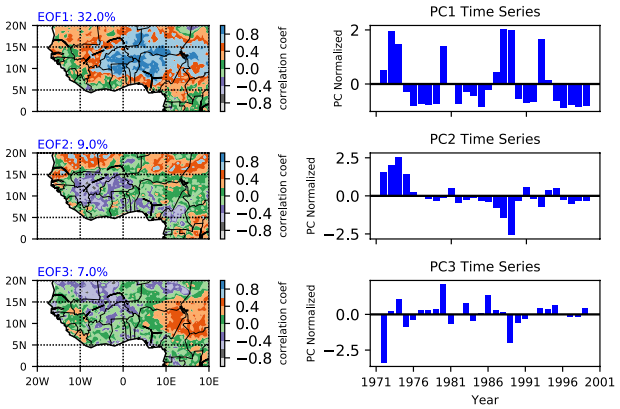

c: *Extreme wet*

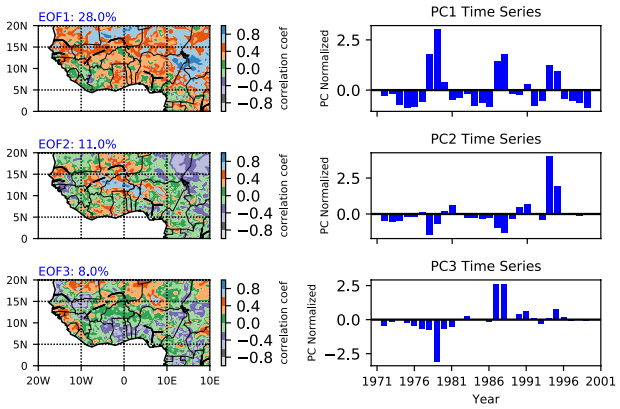

b: *Severity dry*

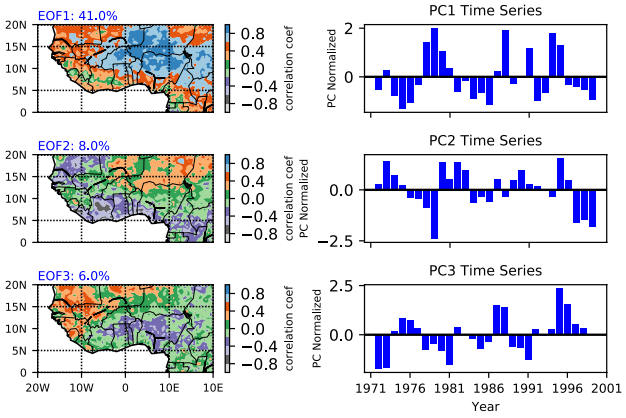

d: *Severity wet*

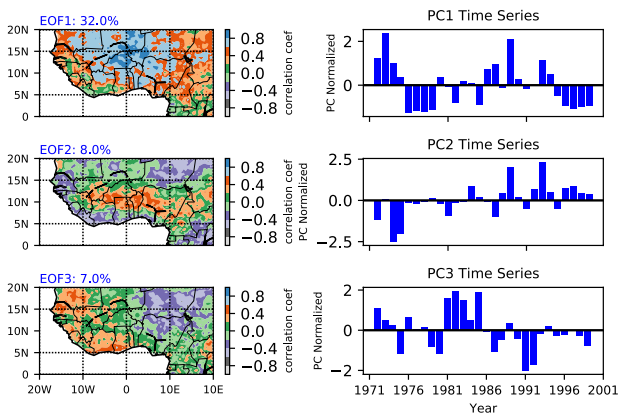

Figure 4.10 : Spatial-temporal distribution of dry and wet areas in West-Africa into period 1971-2000 : evaluation of extreme and severity dry (a, b) and extreme and severity wet (c, d)

4.1.4 Climate models evaluation under the projection periods using the SPEI variability

In this section, the horizontal stripe (-) on figures 4.11 to 4.15 indicates that at least 80% of the RCA4 models show a decreasing trend, while the cross (+) indicates that more than 80% of the models express an increasing trend of the event studied.

4.1.4.1 Assessment of SPEI projection

The analysis of the Figure 4.11 shows that globally at all warming levels, at least 80% of the RCA4 models project a decrease of the drought index trend. However, with the drought intensity, the magnitude of the decrease varies according to the region and drought types studied and also grows with the increasing of the GWLs. For instance, with the GWL1.5, at all drought types, the SPEI values decrease gradually northwardly. The Gulf of Guinea is projected to be wetter (with the highest drought index), the Savanna moderately dry, and the Sahel is projected to be the driest zone(with the lowest decrease of the drought index when it compares to the historical period). Interested in the other GWLs (where the global warming level is 2.0℃, 2.5℃, and 3.0℃) the SPEI's distribution varies slightly with the increasing of SPEI scale (drought types). At the meteorological drought scale, the SPEI variability is uniformly distributed with SPEI closed to zero (SPEI ≈0). At agricultural scale, the drought intensity decrease with the GWLs, the Gulf of Guinea is wet for the GWLs 2.0℃ and 2.5℃, whilst with GWL 3.0℃ there is decreasing of the drought index. For the hydrological drought scale case's, the same global analysis with the one from the agricultural scale is valid with an intensification of its magnitude, but in this study, a slight increase trend of the SPEI is noticed around the south of Chad and eastern part of Nigeria. A clear investigation of the characterization of the projected drought events in the study area is shown below.

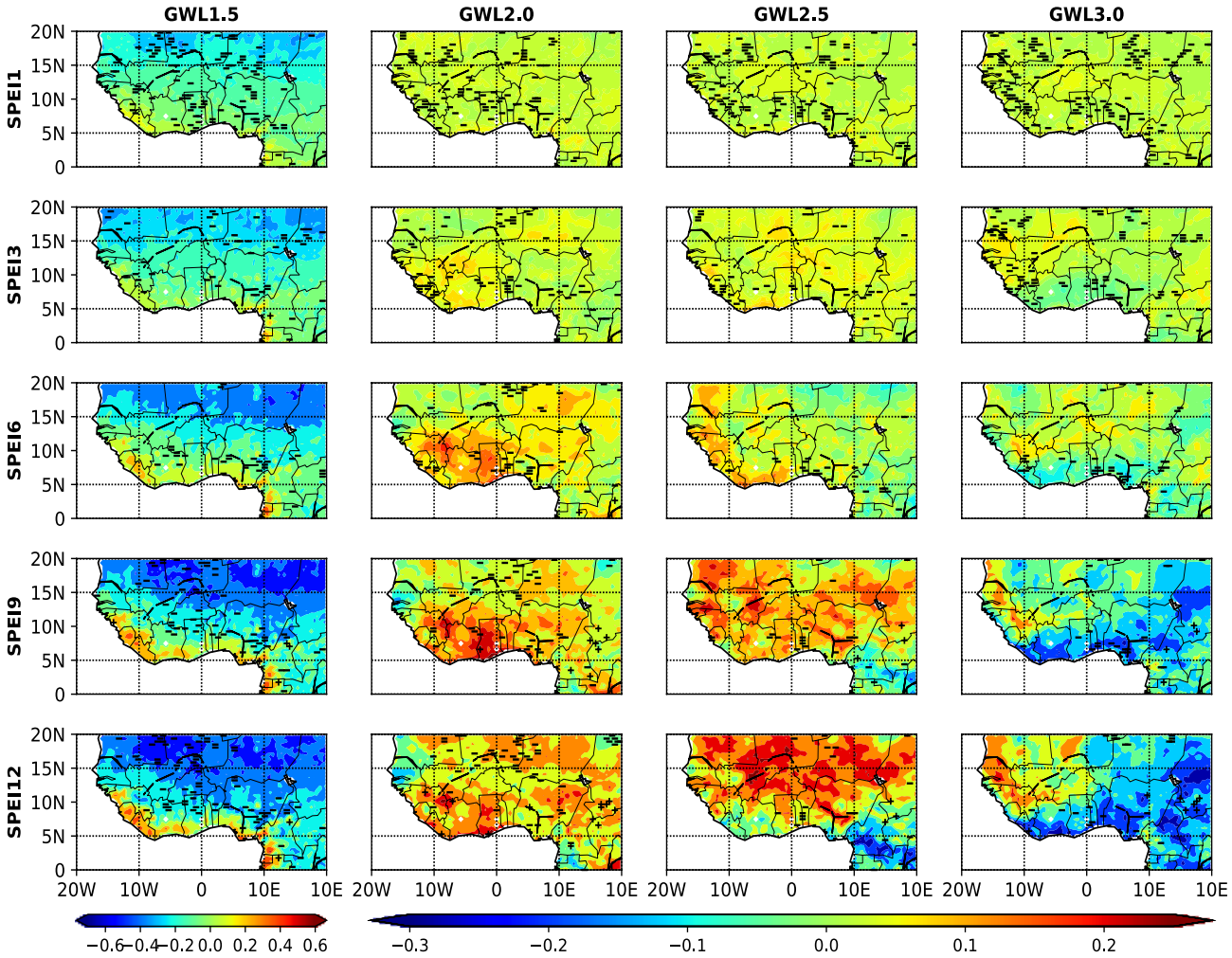

Figure 4.11: Standardized Precipitation Evapotranspiration Index (SPEI) over West Africa for projection periods for various drought types (SPEI1: meteorological drought, SPEI3 and SPEI6: agricultural drought, SPEI9 and SPEI12: hydrological drought). RCMEAN is the ensemble-mean of CORDEX-RCA4 models, CRU is the observed dataset, and BIAS = RCMEAN-CRU is the difference between the model ensemble mean and the observed

4.1.4.2 Assessment of the extreme dry events

The Figure 4.12 presents the variability of extreme dry events under different GWLs and various drought types. Based on the evaluation criteria, more than 80% of RCA4 models shows that the whole West Africa under the GWL1.5℃ experienced an increasing trend of extreme dry events (i.e., there is an increase of the frequency of extreme drought events compared to the historical period) which is materialized with the cross. The decreasing of the extreme dry events is southward from the meteorological drought to hydrological drought (i.e., the extreme dry events is gradually less important from the Sahel to the Gulf of guinea when the assessment is based from the meteorological drought to the hydrological drought). In term of the extreme dry frequency, it may be noticed the existence of a northward gradient. In the Sahel, the magnitude of the frequency of the extreme dry is above of 4 events per decade and about 3 events per decade in the Savanna, while in the Gulf of Guinea this frequency is about 2 events per decade. The impact of the increasing of the temperature from 1.5℃ to above (2.0℃, 2.5℃, and 3.0℃) on the extreme dry events, is well noticed. At meteorological drought level, the Gulf of Guinea and Savanna experienced an increase of the trend of the extreme drought with frequency about 1 event per decade, whilst in the Sahel, more than 80% of the models proven a decreasing trend of the extreme dry event. The decrease of the extreme dry event is important in the Sahel and Savanna for the agricultural and hydrological drought events study. This decrease extends also to the Gulf of Guinea for the SPEI9 under GWL2.5. Only some coastal countries such as Ghana, Cote d'Ivoire, and Cameroon experienced an increase in the extreme dry events during the projected periods. Globally, the frequency of the extreme drought is between 1 to 1.5 events per decade for the GWLs 2.0℃, 2.5℃, and 3.0℃.

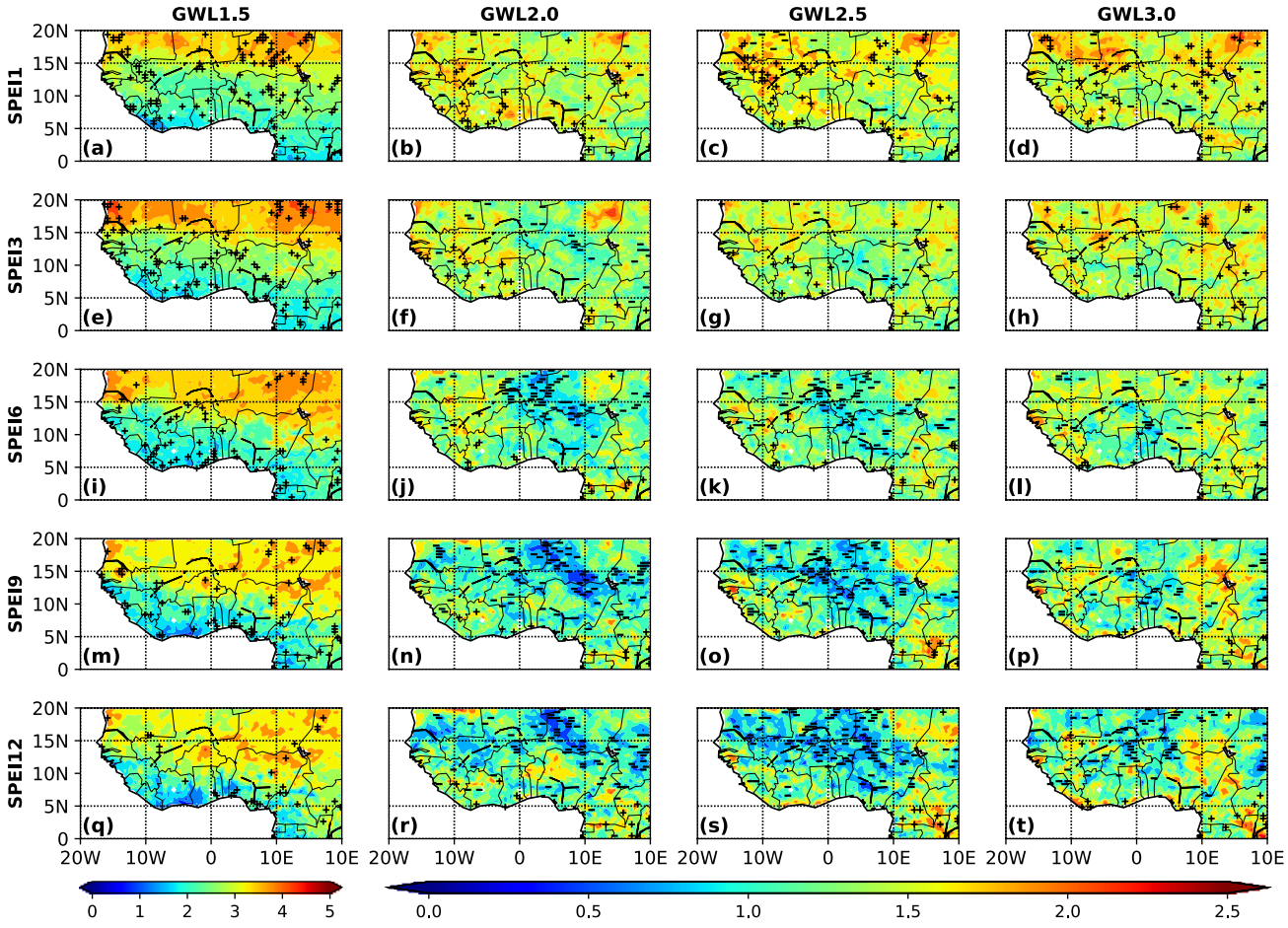

Figure 4.12: The frequency of the extreme dry over West Africa for various drought types (SPEI1: meteorological drought, SPEI3 and SPEI6: agricultural drought, SPEI9 and SPEI12: hydrological drought) at different GWLs during the projection periods. The horizontal stripe (-) indicates that more than 80% of the models agree with a decreasing trend of extreme dry events, whilst the cross(+) shows that at least 80% of the models agree with an increasing trend of extreme dry events.

4.1.4.3 Assessment of the severe dry events

Conversely, to the case of the analysis of the spatial distribution of the extreme drought events, under the GWL1.5, West Africa experiences a uniform decrease of severe drought events (Figure 4.13, proved with the horizontal stripe). A southward frequency of the severe drought events is shown. The lower frequencies are recorded in the Sahel (the lowest in Niger and Chad about 3 events per decade) and the highest (about 8 events per decade) in the Gulf of Guinea at all drought types. At GWLs 2.0℃, 2.5℃ and 3.0℃, the trend is variable. For instance, at the meteorological drought scale under GWL2.0 globally, the Gulf of Guinea and Sahel experienced an increasing trend of severe drought, whilst at Savanna, it observed a decreasing trend of the severe drought events. Under GWLs 2.5 and 3.0 the severe drought increase in the Gulf of Guinea and Savanna and some part in the Sahel. Some particular countries as Niger, Burkina-Faso, and Mauritania have a decreasing trend. Although West Africa records various decreasing or increasing trend of the severe drought, the magnitude of the frequency seems stable over the whole study domain and varies about 7 events per decade. The analysis at the agricultural GWLs 2.0, 2.5 and 3.0 reveals that countries like Cameroon, Ghana, Burkina-Faso and the Central African Republic has a decreasing trend, whilst for the GWLs 2.0 and 3.0, Mauritania, Chad and northern Mali experienced increase trend. The frequency of the severe drought events for the hydrological scale globally, is about 7 events per decade, except in Nigeria and Ghana where it is about 4 events per decade for GWL2.0; in northern Niger and Chad, it is about 4 events per decade for GWL2.5. This difference in value is due to the decreasing trend of droughts over those areas.

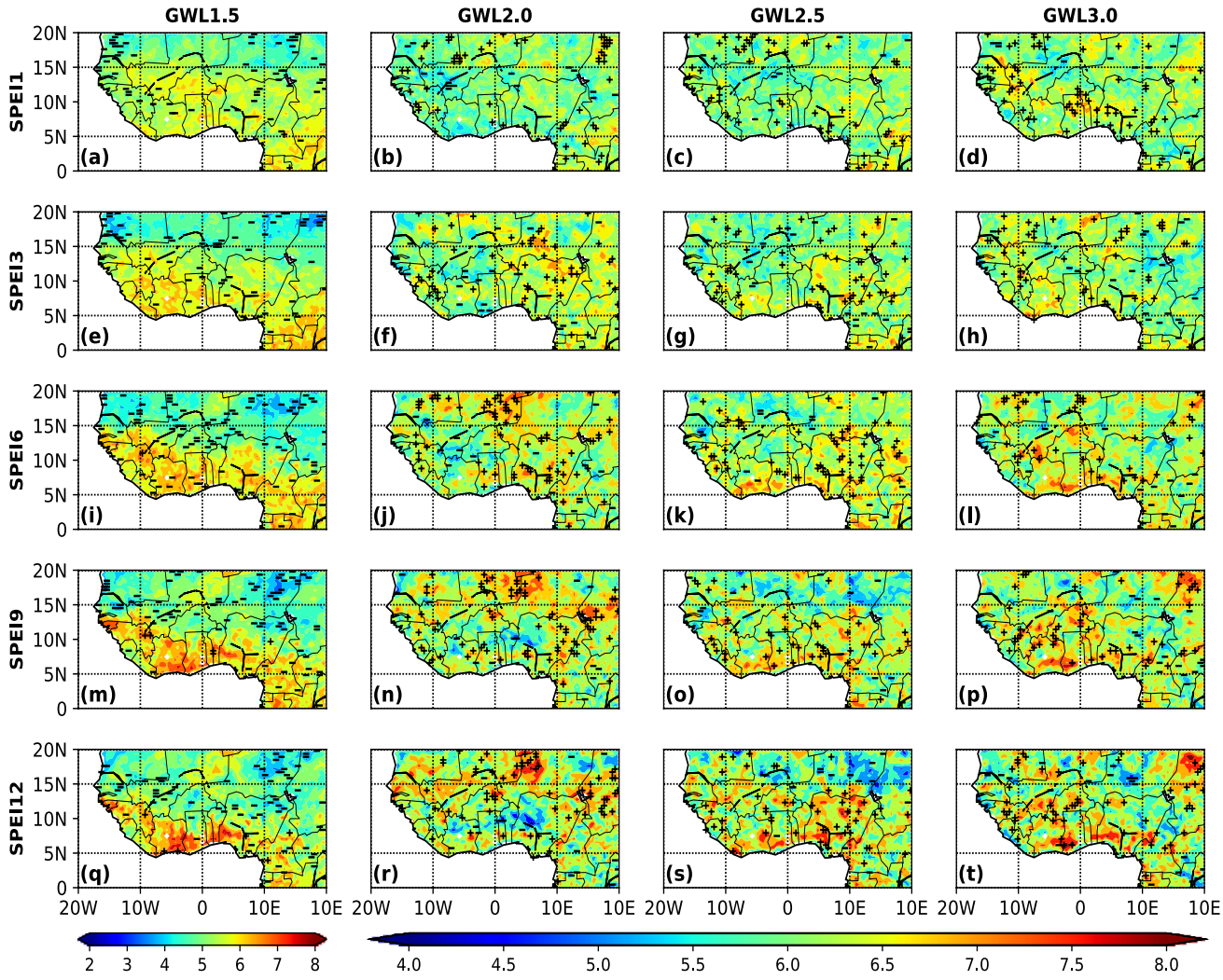

Figure 4.13: The frequency of the severe dry over West Africa for various drought types (SPEI1: meteorological drought, SPEI3 and SPEI6: agricultural drought, SPEI9 and SPEI12: hydrological drought) at different GWLs during the projection periods. The horizontal stripe (-) indicates that more than 80% of the models agree with a decreasing trend of extreme dry events, whilst the cross(+) shows that at least 80% of the models agree with an increasing trend of extreme dry events.

4.1.4.4 Assessment of the extreme wet events

At the meteorological scale, the central area of the study domain showed in general much decreasing trend of extreme wet events. At meteorological and agricultural scales, the western and eastern part of West Africa experienced an increasing trend which is linked to the GWLs (i.e., increase with the GWLs). At all drought types during the GWL1.5, the Gulf of Guinea and the Savanna register an increasing trend, whilst the Sahel has a decreasing trend. More the scale of the drought index (drought type) increase more the frequency of the extreme wet events decrease. For each GWL and drought type, the projected highest value is obtained over the coastal countries. More the drought type increase more the decreasing trend is northward. At GWL 2.0, 2.5 and 3.0 the agricultural and hydrological drought events decrease in the Sahel and Savanna particularly over countries like Niger, Burkina-Faso, Mali, and Benin, with a spatial average frequency of the extreme wet events about 2 events per decade, whilst in the Gulf of Guinea it is noticed an increase of the extreme wet events. For the agricultural and hydrological scales, the eastern part of the study area acquaints an increasing trend. In summary, the model projects more decrease of extreme wet events in West-Africa, particularly in the Sahel and Savanna.

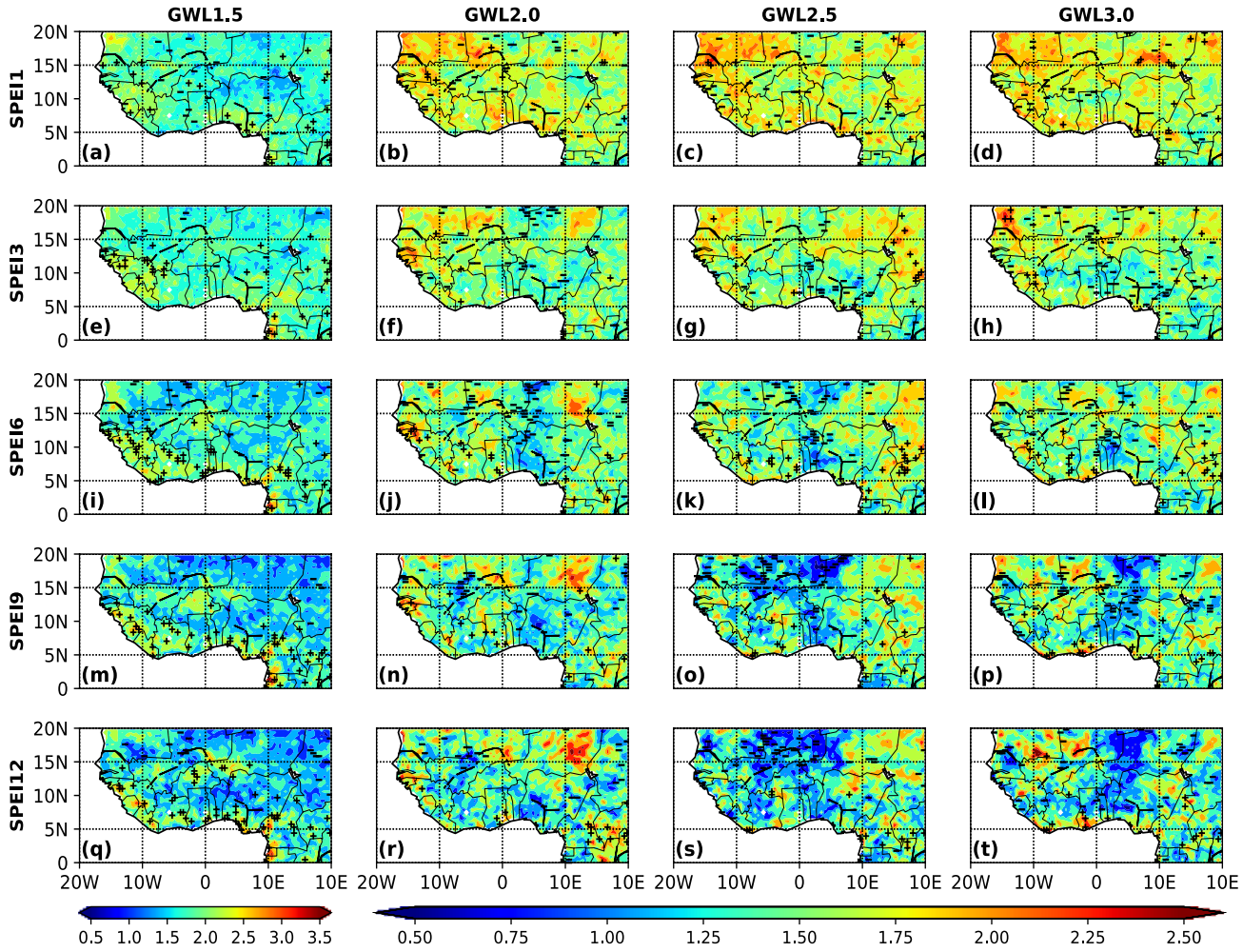

Figure 4.14: The frequency of the extreme wet over West Africa for various drought types (SPEI1: meteorological drought, SPEI3 and SPEI6: agricultural drought, SPEI9 and SPEI12: hydrological drought) at different GWLs during the projection periods. The horizontal stripe (-) indicates that more than 80% of the models agree with a decreasing trend of extreme dry events, whilst the cross(+) shows that at least 80% of the models agree with an increasing trend of extreme dry events.

4.1.4.5 Assessment of the severe wet events

Compare to historical, Figure 4.15 shows that at least 80% of the models reveal a decreasing of the severe wet events over the whole study domain under the GWL1.5. It can also be noticed a northward decrease in the frequency. The highest frequency at GWL1.5 is recorded over the Gulf of Guinea and is about 6 events per decade, whilst the lower values (about 4 events per decade) are located in the Sahel leading to a southward gradient. The area around the boundary of Niger, Burkina-Faso experienced the lowest (about 3 events per decade) for the hydrological drought index during the GWL1.5, while at GWLs 2.5, and 3.0 they acquainted higher frequencies (about 8 events per decade). At GWLs 2.0, 2.5, and 3.0 the variability is not uniform, but there is overall more decrease severe wet events. At the meteorological drought scale, the lower frequencies are located in the Sahel and the higher scattered located in diverse regions. At the agricultural drought scale, northern of Mali, Niger, Burkina-Faso, Ghana, and Benin experienced an increase of severe wet events, whilst the north-eastern of the study domain involvement in a decreasing trend. For the hydrological drought scale, a strong decrease of the severe wet event is noticed at the circled area in Figure 4.15.

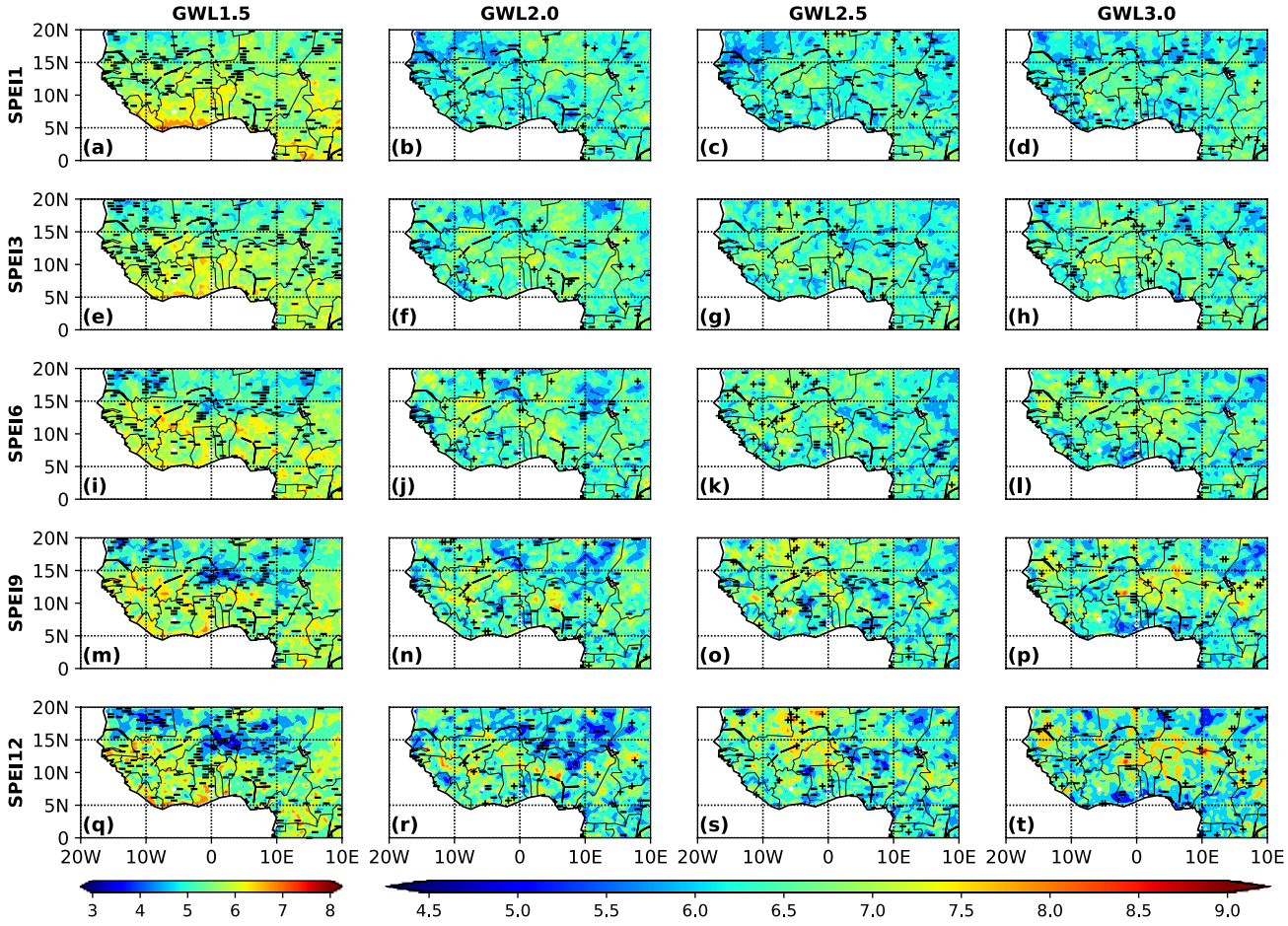

Figure 4.15 : The frequency of the severe wet over West Africa for various drought types (SPEI1: meteorological drought, SPEI3 and SPEI6: agricultural drought, SPEI9 and SPEI12: hydrological drought) at different GWLs during the projection periods. The horizontal stripe (-) indicates that more than 80% of the models agree with a decreasing trend of extreme dry events, whilst the cross(+) shows that at least 80% of the models agree with an increasing trend of extreme dry events.

In summary, under the interested GWLs used in the study, many variabilities have been noticed with the reference period. The ensemble-mean of models shows either important extreme and severe dry events, or a consistence extreme and severe wet events. Globally, under the GWL1.5 for all drought types studied, a recurrent increase of extreme events (dry and wet) was noticed, particularly the Gulf of Guinea and Savanna for both events experienced an increasing trend, whilst the Sahel illustrated an increase of the extreme dry events and a decrease of the extreme wet events. At least 80% of the RCA4 models considered in this study show a decrease of severe (both for dry and wet) events. The lower frequency is located in the Sahel and the higher around the coastal countries. Here, the frequency of the extreme dry events is high and up to 4 events per decade in the Sahel. For the GWL2.0, 2.5 and 3.0, at agricultural and hydrological drought scales, a high important decrease of the extremely dry and extreme wet events are perceived over the Savanna and the Sahel particularly around countries as Niger, Mali, Burkina-Faso, Benin, and Nigeria. The coastal countries detected an increase in extremely dry and wet events, whilst the south-eastern area noted an increase of both the extremely dry and wet events. Important variabilities also are observed for the severe wet and dry events over the study area. For the hydrological drought scale, there is a decrease of severe wet events in the boxed area, which groups countries like Nigeria, Niger, Burkina-Faso, Benin, Ghana, and Togo under the GWL 2.0, 2.5, and 3.0. Conversely, at least 80% of the models show that this area experienced an increase about 1.5 events per decade of the severe dry events, except a country like Benin which shows a decreasing trend.

4.1.5 Precipitation concentration distribution in West Africa

This section presents the results obtained from the study. Based on the variability between the historical and the various GWLs periods. The section 4.1.5.1 shows the annual and seasonal precipitation concentration patterns, whilst the section 4.1.5.2 focuses on the variability of precipitation concentration degree and period. The section 4.1.5.3 evaluates the daily precipitaton variability.

4.1.5.1 Variability of the Precipitation Concentration Index

4.1.5.1.1 Annual variability of the precipitation concentration index

The annual scale of the PCI calculated in this study varies generally across the study area from values greater or equal to 12, to higher than 20; according to Oliver's (1980) classification, this denotes a seasonal rainfall regime. From Figure 4.16 (a)-(e), the lower values recorded during the historical period (here called the control period or CTL) is between 12 and 13 on the Gulf of Guinea, thus illustrating a moderate precipitation concentration over this area. The seasonality is more pronounced in the transition area (the Savanna) with a PCI between 17 and 18, which shows how the precipitation concentration is irregularly distributed; lastly, the Sahel area has a high precipitation concentration (PCI>20), which means that the precipitation is strongly irregularly distributed.

For the different GWLs studied, it is observed that, for the Gulf of Guinea and the Savanna, an irregular precipitation concentration exists, except for some countries (Liberia and Côte d'Ivoire), which have a low precipitation concentration, while a strong irregular precipitation distribution is observed in the Sahel.

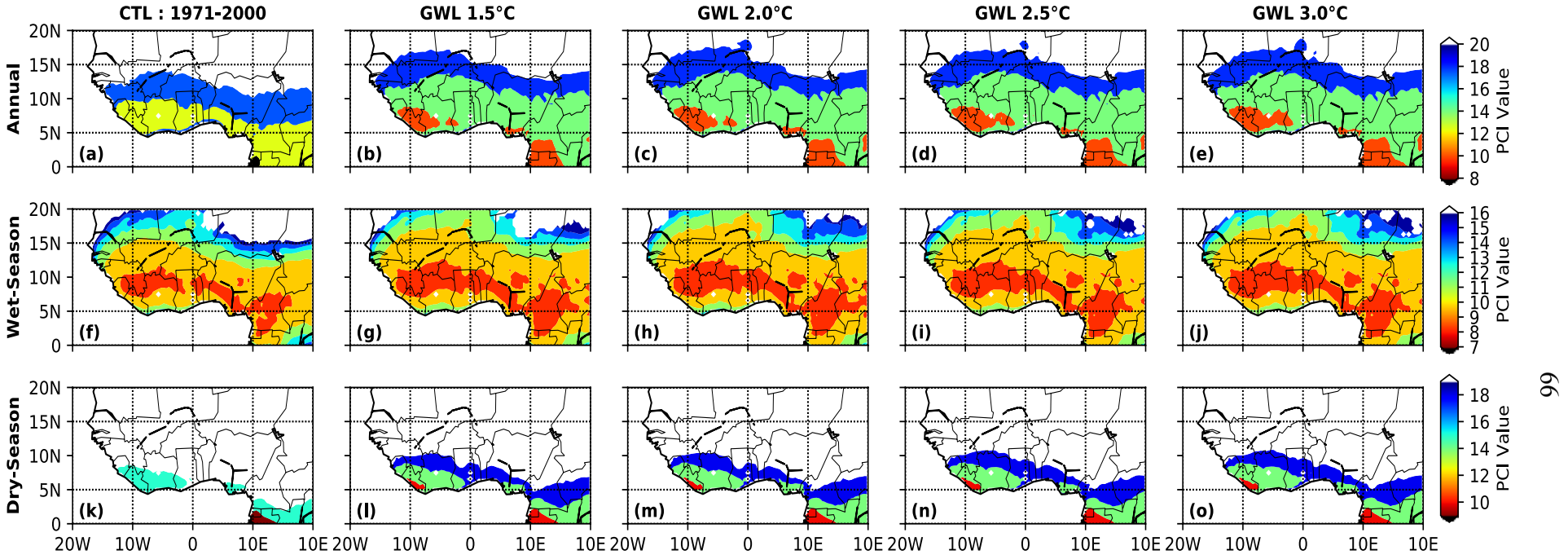

Figure 4.16: Variability of PCI at annual and seasonal scales for the historical period (CTL: 1971-2000) and for projections of GWLs 1.5°C, 2.0°C, 2.5°C, and 3.0°C.

4.1.5.1.2 Seasonal variability of the precipitation concentration index

There are two major seasons over the study area. For the purposes of this analysis, the rainy season is assumed to last from early May to the end of September (MJJAS). The PCI calculated for the seasonal scale shows complex spatial patterns of precipitation distribution in the area of study. Thus, Figure 4.16 f-j illustrate the uniform precipitation concentration (i.e., almost the same amount of precipitation occurs in each month) over the Gulf of Guinea and the Savanna. For the specified GWLs, the average of the uniform precipitation distribution extends toward the Sahel. The northern part of the study area records an irregular precipitation concentration during the wet season.

Figure 4.16 k-o show that, during this period of the year selected, an irregular precipitation concentration is only observed over the Gulf of Guinea. All the other areas, such as the Savanna and the Sahel, have a strong irregular precipitation concentration, which means that the total precipitation occurs within a single month.

The results from Figure 4.16 (with regard to annual and seasonal evaluation) confirm that the precipitation in West Africa is uniformly distributed during MJJAS in the Gulf of Guinea and the Savanna. Despite the global warming effect for all levels, this precipitation concentration does not change; on the contrary, it extends towards the Sahel. In general, the highest values of PCI are recorded over the Sahel, whereas the lowest occur over the Gulf of Guinea.

4.1.5.1.3 Evaluation of the models' robustness

Figure 4.17, which presents the differences between the projected PCI in respect of the historical period, shows that the level of variability is similar from one GWL to another. The annual and seasonal concentrations reduce gradually from the Sahel to the Gulf of Guinea, and confirm the variability illustrated by Figure 4.16, which shows the regression of irregular and strong irregular precipitation concentrations. Figure 4.17 also illustrates the robustness of the simulations. At least 80% of models (indicated here with vertical green stripes) demonstrate that the precipitation concentration over the eastern part of the study area has changed. This change, which increases according to the GWLs, is also shown over several countries, such as Niger during the rainy season. At least 80% of the models demonstrated that the change is significant (as indicated by the horizontal blue stripes), with a confidence level of 95%. Here too, Niger and Nigeria are projected to experience significant changes, which will increase with the GWLs. The red cross (+) is observed in the area where at least 80% of the simulations agree with regard to the change, and where these changes have a 95% confidence level. Therefore, during the rainy season and under GWL3.0, countries such as Ghana, Togo, and Burkina Faso present a more uniform precipitation distribution, in contrast to variabilities for the historical period and the projections (Figure 4.16).

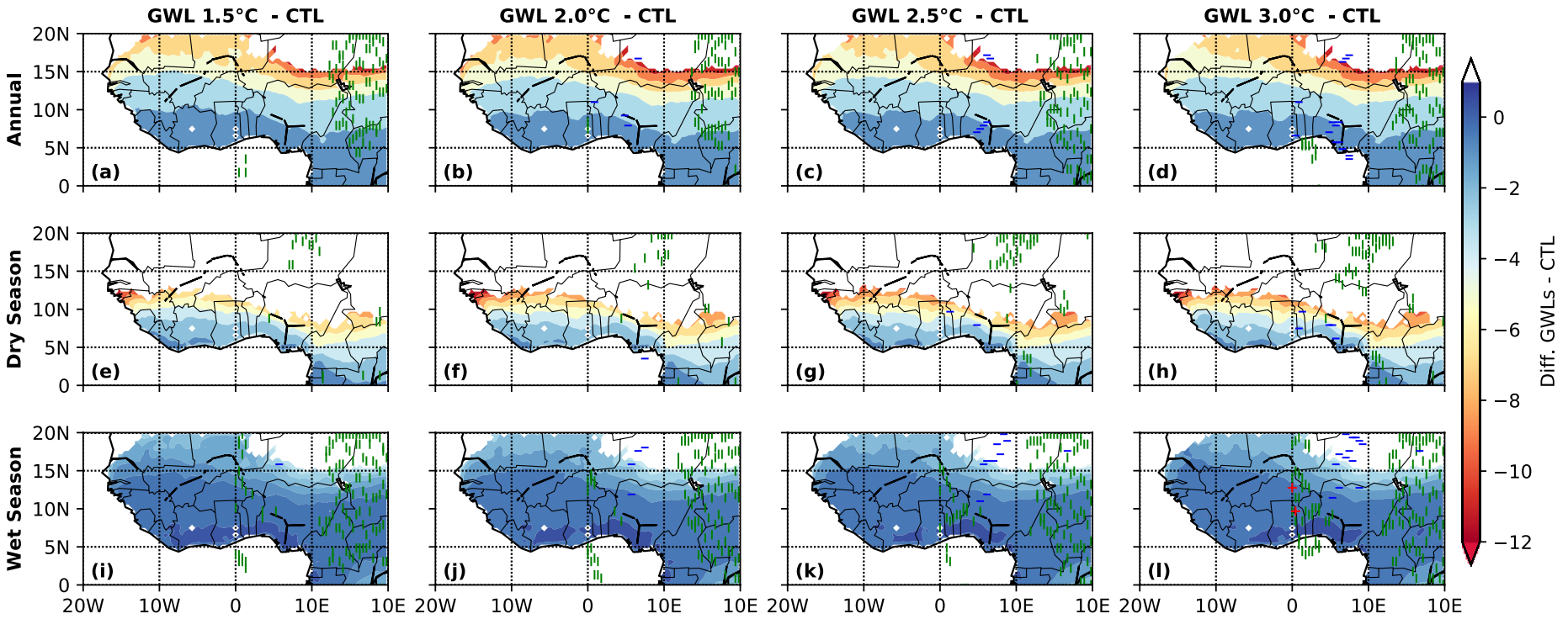

Figure 4.17: Evaluation over West Africa of the difference between the changes at 1.5°C, 2.0°C, 2.5°C, and 3.0°C GWLs of PCI using the CORDEX Africa ensemble. The vertical green stripe (|) indicates where at least 80% of the models agree on the sign of the changes, whilst horizontal blue stripe (-) indicates where at least 80% of the simulations agree that the projected change is statistically significant with 95% as confidence level. The red cross (+) indicates where both conditions are satisfied.

4.1.5.2 Variability of the Precipitation Concentration Degree and the Precipitation Concentration Period

Figure 4.18 shows the PCP and PCD. Figure 4.18 a-e illustrates that the range of PCPs over the whole West African region for present or future periods of study is between 7±2. This means that the yearly mean PCP over West Africa occurs from June to September, which confirms current knowledge about the period of the precipitation producing system in West Africa, viz., that it is governed by the West African Monsoon (WAM). The highest value for the historical time (1971-2000, also referred to as the control period) is recorded over the north-western part of the study domain, whilst for the projections, this value is located over the Sahel. This result confirms that the rainy season arrives earlier in the southern areas, followed by the transition area (the Savanna), before reaching the Sahel. The mean yearly PCDs (Figure 4.18 f-j) vary from 0.17 to 0.90, denoting the high variability of the precipitation concentration over West Africa. During the present period (Figure 4.18.f), the PCD values increase, suggesting the existence of a gradient across the Gulf of Guinea and over the Sahel. The lower values (0.17-0.60) are recorded over the Gulf of Guinea and the highest (>0.80) in the Sahel. This gradient explains that precipitation is more concentrated in a few months over the Sahel than over the coastal areas. The same dynamics in respect of the gradient are observed in the case of future projections, although the PCD values are reduced, compared to the historical period. The lower values here lie between 0.17 and 0.50, and the higher values are between 0.5 and 0.6. During the future period, the precipitation concentration will decrease, and the Savanna and Sahel will have the same precipitation distribution. But in terms of the period, all the GWLs show that the rainy season will state earlier than in the present (historical period). The highest concentration period for

the Gulf of Guinea and the Savanna will be from May to July, while the concentration over the Sahel will be highest in August.

4.1.5.3 Daily variability of precipitation

The consecutive wet days (CWD) and consecutive dry days (CDD) were calculated over the study domain to evaluate the daily variability of the precipitation distribution. CWD and CDD also indicate extremes in rainfall. CDD is furthermore a useful indicator for studying short-term droughts (Frich et al., 2002) and drought tendencies (Orlowsky and Seneviratne, 2012), as it could indicate enhanced dryness and high risk for seasonal droughts (Klutse et al., 2018). Changes in CDD and CWD can lead to uneven temporal distributions of rainfall, which could have a significant consequence for agricultural practices (Barron et al., 2003; FAO et al., 2015; Wiebe et al., 2017). The CDD was calculated both at annual (cdd) and seasonal scales (in this study, May-September: MScdd), in order to evaluate both dry and wet spells within the rainfall season; knowing this is very important for agricultural practices in the region (Klutse et al., 2018). Figure 4.19 presents the variations between the projection of each GWL and the present period. Higher values of CDD are observed in the northern part of the study area, while higher CWD values occur in the coastal areas. When we compare the patterns of Figure 4.19 a-d and Figure 4.19 (i)-(l), it can be seen that the CDD decreases about 10±5 days over the north-eastern part of the study domain, both annually and during the rainy season. In the northern part, a significant variability of dry days occur within the rainy season (for instance, a reduction over the north-eastern area and an increase over the north-western area), which means that the north-eastern of the study domain is wetter under GWLs and

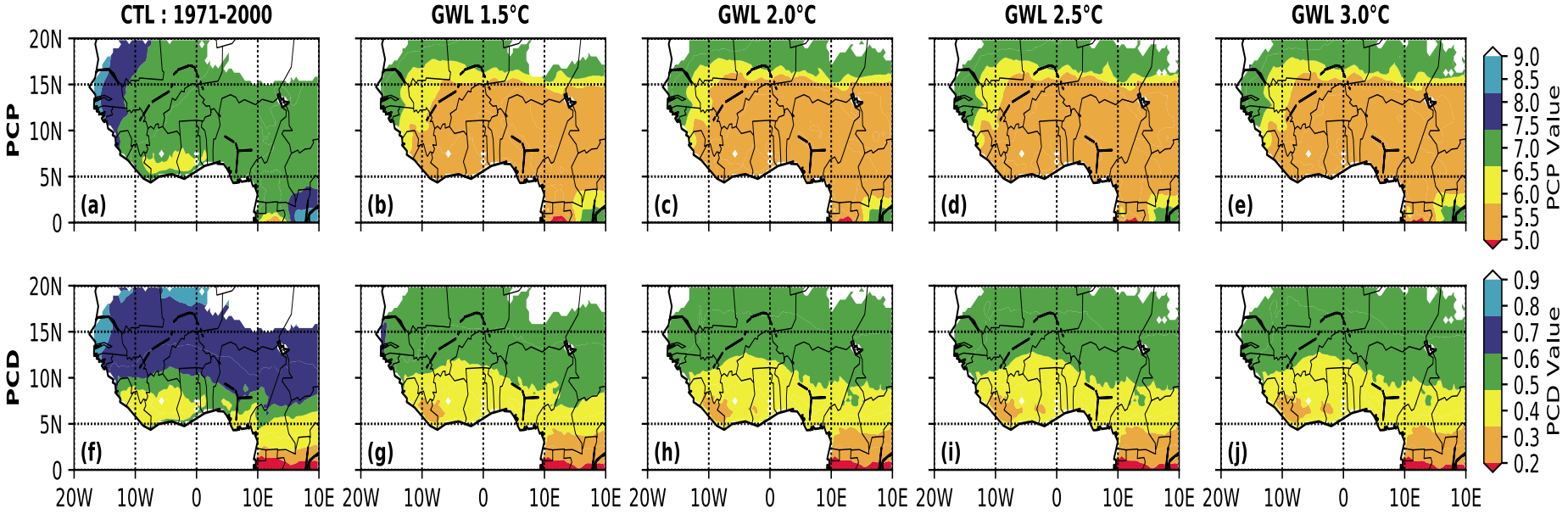

Figure 4.18: Spatial distribution of yearly mean PCD and PCP for the historical period (CTL: 1971-2000) and at projections of GWLs 1.5°C, 2.0°C, 2.5°C, and 3.0°C.

the north-western area is drier. The Gulf of Guinea has a very slight variability in respect of CDD for all GWLs studied, at both annual and rainy season scales. The projections of the GWLs 1.5℃, 2.0℃, 2.5℃ show essentially the same variability in the annual CDD, whilst the GWL 3.0℃ (Figure 4.19i) shows a significant increase in the annual CDD. The CDD are projected to increase for 4-5 days over the Gulf of Guinea; in Mauritania and Senegal, the increase is projected to be 10±2 days. Niger and Chad (which are characterized by a dry north-easterly flow crossing the Sahara desert) are projected to record a reduction of CDD with a range of 12±2 days. This agrees with the results of Klutse et al. (2018), who illustrated a decrease for GWLs 1.5℃ and 2.0℃, in terms of the number of CDD in West Africa during the rainy season, and the results of Sultan and Gaetani (2016), who reported a reduction in the number of dry days over central Africa.

In general, the CWD did not appear to record as many variations as was the case with the CDD. It varied slightly with 0±3 days. Nonetheless, high and important variations could be noticed at several specific points. Figure 4.19 e-h show CWD is projected to decrease by 10±2 over the southern parts of Benin and Nigeria. A small increase in CWD of up to two days is also likely to be recorded over the Sahel.

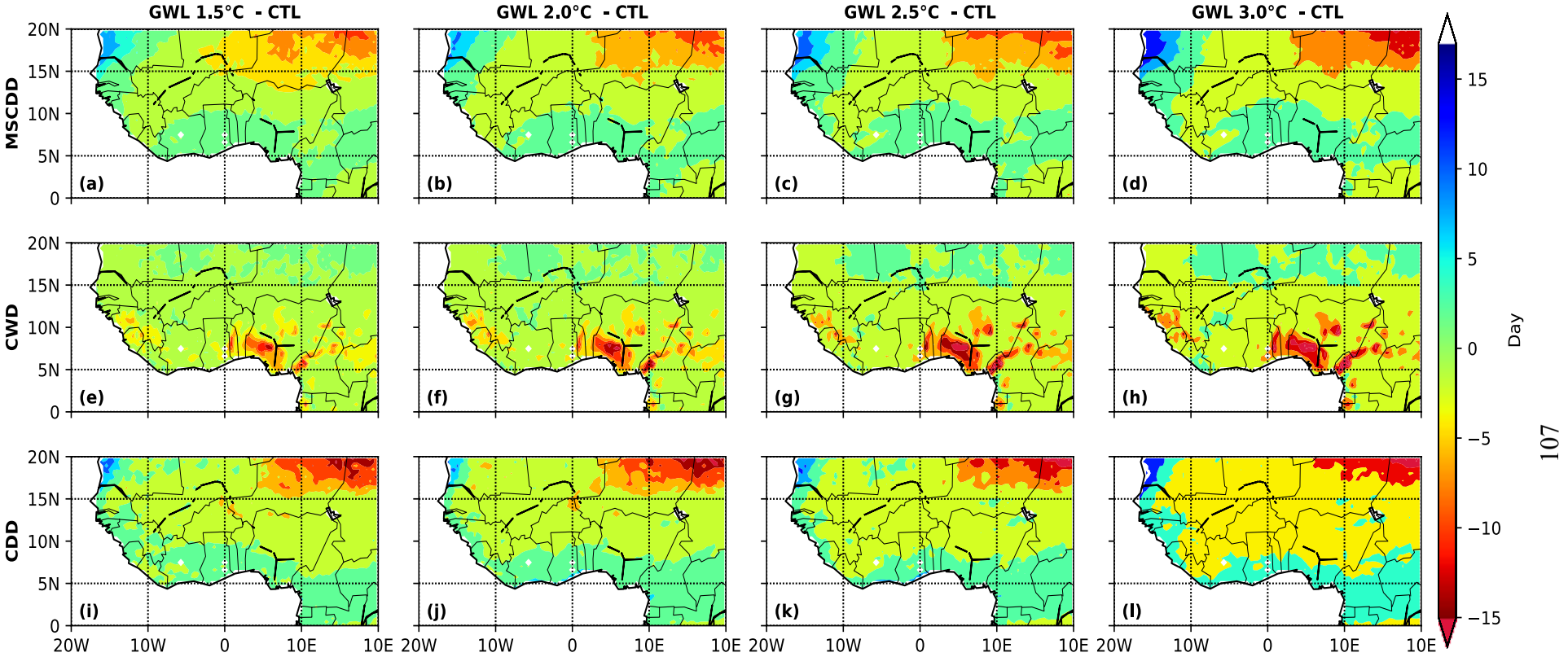

Figure 4.19 : Spatial distribution of the change in CDD during the rainy season (MSCDD), as well as the annual consecutive dry days (CDD) and the consecutive wet days (CWD).

In order to investigate the spatial variability of extreme rainfall events, which play such an important role in the availability of water resources and agriculture, etc. the frequency of intense rainfall events (RxD10mm: $R \geq 10$ mm/day), very intense rainfall events (RxD20mm: $R \geq 20$ mm/day) and heavy rainfall events (RxD25mm: $R \geq 25$ mm/day) were calculated; they are displayed in Figure 4.20. These variables indicate whether there were changes in the amount of precipitation received over consecutive 5 days with the highest precipitation. Figure 4.20 a-d illustrate that, compared to the control period, each GWL detects an increasing RxD10mm over the orographic regions and the ocean boundary (Gulf of Guinea). There is a very slight increase in the number of RxD10mm over the Savanna and Sahel zones. In general, the results clearly show that, as the GWL increases, the more the projected RxD10mm increases too (e.g., for GWL 1.5℃, the increase is about 7±2 over the Gulf of Guinea and 1±1 for the Savanna and Sahel, whilst for GWL 3.0℃, the increase is about 9±2 over the Gulf of Guinea and 3±1 for the Savanna and Sahel). In the case of RxD20mm and RxD25mm, the general increase in response to increasing GWLs is noticed too. Only the coastal countries record significant increases in RxD20mm and RxD25mm, which could be due to the south-westerly moist flow from the Gulf of Guinea inland.

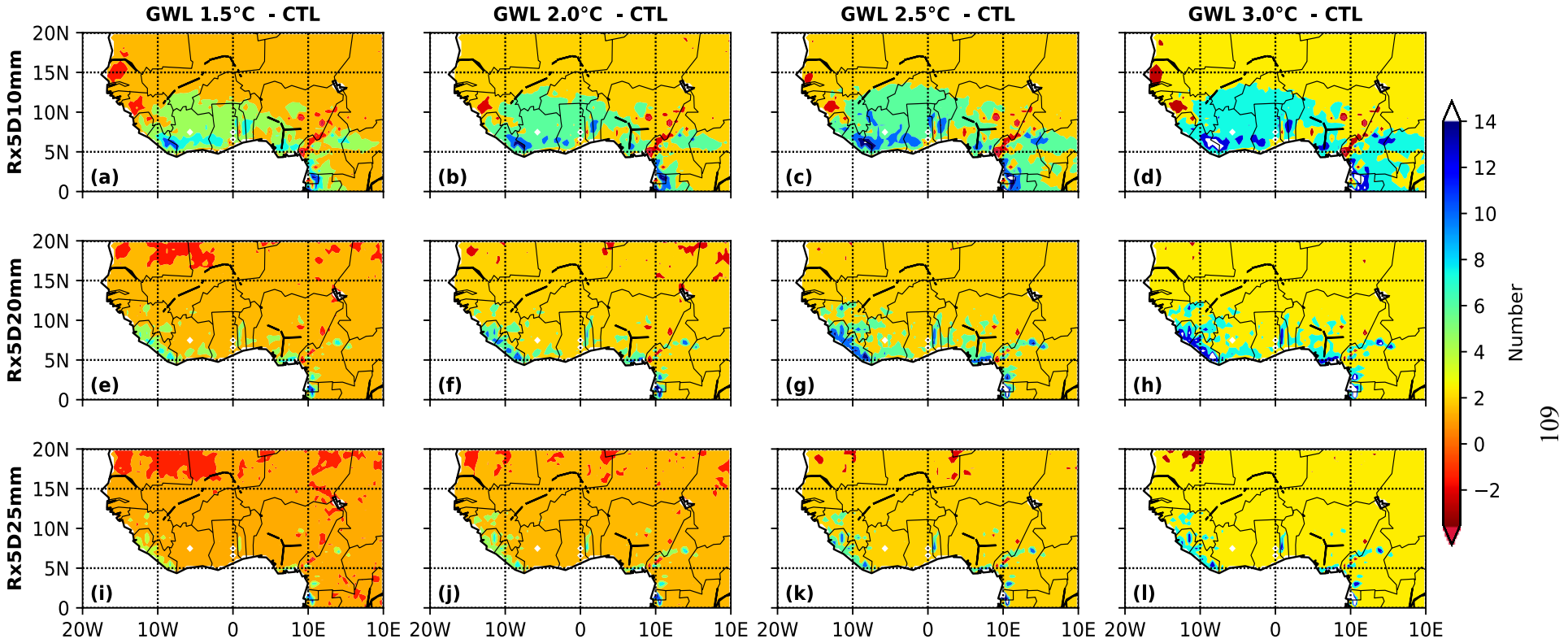

Figure 4.20: Spatial distribution of the change in frequency of intense rainfall events (RxD10mm), very intense rainfall events (RxD20mm), and heavy rainfall events (RxD25mm).

4.1.6 Adaptation strategies to mitigate the impact of the high variability of the precipitation

Since the spectacular drought events of the 1970s, it has become clear that the high variability in precipitation constitutes one of the major challenges faced by the West African region. Agriculture is one of the major economic activities of West Africa, and thus significant changes in rainfall due to climate change will negatively affect the entire region. These concerns have generated ongoing scientific, social and political debate. Moreover, some parts of West Africa (mostly along the Guinean Coast) have recorded recurrent flood events since 2000. Thus, both climate variability and increasing trends in droughts and floods and other severe weather events pose a challenge for the primarily rain-fed agriculture systems in West Africa (Sultan and Gaetani, 2016). Therefore, any adaptations must enable inhabitants to cope successfully with short-term climate variability as well as to reduce the long-term negative impacts of climate change (Lobell, 2014; Saba et al., 2013). Households and communities must become accustomed to and able to respond creatively and effectively to disruptions of their livelihoods. Indeed, in order to be successful, adaptations must be anchored in all processes affecting life. Some of the possible adaptation strategies, especially relating to floods, droughts and food crops, are illustrated in this study.

According to the results above, at increasing GWLs, precipitation over the Gulf of Guinea and the Savanna will shift and start earlier (in May) and that the highest precipitation concentration will occur in May-June over that area. In addition, intense rainfall events and consecutive wet days will increase in frequency, which can expose the Gulf of Guinea and Savanna to flood events from June onwards. This confirms the results from Donat et al. (2016), which showed that the intensification of the hydrological cycle both in recent decades and in future projections, will lead to an

increased risk of flooding in dry regions as the climate warms. Groundnut, cassava, and maize are important crops for the Gulf of Guinea, especially for Nigeria, southern Mali, Benin, Ivory Coast, Burkina Faso, Ghana, and Senegal, while over the Savanna, the main crops are yam, millet, and sorghum. Therefore, to inform farmers about short-term coping and adaptation practices, scientists are encouraged to simulate crop models, and to assess their uncertainties according to the shift in the times of the projected precipitation distribution and the increase in the soil temperature. Alternative strategies, such as constructing infrastructure or irrigation systems could also be used to mitigate the impact of exposure.

Regional provisions and strategies that include all West African countries should be developed to meet the challenge of combating GHG production. The framework agreements must link and bind countries to ensure strict compliance with community-based adaptation measures. At the local level, moreover, each country will have to develop precautionary flood and drought warning systems to limit the loss of human life. Scientific community frameworks need to be developed at the local level to improve the seasonal prediction of rainfall models that must be updated frequently in order to generate reliable information. Better research findings are needed to increase knowledge of how information structures could be framed and used to reduce the power of parochial conflicting benefits and overcome inertia, apathy, and lack of political drive. Finally, communication systems geared towards achieving specific targets (e.g., to assist farmers) will have to be developed. Informing media platforms about climate sciences and adaptation strategy policies and discussions, for instance, would educate the public about the impacts of global warming, the importance of reducing GHG emissions, and the need for developing and implementing mitigation and adaptation strategies.

In summary, this part of the present research work led to understanding the spatial variability of rainfall in West Africa. This variability correlates with the spatial concentration of the rainfall and creates a convergence of drought and flooding areas in West Africa. The study expects to record in short time a very important amount of rainfall particularly over coastal countries of Gulf of Guinea and also plans some potential flood episodes years in the future according to the analysis on the projections of global warming levels 1.5ºC, 2.0ºC, 2.0ºC and 3.0ºC under RCP8.5. Savanna's changes should not be much significant, because the CWD and CDD did not change enough and the distribution of the PCI showed a uniform distribution of precipitation during the rainy season and moderate distribution over the year. Under GWL perspectives, this research identified an earlier onset of rainfall and a considerable increase of both the variability of CDDs and CWDs and the intensity of rainfall especially over the Gulf of Guinea. Such significant information is useful for farmers and decision-makers to ensure the survival and prosperity of the population. Therefore, the study has extended its interest by addressing some adaptation strategies.

For a practical experiment, the study suggests using a regional climate model investigate on the prediction of a hydrological climate event, especially the flooding events in West Africa. For this purpose, the atmosphere-hydrology coupled model WRF-Hydro has been selected as a good candidate.

4.2 Present-day Climate Assessment with WRF-only and WRF/WRF-Hydro

4.2.1 WRF-Hydro calibration in offline mode

This section aims at implementing a seasonal flood forecasting with WRF-Hydro model. The study focuses on the evaluation of the precipitation and streamflow of the sub-basins. Therefore, the hourly simulations of WRF-Hydro streamflow are averaged to daily in order to match the timescale of the available observations. The WRF-Hydro is forced by WRF simulations (referred to as WRF-only) both on uncoupled and fully coupled modules.

4.2.1.1 WRF-only simulation

Figure 4.21 shows the comparison between the simulated WRF-only and observed datasets. The weekly WRF precipitation for the Savè catchment is relatively close to value derived from CHIRPS (Figure 4.21a) and TRMM (Figure 4.21b), with a mean coefficient of determination (R^2) equal to 0.64, and 0.59 respectively. The agreement between the two observed datasets (CHIRPS and TRMM) is about 0.87 for R^2 (Figure 4.21c), showing that the observed precipitation datasets are close with little uncertainty.

Figure 4.21d shows the annual cycle of the daily rate of precipitation at Savè for the WRF simulation, and observed datasets (CHIRPS and TRMM). WRF-only simulates well the observed precipitation CHIRPS dataset is closed to WRF-only as showed both the Figure 4.21b and Figure 4.21d, this is consequently due to the high resolution of the two datasets (WRF-only and CHIRPS), recall that the spatial resolution of WRF-only is 5-km and the one for CHIRPS is 0.05º.

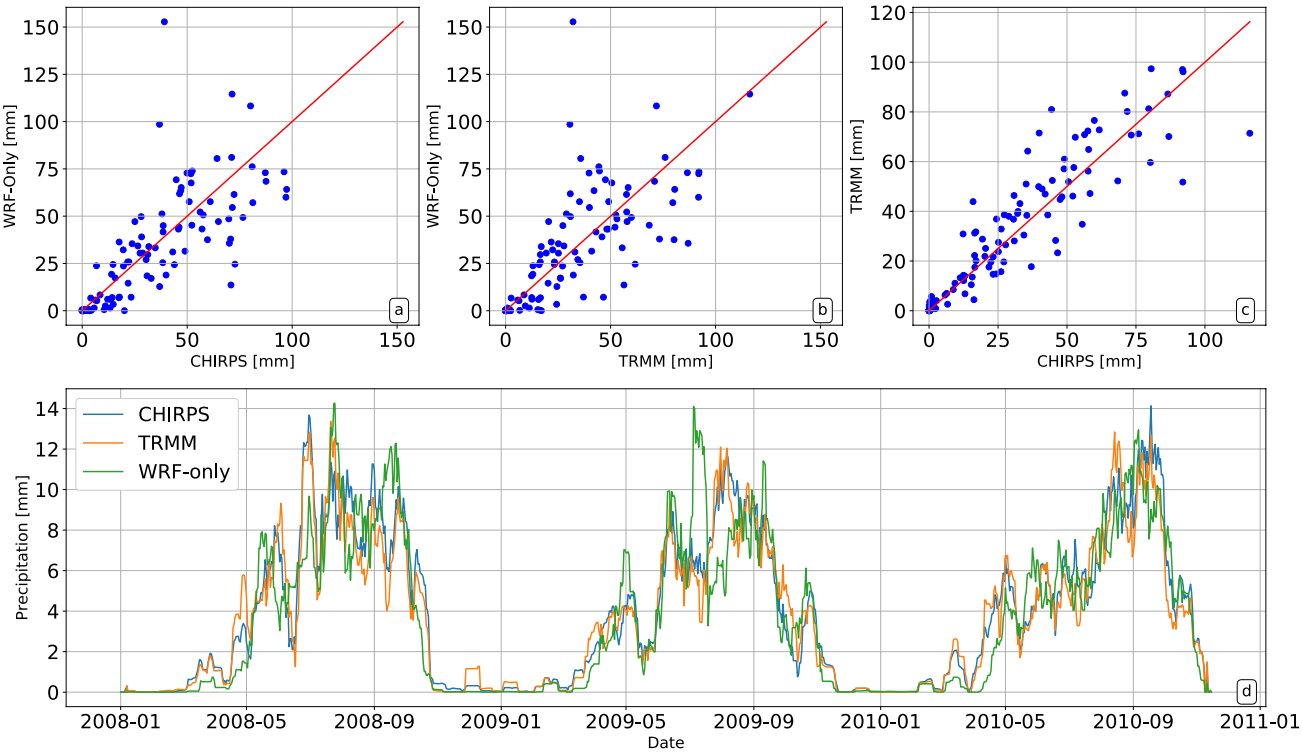

Figure 4.21: Scatter plots of simulated WRF-only vs. observed (a- CHIRPS , and b- TRMM) weekly cumulative precipitation for period the 2008-2010, c) comparison between observed, and d) analysis of 7-day filtered daily precipitation for WRF-only, CHIRPS , and TRMM.

4.2.1.2 Calibration and evaluation of WRF-Hydro

There are a number of parameters in the Noah LSM which are associated with large uncertainties that impact hydrological model outputs. In view of this, model calibration is necessary before its application (Gochis et al., 2015). Prior to use the model WRF-Hydro for flood forecasting, the study purposes to simulate at offline module the model with the default parameters over the Ouémé-river at Save outlet (referred to as Savè) using the forcing from WRF and WRF-modified (the precipitation in WRF output is replaced by TRMM after its interpolation from 3-hourly to hourly). Figure 4.22 presents the results of this offline assessment of the model WRF-Hydro with WRF output as forcing. It is noticed that the model capture fairly the temporal variation of the observed, but misrepresents the magnitude and reproduce somehow the peaks. The correlation coefficient (Corr) is high because this efficiency coefficient focuses on the similitude trend of the shape of the model and the observed. The NSE and the KGE coefficient respectively 0.20 and 0.09, inform on the misjudgment of the model in respect to the observed, it underestimates the high flow and overestimates the low streamflow. Even these values of NSE and KGE obtain for the simulation are influenced by the low discharge during the dry season at Savè (January-June). To achieve the goal of the study, we task to calibrate the model over Savè by selecting the optimized parameters in offline simulations. The calibration method adopted is inspired from Yucel et al. (2015), which is otherwise referred to as "stepwise approach". This kind of method is based on manual calibration approach because the automatic calibration methods require a high number of model runs with excessive computational time; an option which is not possible in the current study (Yucel et al., 2015). The calibration period considered here is the whole year 2008, as mentioned by Senatore et al. (2015) one-year calibration is considered long enough to evaluate the basic parameter sensitivities. As used in the case of the

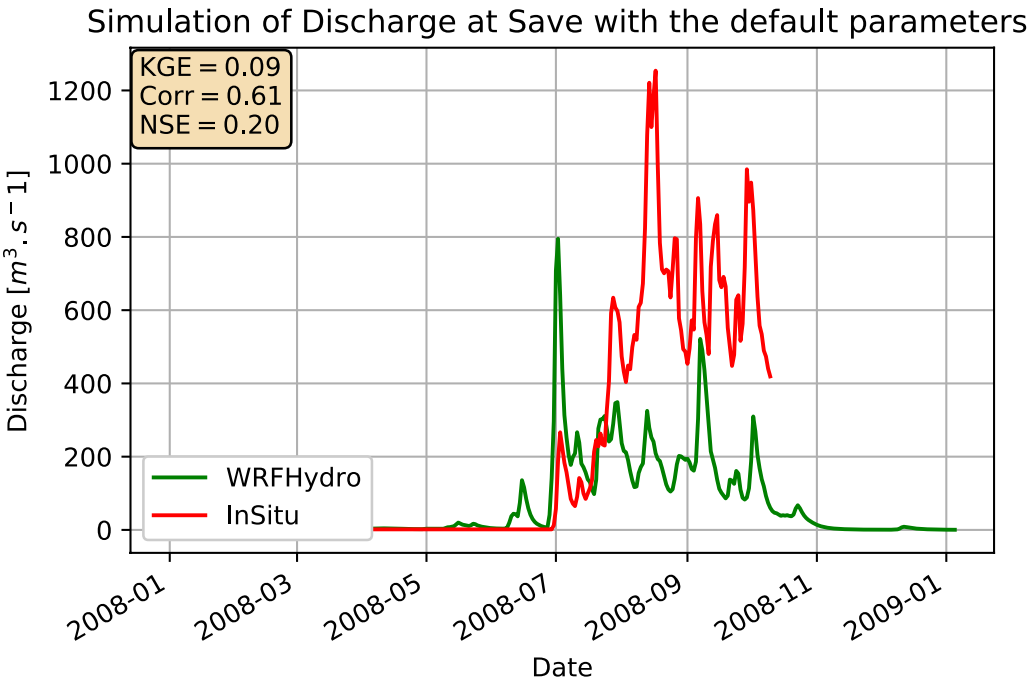

Figure 4.22: Simulation of the uncoupled WRF-Hydro model with the default parameters for the period 01 January 2008 to 01 January 2009 at Savè catchment.

evaluation of the model with default parameters, the optimized parameters are selected based on those statistics, namely the correlation (Corr), the Nash-Sutcliffe efficiency (NSE) and the KGE used as efficiency criteria. The NSE checks the correspondence between modeled and observed discharge. It can be used to indicate how well the plot of observed versus the modeled discharge fits the line $y = x$ (Moriasi et al., 2007). The NSE is ranged from $-\infty$ to 1 with values between 0 and 1 that indicate acceptable performance, while values ≤ 0 shows that the mean of observed data is a better predictor than the modeled thus the results are considered unacceptable (Moriasi et al., 2007).

The Table 4.2 presents some of the results of the calibration and shows that in this study, the calibration is performed for the Savè catchment for the sensitive parameters such as REFKDT, SLOPE, RETDEPRTFAC, OVROUGHRTFAC, and MannN. The REFKDT is ranged between 0.1 and 10 with a default value 3.0, while the RETDEPRTFAC settable with the same range has as default value 1.0 (Gochis et al., 2015). The SLOPE varied between 0.1 and 1.0 as well as the OVROUGHRTFAC. The first parameter evaluated is one of the parameters controlling the total water volume (REFKDT) with the value ranging from 0.1 to 8.0 with 0.1 increments. Since the default simulation (REFKDT = 3.0) show the underestimation of the observed, the REFKDT value shall be reduced to disable many infiltrations. As in Arnault et al. (2016) for the case of the Sissili in West-Africa and Kerandi et al. (2017) in Kenya, we find that the model discharge performance is highly sensitive to parameter REFKDT. The REFKDT = 1.5 represents the one which perform the observed better than the default simulation with the statistics considered (NSE = 0.52, KGE = 0.49, and Corr = 0.58). For the evaluation of the RETDEPRTFAC aim to adjust the initial retention depth (which is equal to 1 mm in the model). Scaling factors (RETDEPRTFAC) between 0 and 10 with 1.0 increment show that the modeled discharge remains the same regardless of the change in

Table 4.2: Selected objective criteria (correlation coefficient: Corr, Nash-Sutcliffe efficiency: NSE and Kling-Gupta Efficiency: KGE) between simulated WRF-Hydro and observed discharge at Savè based on the infiltration-runoff parameter REFKDT, retention factor RETDEPRTFAC, the SLOPE, the overland flow roughness scaling factor OVROUGHTFAC and the Manning's roughness coefficients MannN. Experiments in italics bold show the selected parameters' value and the best Corr, NSE and KGE after calibration.

REFKDT									
Range	0.1	0.5	0.8	1.0	**1.5**	2.0	3.0	3.5	4.5
NSE	0.29	0.33	0.38	0.46	**0.52**	0.34	0.20	0.17	0.11
Corr	0.64	0.67	0.63	0.63	**0.58**	0.60	0.61	0.64	0.60
KGE	0.38	0.39	0.41	0.47	**0.49**	0.32	0.09	0.07	0.07
RETDEPRTFAC									
Range	0.0	**1.0**	2.0	3.0	4.0	5.0	6.0	7.0	8.0
NSE	0.50	**0.52**	0.49	0.49	0.49	0.49	0.49	0.49	0.49
Corr	0.58	**0.58**	0.59	0.59	0.59	0.59	0.59	0.58	0.58
KGE	0.48	**0.49**	0.49	0.49	0.48	0.46	0.47	0.46	0.46
SLOPE									
Range	0.1	**0.2**	0.3	0.4	0.5	0.6	0.7	0.8	0.9
NSE	0.52	**0.61**	0.60	0.50	0.37	0.20	0.12	-0.03	-0.23
Corr	0.58	**0.62**	0.65	0.65	0.66	0.61	0.63	0.55	0.61
KGE	0.49	**0.56**	0.52	0.39	0.33	0.24	0.19	0.11	0.04
OVROUGHRTFAC									
Range	0.2	0.3	0.4	0.5	**0.6**	0.7	0.8	0.9	1.0
NSE	0.60	0.60	0.60	0.61	**0.63**	0.62	0.62	0.61	0.61
Corr	0.67	0.65	0.61	0.60	**0.66**	0.66	0.64	0.64	0.62
KGE	0.56	0.56	0.57	0.60	**0.60**	0.60	0.59	0.56	0.56
MannN									
Range	0.2	0.4	0.6	0.8	1.0	1.4	**1.6**	1.8	2.0
NSE	0.42	0.44	0.50	0.56	0.61	0.62	**0.66**	0.62	0.60
Corr	0.66	0.63	0.73	0.68	0.70	0.72	**0.67**	0.69	0.67
KGE	0.36	0.37	0.41	0.48	0.50	0.57	**0.63**	0.60	0.61

RETDEPRTFAC, as the scores are very close to each other. As mention by Gochis et al. (2015), increases in the RETDEPRTFAC on channel pixels can encourage more local infiltration near the river channel leading to wetter soils. Therefore the default RETDEPRTFAC = 1.0 seems to provide better results and will be considered such for the next calibration steps. In the case of the present study, the uncoupled model WRF-Hydro is also very sensitive to the parameter SLOPE. The optimized value of the parameter SLOPE is 0.2. The parameters controlling the hydrograph shape are also investigated. As illustrated by Yucel et al. (2015) the surface roughness (OVROUGHRT) plays an important role in transmitting infiltration excess water to channel networks and is calibrated in WRF-Hydro using a scaling factor (OVROUGHRTFAC) between 0.2 and 1.0 with 0.1 increments. Considering the correlation coefficient (Corr), the NSE and the KGE statistics and hydrograph shape match between simulated and observed hydrographs at Savè, the scaling factor value of OVROUGHRTFAC = 0.6 is judged as the best to fit the simulated hydrograph to the observed hydrograph.

After the surface runoff is transmitted to the river network, the conveyance of water along the channels also affects hydrograph shape Yucel et al. (2015). Channel properties are introduced into the model as average channel base width (Bw), initial water depth (HLINK), channel slope (Ch SSlp), and Manning coefficient (MannN) based on each stream order (St Order). The default channel parameter values are provided in Table 4.3. Only the channel roughness (Manning coefficient: MannN) parameter is calibrated, the others are maintained constant. The scaling factor (MANN) is ranging between 0.2 and 2.0 with 0.2 increments. The calibrated value is then obtained with the scaling factor MANN = 1.6.

Table 4.3: Channel parameter values of base width (Bw), initial water depth (HLINK), channel slope (Ch SSlp), and Manning coefficient (MannN) based on each stream order (St Order) : default channel parameter values

St order	Bw	HLINK	Ch SSlp	MannN
1	5	0.02	1	0.65
2	10	0.02	0.6	0.50
3	20	0.02	0.3	0.45
4	30	0.03	0.18	0.35
5	40	0.03	0.05	0.20
6	60	0.03	0.05	0.12
7	60	0.03	0.05	0.03
8	60	0.1	0.05	0.03
9	60	0.3	0.05	0.03
10	60	0.3	0.05	0.03

The five parameters evaluated are summarized in Table 4.2 within italics-bold the selected parameters' values and the best NSE, Corr, and KGE after calibration. It can be seen that the observed discharge hydrograph at Savè is reasonably well reproduced with KGE, and Corr equal to 0.63, and 0.67 respectively, between March and December 2008 (Figure 4.23a). In all subsequent simulations, the calibrated parameters for the Savè catchment are held as such.

The calibrated model is evaluated offline for the period P_2: 2009-2010 (Figure 4.23b). The above-mentioned efficiency criteria allow us to evaluate the performance of the model. It can be noticed that it fairly well simulates the trend and peaks of the observed discharge, even slightly better in comparison to the calibration period, with model efficiencies KGE of 0.86 and Corr of 0.87. This enhanced performance for the validation period is related to the much higher discharge peak in 2010, i.e. the flooding year, which is fairly well reproduced by the model. Globally, for the simulation period P (2008-2010), WRH-Hydro in offline mode is able to simulate discharge with KGE and Corr equal to 0.70 and 0.74.

The robustness of the calibrated model in the uncoupled module is also evaluated over the Bétérou catchment (an inner-domain to Savè basin). Figure 4.24 shows a best-fit performance of the model in simulating the shape of the observed hydrograph at Bétérou. It reproduce somehow well the peaks of discharge, the trend of the shape of the observed hydrograph is also well reproduced. The performances of the model are revealed by the statistics KGE = 0.74, Corr = 0.85 and NSE = 0.68 for the calibration period over Bétérou catchment for the uncoupled module simulation.

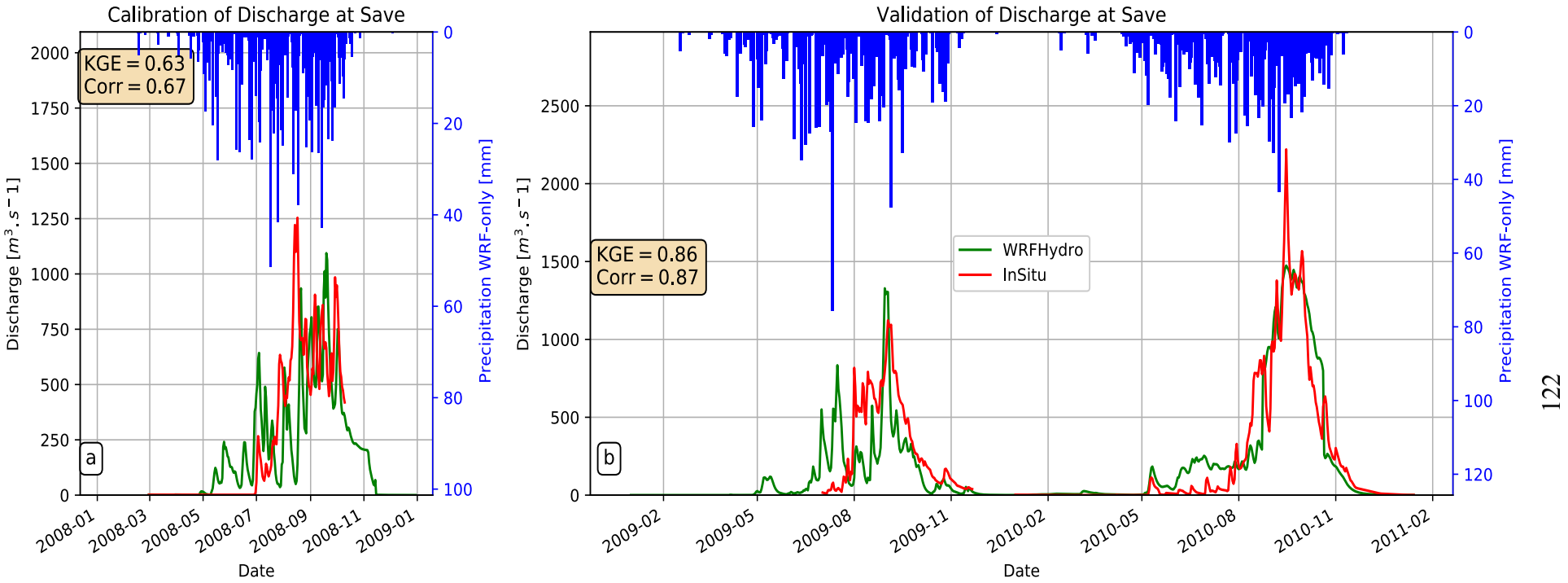

Figure 4.23 : Observed and simulated (uncoupled WRF-Hydro) daily hydrographs at Savè, and catchment-averaged daily precipitation derived from WRF-only: a) calibration period 2008; b) validation period 2009-2010.

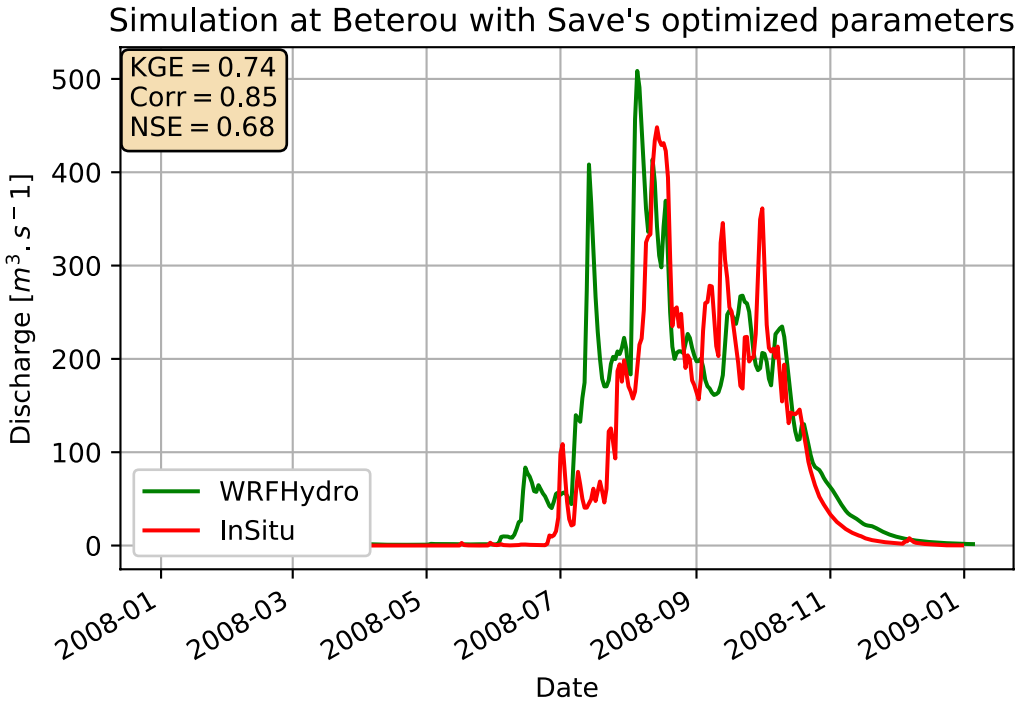

Figure 4.24: Evaluation of the uncoupled calibrated WRF-Hydro model over Bétérou catchment during the calibrated year (2008)

The assessment of the calibrated model WRF-Hydro in the online module (fully coupled mode) is performed by simulating the coupled WRF-Hydro model with an update of optimized parameters resulting from uncoupled WRF-Hydro. This calibrated model of WRF-Hydro will be referred to as WRF-H. It is used to assess the performance of the WRF-Hydro to simulate discharge and precipitation in the research area. Figure 4.25 presents the simulation result of WRF-H at Savè for the three years 2008-2010, whilst Figure 4.26 presents the simulation result at Bétérou for the same period. At Savè, the daily discharge is well reproduced for each simulation with only 13% bias and NSE about 0.64, the KGE resulting is 0.76 and the Correlation coefficient 0.84. These statistics demonstrate how better is the performance of WRF-H compare to the uncoupled simulation WRF-Hydro. The same better performance of WRF-H is noticed in the case of simulation at Bétérou with also a low bias comparing the simulated model to the observed. The Nash-Sutcliffe Efficiency (NSE = 0.46) is a bit lower than Savè, while the KGE and the Corr are respectively equal to 0.66 and 0.79. At Bétérou the model overestimates the low flow for the year 2008 and 2009, and simulate well the relevant peaks.

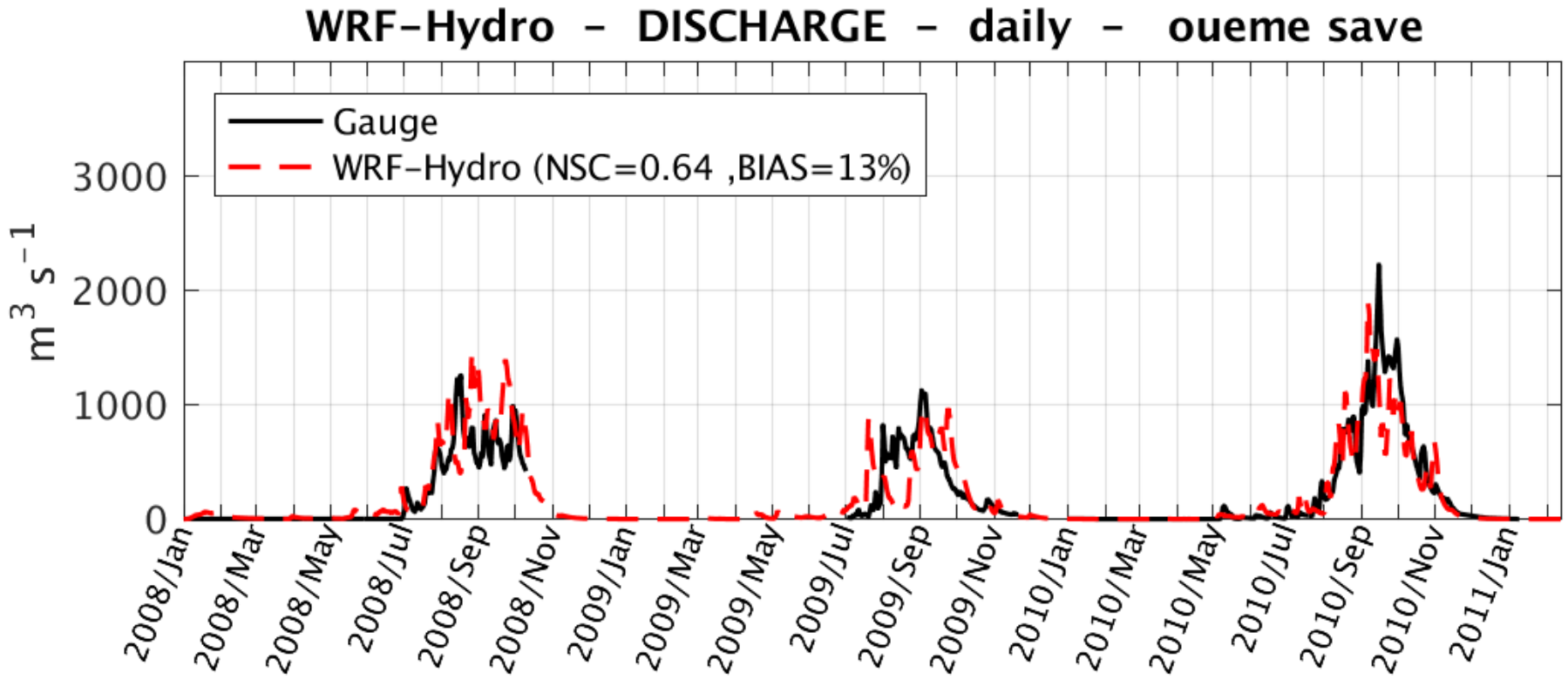

Figure 4.25: Fully coupled simulation of WRF-Hydro (WRF-H) at Savè for whole experimental period. The Gauge represents the observed discharge at Savè outlet, and WRF-Hydro is the simulated discharge with WRF-H.

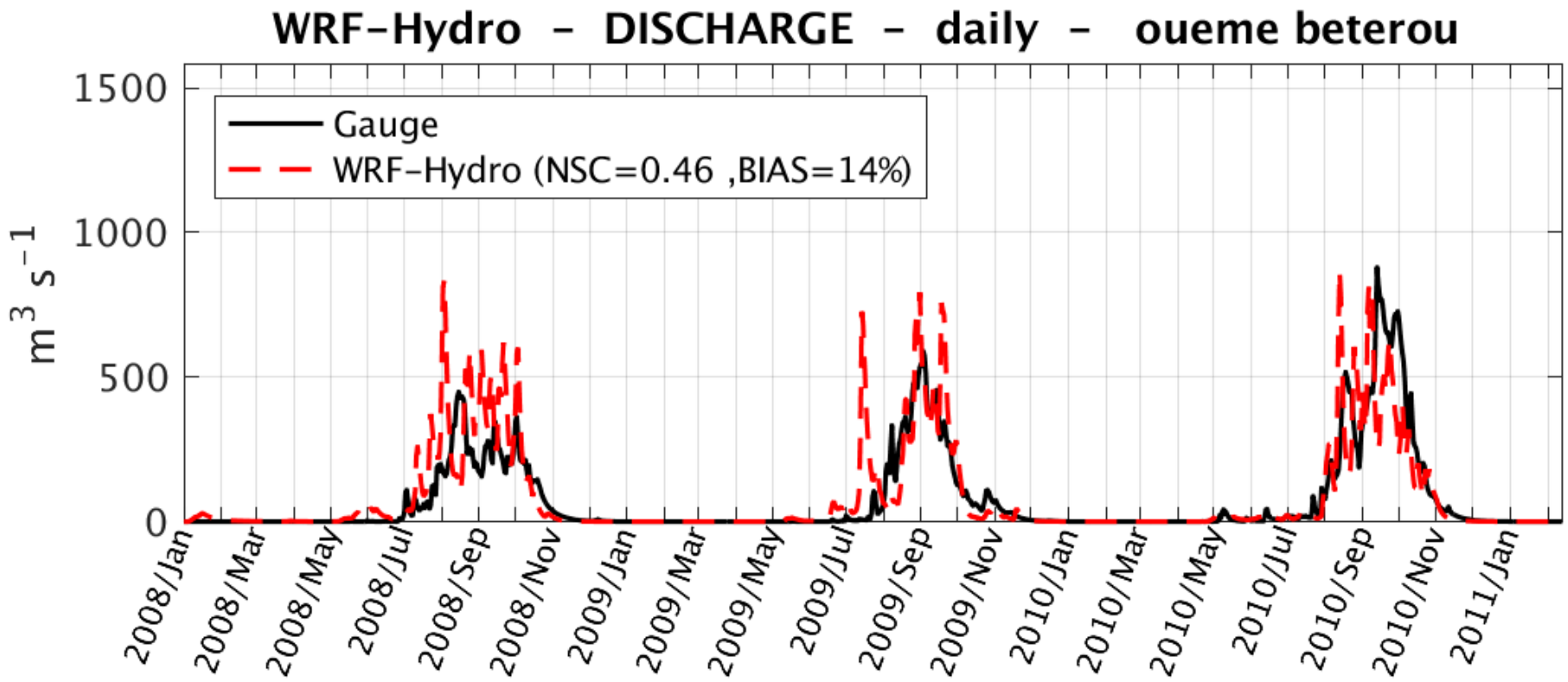

Figure 4.26: Fully coupled simulation of WRF-Hydro (WRF-H) at Bétérou for whole experimental period. The Gauge represents the observed discharge at Bétérou outlet, and WRF-Hydro is the simulated discharge with WRF-H.

4.2.2 Evaluation of WRF-H

In this section, the assessment of the WRF-H in the research area is leading into two variables: the precipitation and the discharge.

4.2.2.1 Precipitation simulations

The simulated precipitation of the model WRF-H is assessed both temporally and spatially scales for the rainy season of the period 2008-2010 according to the research interest (flood). Figure 4.27 exposes comparison between the weekly precipitations from WRF-only, WRF-H, and observed datasets. The R^2 in Figure 4.27.a, which compares WRF-H and WRF-only, is equal to 0.88. This shows clearly that WRF-only and WRF-H simulate differently precipitation, which was already illustrated by Givati et al. (2016), Naabil (2017) and Senatore et al. (2015). Figure 4.27b and 4.27c compare WRF-H with CHIRPS and TRMM, and it illustrates a good agreement between these datasets. The slightly better agreement of CHIRPS (compared to TRMM) with WRF-only (Figure 4.21b) and WRF-H (Figure 4.27b) could be explained by the high resolution of both CHIRPS and WRF-H precipitation. Indeed, the comparison between Figures 4.21 and 4.27 illustrates that WRF-H performs slightly better than WRF-only in term of daily and weekly precipitation. Figure 4.27d enhances these results with Corr equal to 0.68 between WRF-H CHIRPS against 0.59 between WRF-H and CHIRPS.

Klein et al. (2015) showed that the high variability of precipitation in West Africa results from a large uncertainty in WRF simulations. This uncertainty is investigated in details in section 4.3 by modifying boundary conditions with a stochastic perturbation. The difference between simulated precipitation and CHIRPS is analyzed in Figures 4.28 and 4.29. Figure 4.28 presents the monthly trend of precipitation and shows that precipitation records during the two last months (August and September) in 2010 are

highest in comparison to 2008 and 2009. The simulated precipitation WRF-H follow well the trend of the observation CHIRPS. The Figure 4.29 presents the spatial distribution of precipitation in domain D2 during the rainy season period June to September (JJAS) in 2010 (the flooding year). The difference between the two models (Figure 4.28c) shows either WRF-H underestimated or overestimated simulation in comparison to WRF-only, depending on the location (as in Wagner et al., 2016). The mean precipitation in domain D2 is about 864 mm for WRF-only, and 947 mm for WRF-H. This means that WRF-H increases the simulated precipitation from WRF-only by about 1%. The observed precipitation in this domain is about 817 mm i.e., less than simulated precipitation from both WRF-only and WRF-H. Similar results are obtained for the Savè catchment, with seasonal spatial-averaged precipitation of 1049 mm for WRF-H, 998 mm for WRF-only and 977 mm for CHIRPS.

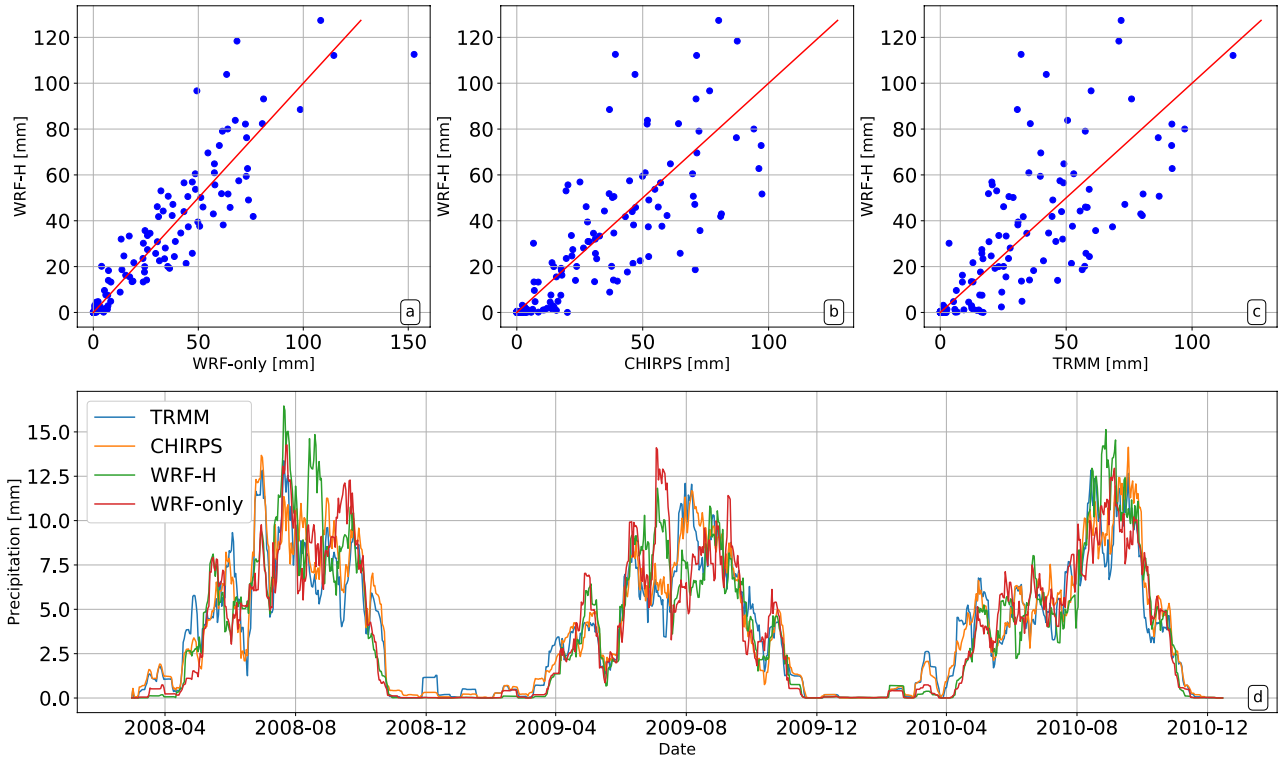

Figure 4.27: Evaluation of weekly simulated precipitations with observed datasets at Save-catchment: a) WRF-H vs. WRF-only, b) WRF-H vs. CHIRPS, c) WRF-H vs. TRMM, and d) analysis of 7-day filtered daily precipitation for WRF-H, WRF-only, CHIRPS and TRMM.

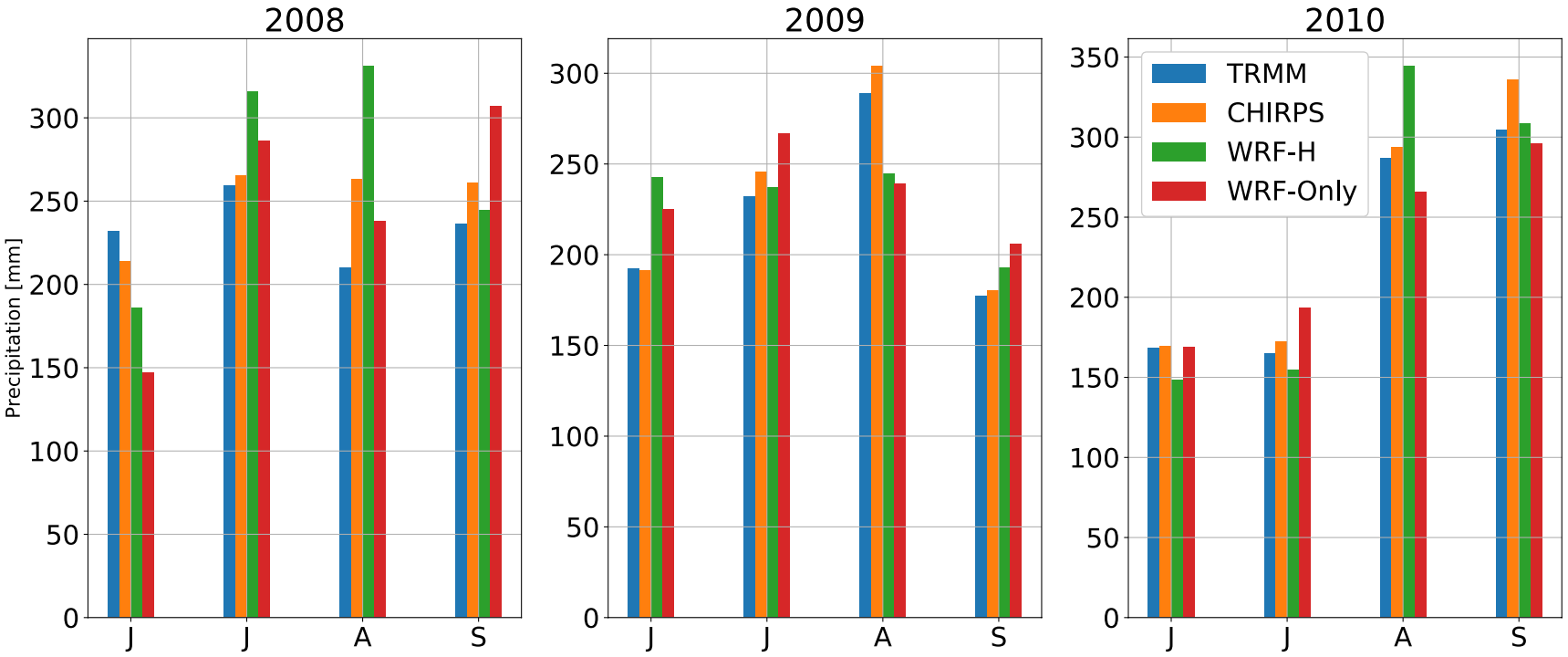

Figure 4.28: Precipitations trend in June-September (JJAS) at Savè catchment for the period 2008-2010

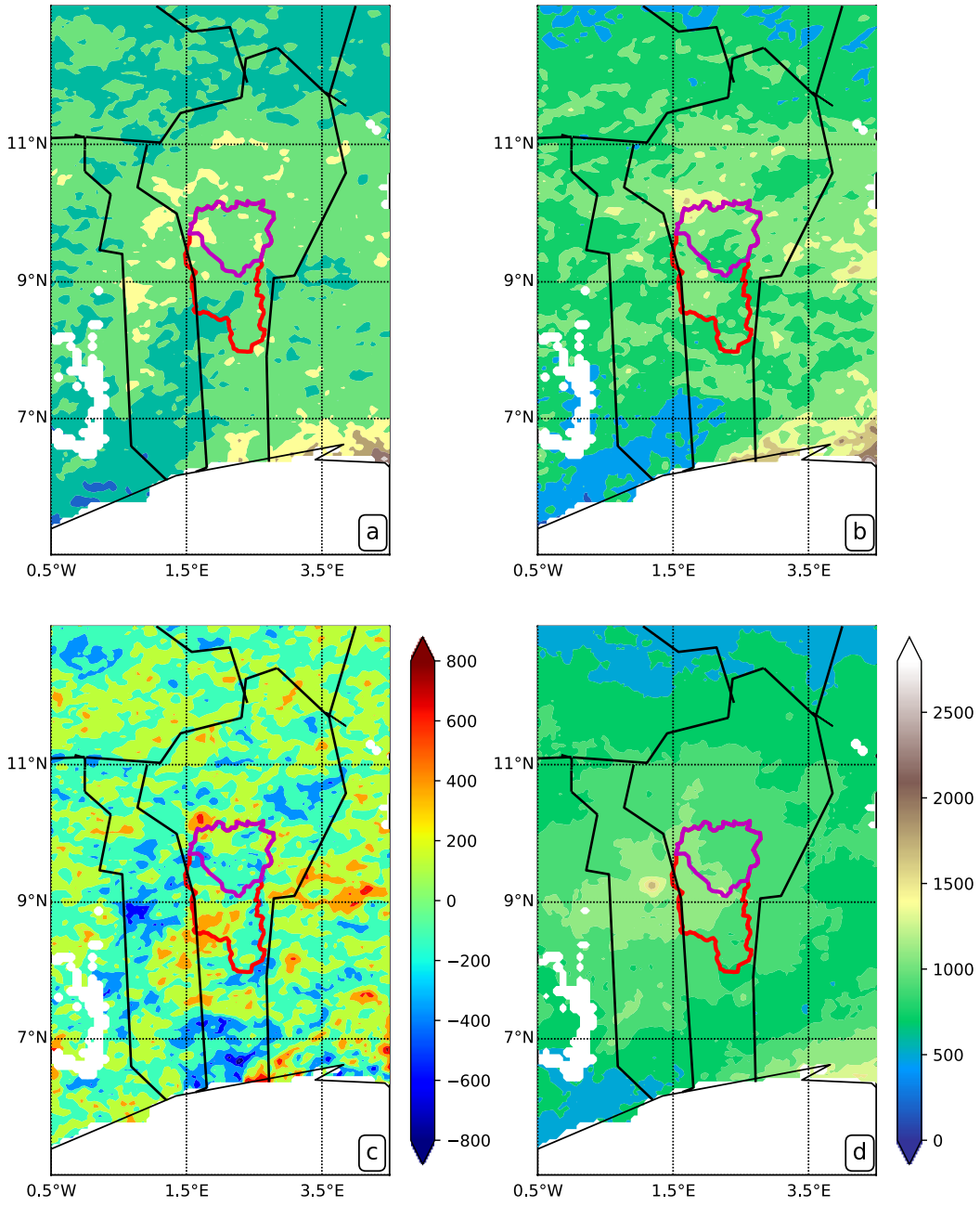

Figure 4.29: JJAS precipitations for the flooding year 2010 with Savè-catchment (red contour), and Beterou-catchment (purple contour): a) WRF-only simulations, b) WRF-Hydro (WRF-H) simulations, c) difference between WRF-H and WRF (WRF-H minus WRF), and d) CHIRPS precipitation. The colorbar of Figure 5d is used as common colorbar for Figure 5a, b, d.

Since the model performed well for both Savè and Bétérou, the following analysis focused on those two basins of Ouémé-river. Figure 4.30 and Figure 4.31 present respectively the cumulative precipitations derived from WRF-H, and the satellite datasets CHIRPS and TRMM at Bétérou and Savè. A perfect reproductivity of observed dataset by WRF-H is noticed, and also the clear rainy season period is also well captured by the model. The total seasonal precipitation is based on one rainy season from April to October over the basins. The cumulative seasonal amount is indicative of the average of annual precipitation for the given year for the region. According to Figures 4.30 and 4.31 we can make the assumption that there is no or negligible rainfall recorded in the dry season. At Bétérou (Figure 4.30), the model fairly underestimates the cumulative precipitation compared to TRMM and CHIRPS, albeit it shows a good capture of seasonal variability over the years. The respective total amounts are WRF-H = 3921 mm, TRMM = 4077 mm and CHIRPS = 4000 mm, which confirm consistency with results discussed above that the WRF-H precipitation simulations are closer to the observed CHIRPS than TRMM. The bias of the cumulative precipitation is between -8.82% and 0.00% in regard to TRMM and between -8.16% and 2.13% for CHIRPS. At Savè (with WRF-H = 3883 mm), conversely to analysis at Bétérou the model fit well the total seasonal cumulative precipitation of TRMM (about 3985 mm) than CHIRPS (4020 mm). The error related to the evaluation of the cumulative precipitation is between -5.82% and 2.18% for TRMM and about -7% and 0% for CHIRPS. Figure 4.28 illustrates that as in the case of Bétérou (Figure 4.28), despite the underestimation of the cumulative precipitation by the model, it captures also well the seasonal variability over the years.

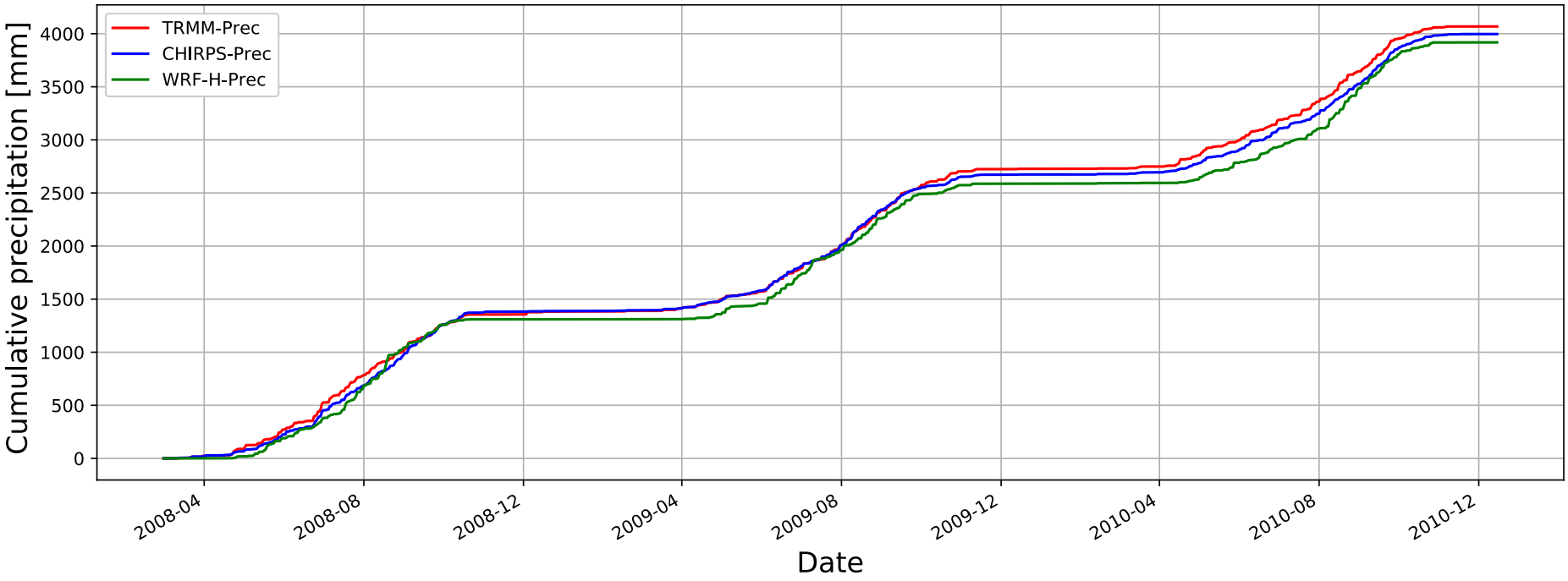

Figure 4.30 : cumulative total precipitation derived from TRMM, CHIRPS and simulated in WRF-H over Bétérou during the period 2008 to 2010

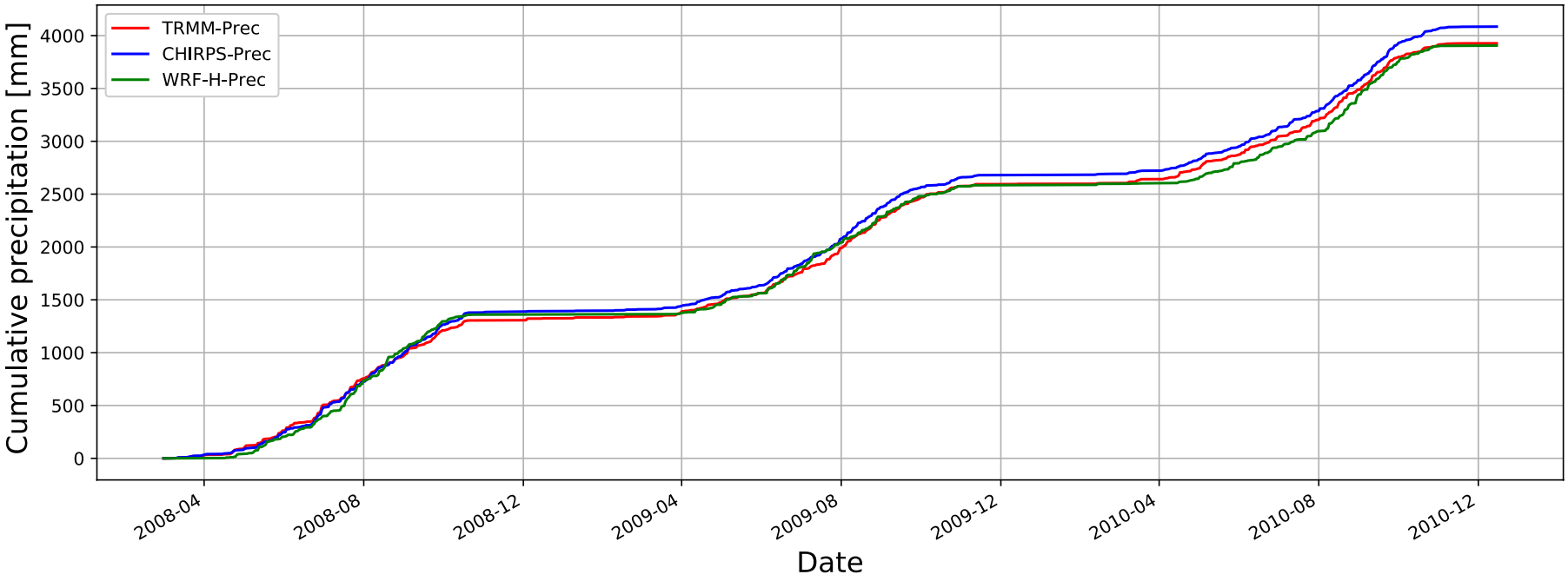

Figure 4.31: cumulative total precipitation derived from TRMM, CHIRPS and simulated in WRF-H over Savè during the period 2008 to 2010.

4.2.2.2 Discharge simulations

Discharge results at Savè are displayed in Figure 4.32a (similar to Figure 4.25), showing the daily time series of simulated (green) and observed (red) stream discharges and related WRF-H precipitation (blue) for the period 2008-2010. A good agreement can be seen between the observed and the simulated hydrographs, and an approximate good representation of the peaks of the discharge as well as hydrograph shapes, as quantified by the performance measures KGE and Corr (0.76 and 0.84 respectively). This performance, in comparison with the offline simulation, could be explained by the time step of the meteorological data in fully-coupled mode, which is 30s and not hourly as in offline mode. Since one of the objectives of the study is to evaluate the performance of WRF-H to simulate the discharge, and therefore to predict potential floods, the study focuses on the ability of the model in reproducing only the rainy seasons. For Savè's case (Figure 4.32), KGE equal to 0.22, 0.64 and 0.80 are obtained for the rainy seasons of 2008, 2009 and 2010 respectively, which give important information about the model's simulation skills. Also, it is noted that the model has a better performance in 2010.

The robustness of the calibrated WRF-H over Savè is evaluated in a second catchment, i.e. the Bétérou (Savè's inner-catchment), which is illustrated in Figure 4.32b. Figure 4.32b shows that WRF-H reproduces well the discharge trend as well as the peaks so that WRF-H can also be used successfully for this inner-catchment. Table 4.4 illustrates the discharge peaks obtained for basins during the three years. An evaluation from a recent work of Hounkpè et al. (2015) revealed that the averages of annual rainfall between 1960 - 2007 are 1205 mm at the Bétérou rainfall station and 1098 mm at Savè. The dynamics of the flow is characterized by a high discharge during the rainy season.

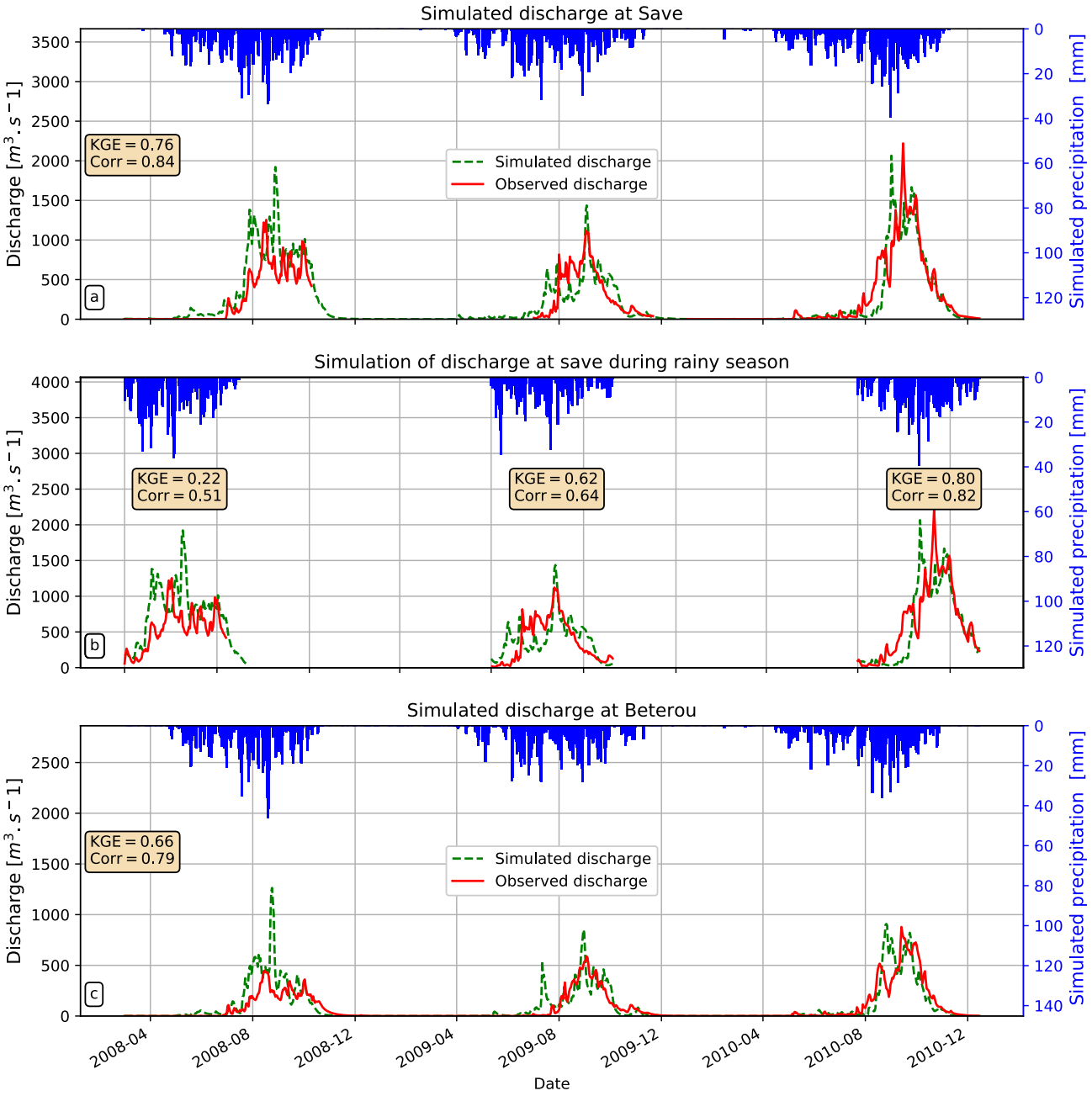

Figure 4.32: Observed and simulated (fully coupled WRF-Hydro) hydrographs and derived precipitation from WRF-Hydro: a) full year at Savè, b) rainy season at Savè, and c) at Bétérou (Savè's inner catchment)

Table 4.4 : Summary of yearly highest and lowest discharge values both for simulated WRF_H and station dataset, following by KGE during the rainy season.

		Catchment	
		Savè	Bétérou
2008	High value observed	1250 m^3/s	500 m^3/s
	High value simulated	1935 m^3/s	1320 m^3/s
	KGE	0.22	0.16
2009	High value observed	1127 m^3/s	572 m^3/s
	High value simulated	1453 m^3/s	854 m^3/s
	KGE	0.62	0.69
2010	High value observed	2200 m^3/s	930 m^3/s
	High value simulated	2090 m^3/s	950 m^3/s
	KGE	0.80	0.84

The maximum flow between May and September over the period 1960-2007 is in order of 240 to 740 m^3/s at Bétérou and 1000 to 1750 m^3/s at Savè outlet. From November to May, almost all the rivers dry up and the averages of low flows are about $5m^3/s$ at Savè, and $2m^3/s$ at Bétérou.

WRF-H is able to capture the flood event, which occurred in September-October 2010 over Savè as well as over Bétérou. In particular, although the predicted highest discharge peak occurs earlier than in the observed datasets at Savè and Bétérou. The second "weak" peak in 2010, which could amplify damage intensities of the flood in the study area, is also well reproduced. According to results from Figure 4.32, this second "weak" peak should result from the highest precipitation simulated and observed in September 2010. The first important peak at Savè in 2010 is also reflected from the highest simulated precipitation of August 2010.

To consolidate the previous analysis, the Figures 4.33 and 4.34 are plotted, and presented respectively over Bétérou and Savè for further comparison on the one hand, the simulated and observed discharge at daily time step for the whole WRF-H evaluation period (2008-2010), and the flooding period (2010) based on linear regression with values of the line 1:1 and coefficient of determination (R^2); and on the other hand, the cumulative discharge of simulated and observed datasets. Figure 4.33a indicates that at Bétérou the WRF-H underestimates the low flows, whilst in contrast at Savè (Figure 4.34a), it fairly well extracts the low flow. This underestimation of the low flow at Bétérou and somehow at Savè is related to the fact that in early August at the beginning of the rainy season over the sub-basins, the model started produce streamflow (2008 and 2009 on Figure 4.32b and Figure 4.32c). The Figure 4.34b demonstrate that the underestimation of the low flow at Savè is due to the lags noticed between the simulated and observed "peaks". Globally, WRF-H captures well the variability of the seasonal

discharge for Savè and Bétérou, but overestimate the cumulative total discharge (Figure 4.33c and Figure 4.34c). These figures also indicate that the discharge is recorded from July to November with high increase in August-September. The total volume of discharge observed at Bétérou during the period 2008-2010 is 86,045 m^3 against 100,182 m^3 for the WRF-H simulation, given rise of 16% as a difference. At Savè, the recorded total volume of water is about 186,475 m^3, while the corresponding simulated discharge is approximately 220,367 m^3, overestimating the observed discharge up to 18%.

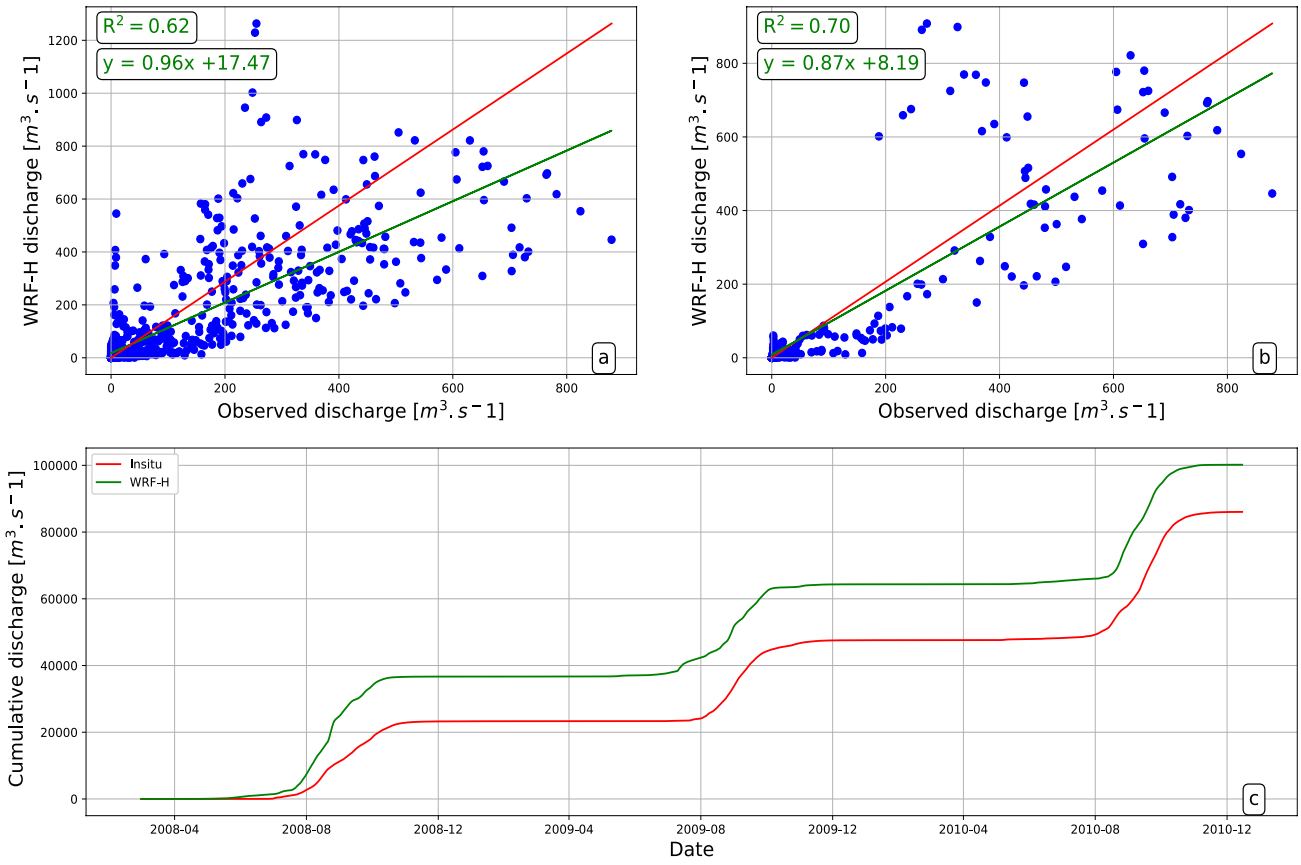

Figure 4.33: Scatter plot showing comparison of simulated and observed discharges (a - for the period 2008-2010, and b- for the flooding year 2010), and the cumulative totals of simulated and observed discharge at Bétérou

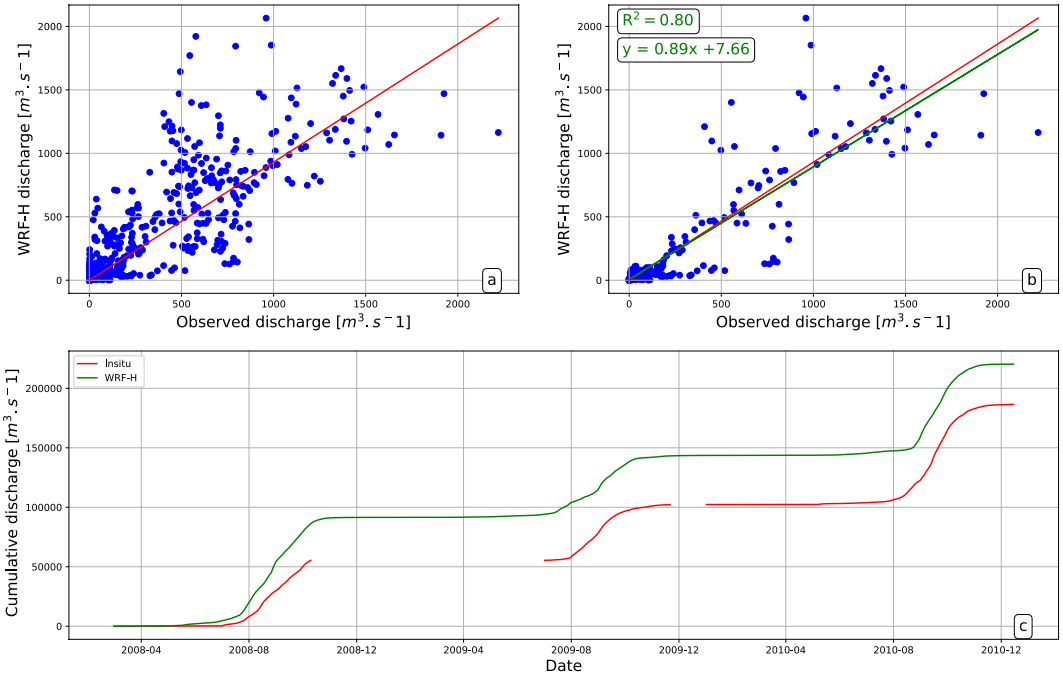

Figure 4.34: Scatter plot showing comparison of simulated and observed discharges (a- for the period 2008-2010, and b- for the flooding year 2010), and the cumulative totals of simulated and observed discharge at Savè.

4.2.3 Evaluation of the uncertainty of WRF-H

In order to evaluate the forecasting uncertainties of WRF-H, we introduce a stochastic kinetic-energy backscatter scheme (SKEBS: Berner et al., 2015, 2009; Shutts, 2005) and evaluated its impact on the predictability of streamflow and the precipitation with WRF-H. The scheme is used and activated in WRF-Hydro; it is referred to as WRF-H-SKEBS. The purpose here is that the SKEBS approach adds random perturbations with prescribed spatial and temporal decorrelations. In particular, SBEKS produces perturbation into the lateral boundary conditions. The amplitude of the stochastic perturbations is chosen as the default in WRF-H. An ensemble of 10-member is performed for this task. Both stochastic physics and initial condition perturbations into WRF-H-SKEBS result in an ensemble spread for the three rainy seasons. Figure 4.35 shows that WRF-H-SKEBS has a relatively large impact on precipitation and discharge results in the study region. The ensemble also results in a large range of simulated discharge performance, as can be seen in Table 4.4. This result demonstrates the sensitivity of WRF-H to lateral boundary perturbations and confirms the uncertainty of the model regarding discharge and precipitation simulations, which is of uttermost importance for flood forecasting.

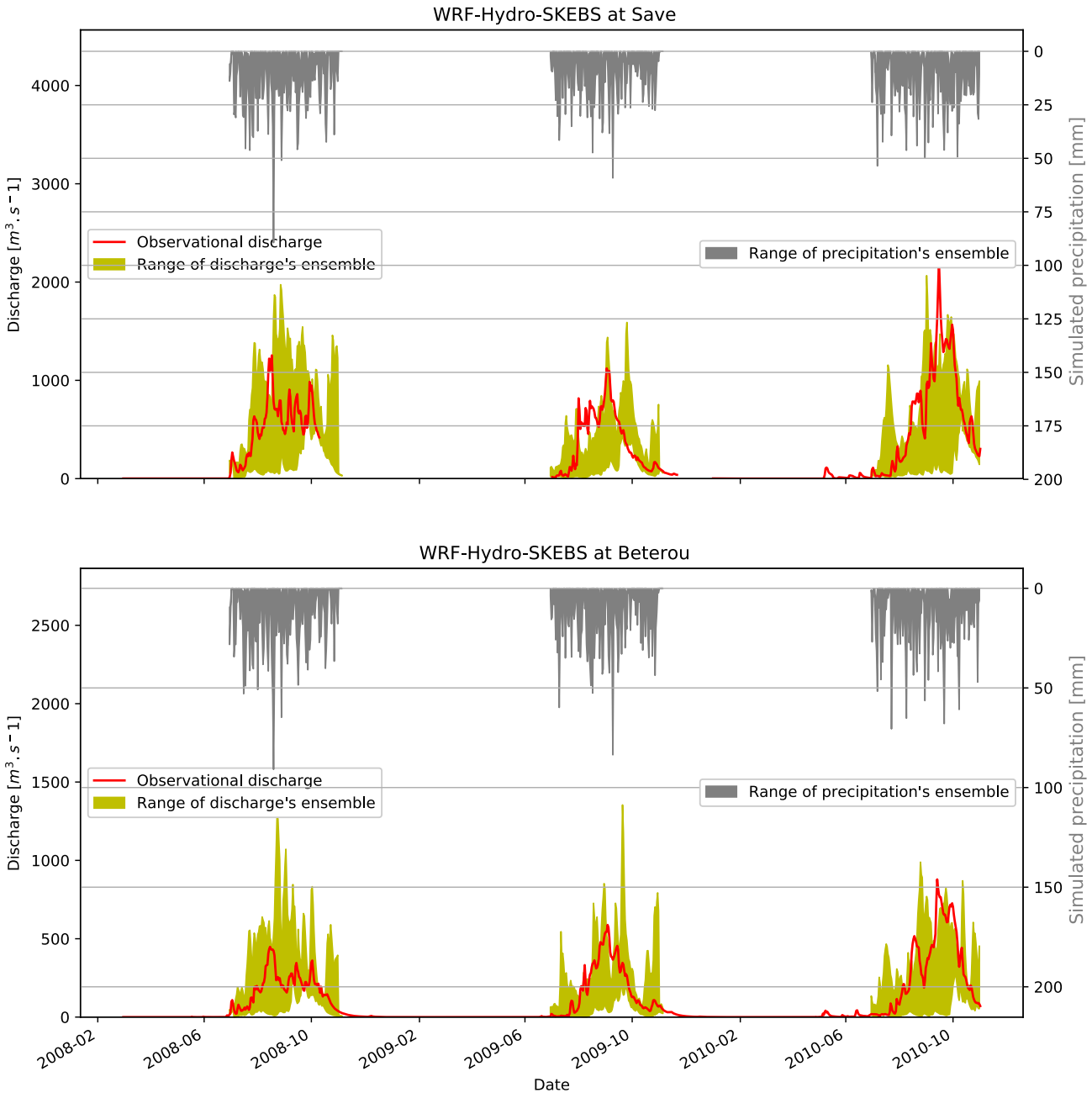

Figure 4.35: Ensemble (WRF-Hydro-SKEBS) of simulated hydrographs and precipitations at Savè and Bétérou

4.2.4 Evaluation of the soil water content

Figures 4.36 and 4.38 show the daily averaged (5-day filtered) soil moisture extracted for soil depth between 0.5-2cm (Dorigo et al., 2014) from the Climate Change Initiative (CCI) of the European Space Agency (ESA : https://www.esa.int/ESA; thereafter refer to as θ_{CCI}) respectively for Bétérou and Savè, and the corresponding volumetric soil water content in the first Noah soil layer between 0 and 10 cm (referred to as θ_{1WRF-H}). The θ_{1WRF-H} is relatively high at the beginning of the simulation (January 2008: about 0.3 $m^3.m^{-3}$), but get a decreasing trend from the first months of the simulation and reached approximatively the same value in February ending with those of other years (Feb-2009 and Feb-2010). This suggests that there is an excess of θ_{1WRF-H} both at Bétérou and Savè at the initial time of the simulation, and that a 2-month spin-up period appears to be sufficient for soil moisture in the first Noah LSM soil layer (Arnault et al., 2016). The θ_{CCI} values are globally lower than WRF-H simulations either for Bétérou or Savè during the rainy season and simulate reasonably well at the onset end the end of the season. However, despite the important bias, WRF-H correlated well with the observed. Furthermore, Figures 4.37 and 4.39 present the daily soil moisture in the four Noah LSM soil layers of the WRF-H simulation respectively for the basins Bétérou and Savè. As observed for the θ_{1WRF-H} (with soil layer between 0-10 cm) where only 2-month spin-up is enough to simulate the soil moisture, the difference between the two years is much for the soil layer 10-200 cm. For instance, the soil moisture value for the second (10-40cm) and the third (40-100 cm) soil layer, the stability is reached after the simulation of more than one year. Therefore, for this study case, we need more time for spin-up (more than a year) to simulate well the soil moisture between 10-200 cm.

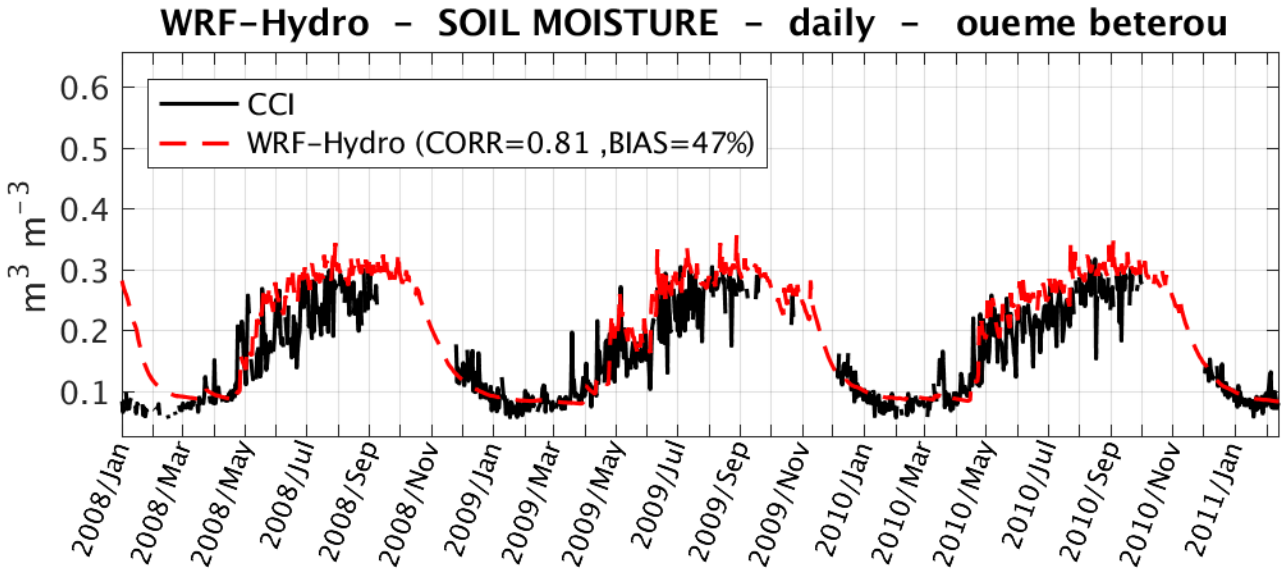

Figure 4.36: Evaluation of the soil moisture between the simulated with WRF-H of the first Noah LSM soil layer (from 0 to 10 cm) and the daily average (5-day filtered) from CCI (from 0.5 to 2 cm) over Bétérou catchment.

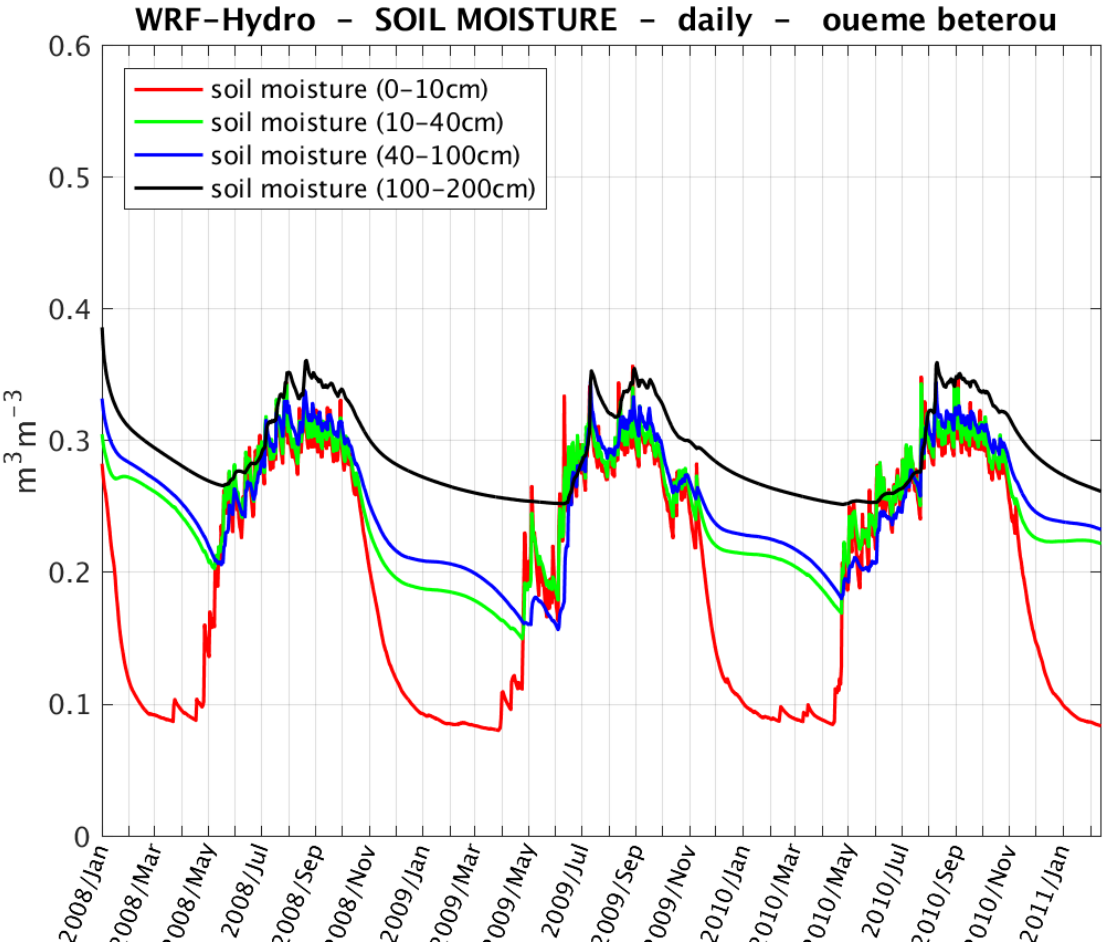

Figure 4.37: Daily average (5-day filtered) time series of soil water content (SWC) of the four Noah LSM soil layers of the WRF-H simulation at Bétérou

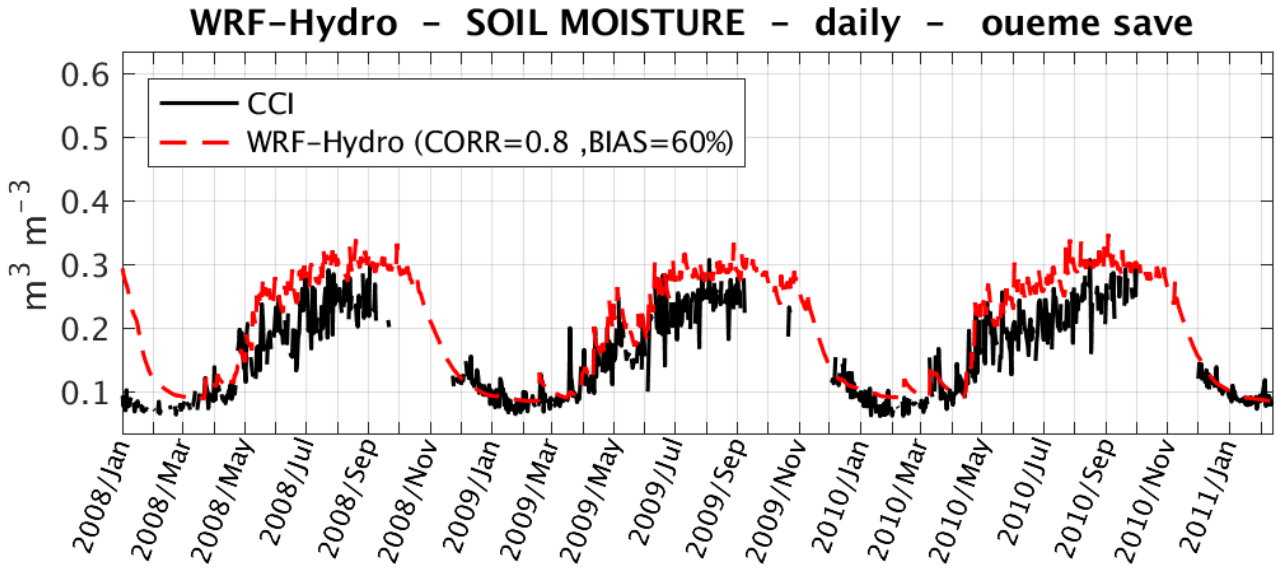

Figure 4.38: Evaluation of the soil moisture between the simulated with WRF-H of the first Noah LSM soil layer (from 0 to 10 cm) and the daily average (5-day filtered) from CCI (from 0.5 to 2 cm) over Savè catchment.

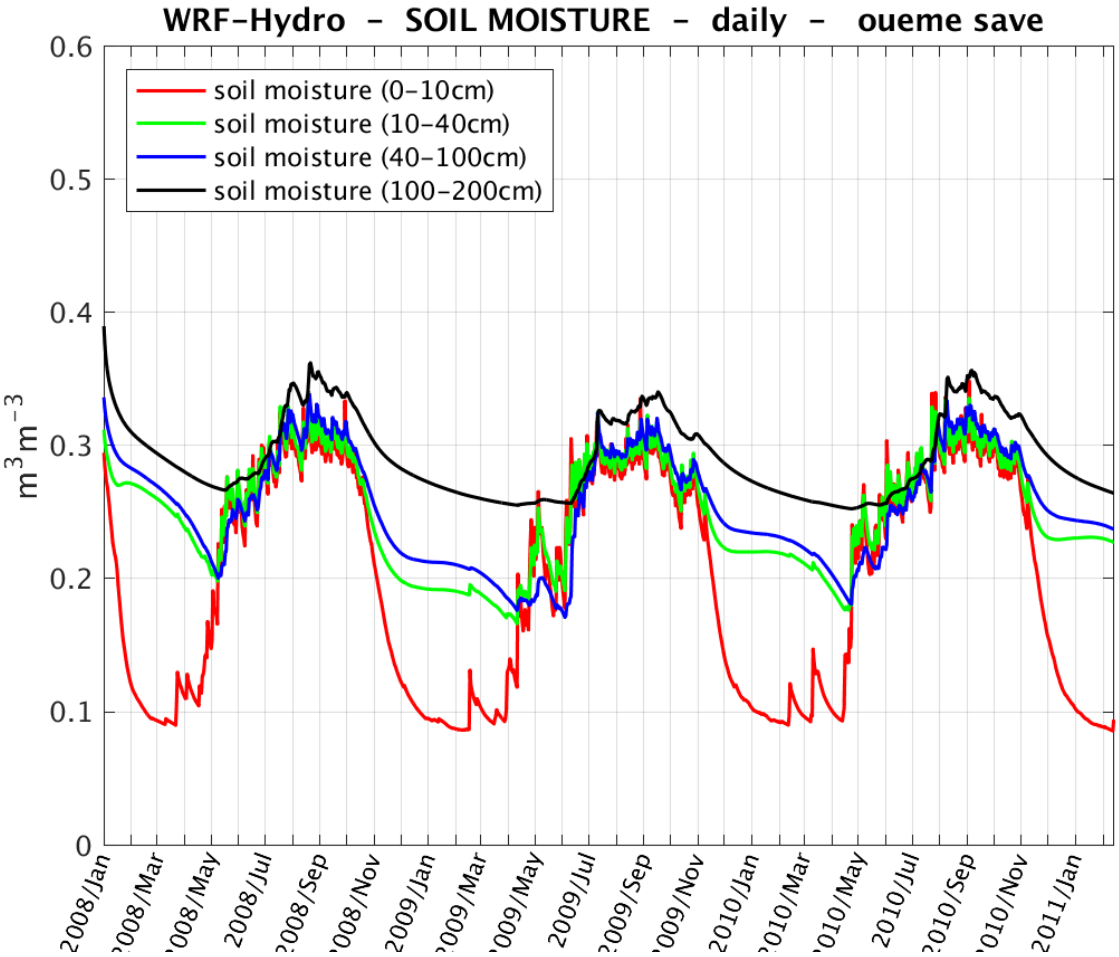

Figure 4.39: Daily average (5-day filtered) time series of soil water content (SWC) of the four Noah LSM soil layers of the WRF-H simulation at Savè.

4.2.5 Evaluation of the water cycle

Figures 4.40 and 4.42 showed the partitioning of the WRF-H simulated precipitations respectively over Bétérou and Savè during the three simulation years. With the closer results of the simulated precipitation with WRF-H to the observed datasets (Figure 4.30 and Figure 4.31), the partitioning of the rainfall during the evaluation period (2008-2010) is presented on those Figures 4.40 and 4.42. At Bétérou (Figure 4.40) the total rainfall simulated with WRF-H is 3921 mm, 7% of this amount contributes to the soil moisture (about 255 mm), and 23% seeps through the percolation to contribute (replenish) to the water resource available in the aquifer. About 21% of the total precipitation simulated at Bétérou passes through the surface runoff. Since there is no sublimation in the study area, the major part of the total precipitation is evaporated and represent 62% (i.e. 2447 mm). This part of the water (precipitation) evaporated is shared between the plant transpiration which is 65% of the total evaporated water. 7% of this evaporated water contribute to the canopy evaporation, the ponded water evaporation represents 1%, and the direct evaporation is about 27% of the total simulated evaporated water. It is noticed a similitude in the shape of the soil moisture of the first Noah LSM soil layer (Figure 4.36) and the direct evaporated water. They are relatively high at the beginning of the simulation but display a sharp decrease during the first simulated month. This suggests that there is an excess of soil moisture at the first soil layer in Savè catchment at the initial time of the simulation, which is drained out through direct evaporation during the first simulated month (Arnault et al., 2016). During the dry season, the total evaporation is almost equal to the plant transpiration. This analysis of precipitation partitioning and the evaporated water balance at Bétérou is identically the same at Savè except for the percentage of each contribution of the balance. At Savè, the

total cumulative precipitation simulated is 3883 mm, and 1% lower than the total precipitation simulated at Beterou.

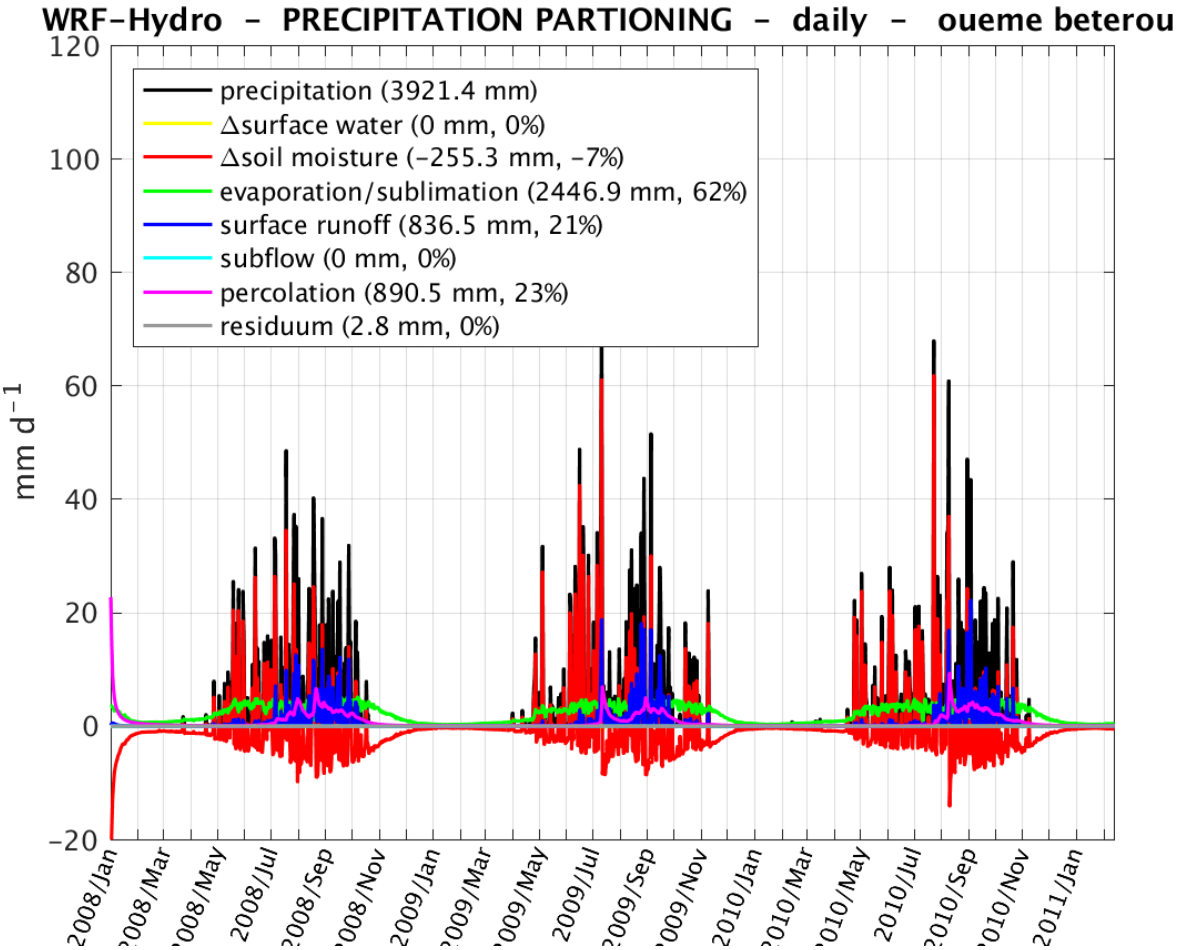

Figure 4.40: WRF-H simulated precipitation partitioning over the three years simulation period at Bétérou.

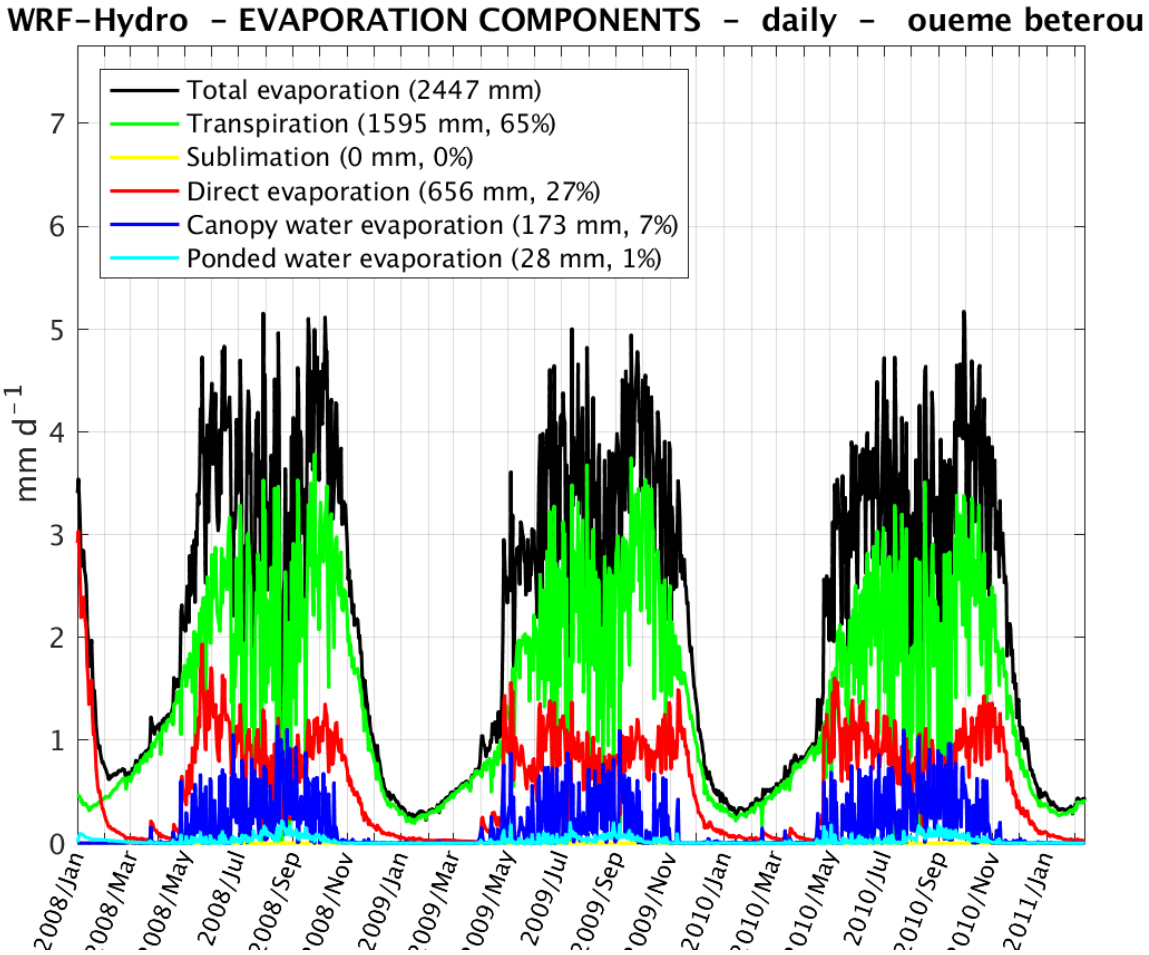

Figure 4.41: WRF-H simulated total evapotranspiration components over the three years simulation period at Bétérou.

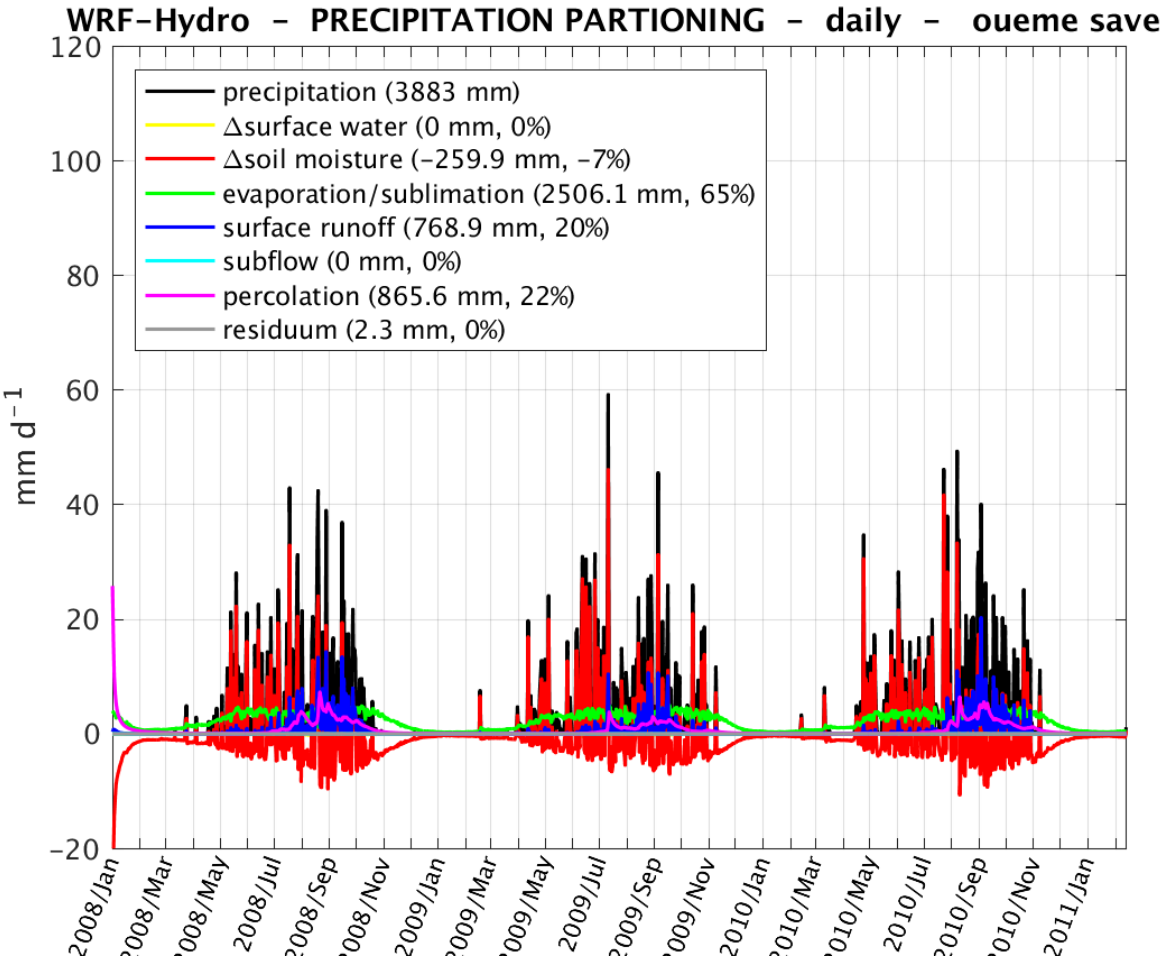

Figure 4.42: WRF-H simulated precipitation partitioning over the three years simulation period at Savè.

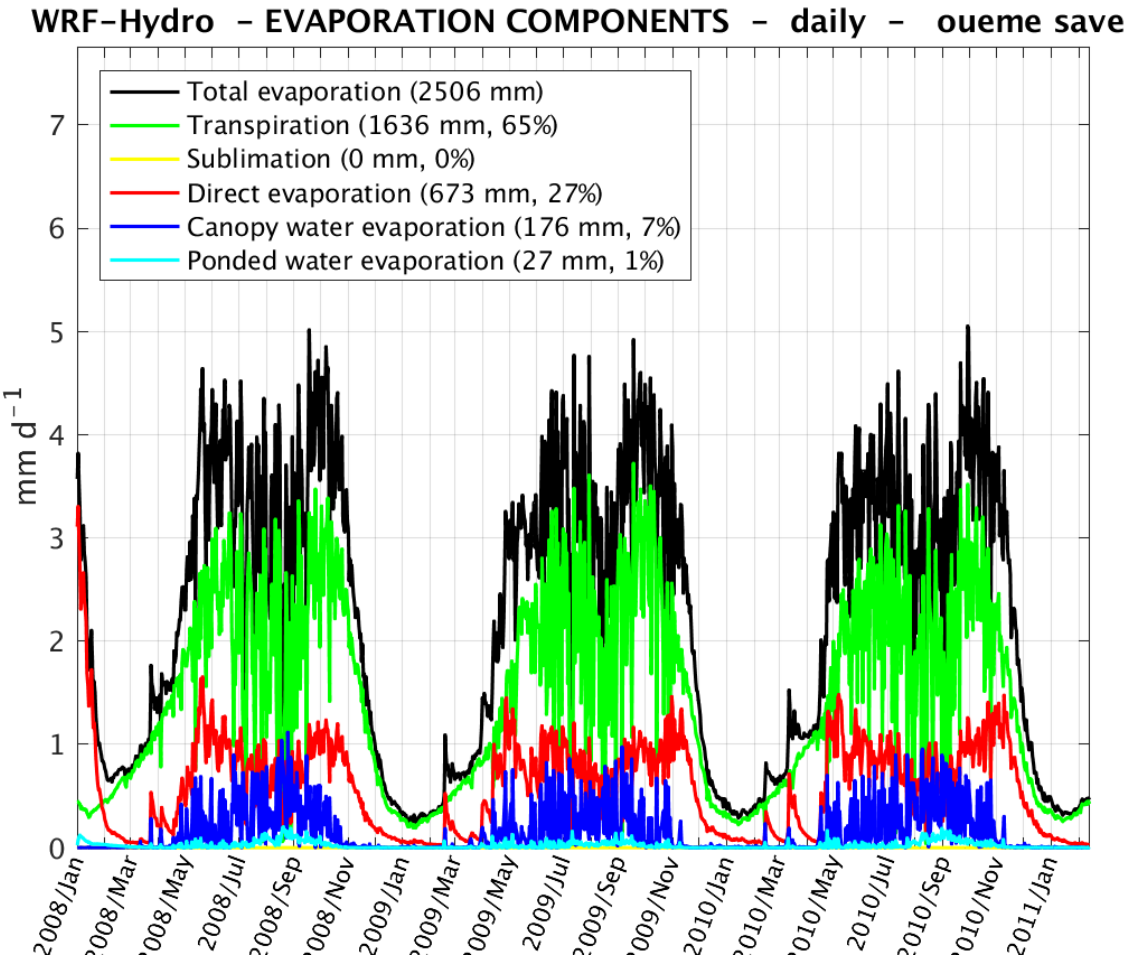

Figure 4.43 : WRF-H simulated total evapotranspiration components over the three years simulation period at Savè

CHAPTER 5

CONCLUSION AND RECOMMENDATIONS

5.1 Conclusion

West Africa is known to be particularly vulnerable to climate change due to high climate variability, high reliance on rain-fed agriculture, and limited economic and institutional capacity to respond to climate variability and change. In this context, better knowledge of how climate will change in West Africa, and how such changes will impact extreme climate events such as drought and flood have constituted the purposes of this study. First, the study used CORDEX climate simulations to analyze the situations of West Africa regarding to these two extremes climate events under four global warming levels (1.5°C, 2.0°C, 2.5°C and 3.0°C). Secondly, an experimental work to early predict one of these climate events (e.g. flooding) have been undertaken.

The spatial distribution of SPEI values examined, showed that during the historical period the Sahel and Savanna experimented extreme and severe droughts, specifically during the years 1971-1974, 1977-1980, 1987-1989, 1994 and 1995, confirming Masih et al. (2014) results, which explained that the occurred droughts in Sahel and Savanna in 1972–1973, 1983–1984 and 1991– 1992 were most intense and widespread. This result is also in agreement with the investigation on drought in West Africa by Hulme et al. (2001), Nicholson, (2005), Van De Giesen et al. (2010), Kasei et al. (2010), Oguntunde et al. (2017) and Diasso and Abiodun (2015) . The Gulf of Guinea and the North-west of West Africa, particularly Mauritania and Senegal were not excluded in 1998-2000 by this drought. But this observation is not static, some wet years also were noticed at the western part of the study domain. The results illustrated that the Savanna

could become relatively wet and the Eastern and North-western part of West Africa more extremely dry under all GWLs; whilst the Sahel will be a little bit dry, clarifying the existence of the gradient Gulf-of-Guinea-Savanna-Sahel where the Gulf-of-Guinea recorded moderate wet condition. Under RCP8.5, the Gulf-of-Guinea will be the wettest area, especially the coastal countries. A reduction under GWLs of the driest episodes could also be noticed, particularly the area covering latitude 12ºN-16ºN; whilst, the coastal part of Liberia and Cameroon, Mali, Burkina-Faso, Niger, Ivory-Coast, Benin, Nigeria, Chad will experiment extreme drought. A better understanding of the contrast between drought and probably flooding areas led the study to assess the PCI both on annual and seasonal time scales. Results of seasonal and annual computation of PCI informed on the changes in the spatial distribution of precipitation.

The findings obtained in this study with regard to the PCI, illustrated that the main rainfall activity period over West Africa was between May and September. During the historical period, rainfall was uniformly well distributed over the Gulf of Guinea and the Savanna, whilst in the Sahel, a more moderate and irregular precipitation concentration was recorded. Under future scenarios, i.e., at all the GWLs of 1.5℃, 2.0℃, 2.5℃ and 3.0℃; the moderate and irregular precipitation concentration was projected to reduce in favour of a more uniform distribution, except over the North-eastern areas (which are part of Niger and Chad), which became the least dry at all four GWLs. In order to obtain further detail about the period of the concentration of rainfall in West Africa, the PCP variable was calculated; it showed that the precipitation concentration increased gradually from the Gulf of Guinea to the Sahel, thus explaining the existence of a south-north gradient. During the historical period (1971-2000), the highest rainfall concentration occurred in July-August over the Gulf of Guinea and the Savanna, while it was highest during September over the Sahel.

The PCP too changed in response to increasing GWLs. The rainfall was found to be more concentrated in June-July over the Gulf of Guinea and the Savanna, and during August for the Sahel. In general, the degree of the concentration seemed to be more important in the Savanna-Sahel (with high values of PCD), due to the WAM system, which is led by the back-and-forth movement of the Inter-Tropical Discontinuity (ITD) between south and north. Indeed, this movement creates an increased precipitation concentration in the Savanna-Sahel area, which is immediately followed by the southward movement of the ITD. This establishes a long-time record of precipitation concentration, which is highlighted by the PCD values over this area. A significant reduction in the CDD is recorded over the north-east (i.e. Niger and Chad), and a slight increase in the number of CWD over the Sahel. Additionally, based on the results from PCI and PCP, Niger and Chad are projected to experience more wet condition under increasing GWLs. The 5-day cumulative rainfall variable shows that the Gulf of Guinea is projected to experience more intense, very intense and heavy rainfall events under increasing GWLs.

All these results together show how much West Africa will be exposed to higher variability of climate change and also to future heavier rainfall and wet conditions. To cope with such changes, reduce the loss of life and better manage the impact on inhabitants of this region, some adaptation strategies are necessary under continual climate change. Two types of strategies are required: a regional framework agreement and local coping strategies. The regional agreement is very important because it forces each stakeholder (country) to respect the framework agreement; this is mostly in line with the mitigation of climate change at the regional scale. Local strategies are important in two ways: Firstly, local strategies should enable West African countries to respect the regional framework agreement. Secondly, they should encourage countries to look for

and develop adequate adaptation possibilities, by responding to the contributions of scientists and decision-makers, which represent an important factor in development. They are the ones who have to provide reliable information to the population, and particularly to farmers, for better management of crops in order to ensure food security.

The experimental work of this study explores the abilities of the fully coupled WRF-Hydro modeling system to simulate discharge and precipitation in Ouémé-river in West-Africa, but also evaluate some other variables. The model has been calibrated in offline mode for one year and tested for two years using hourly outputs from WRF simulations. Optimized parameters from the calibration were used to perform the fully coupled WRF-Hydro model, which was used to investigate the performance skills over Ouémé-basin.

The evaluation of simulated precipitation, shown its good replicability skills and provides confirmation of the uncertainty associated with WRF-H to simulate precipitation (Klein et al., 2015; Miguez-Macho et al., 2007). WRF-H showed also a good performance to simulate discharges. Its performance evaluated with KGE equal to 0.76 for the period 2008-2010 is relatively close to the performance of the model in uncoupled mode on period 2009-2010, which is equal to 0.86. The robustness of WRF-H has been assessed at Bétérou, an inner-catchment of Ouémé-river at Savè, where it provided a good agreement with respect to observed discharge with KGE equal to 0.66. Additionally, it was able to capture the flood event that occurred in 2010 over both Savè and Bétérou, and even captured the peaks. This is due to the fact that in the fully-coupled module of WRF-hydro, the atmospheric and hydrological processes are simulated in a consistent way, which enhanced confidence in the results. The uncertainty of predictability skills of WRF-H with respect to discharge in Ouémé-river at Savè was treated with an ensemble of 10-member. Results showed that the large spread of WRF-

H regarding the stochastic perturbation was introduced to the boundary conditions. The model shows its high sensibility to perturbations introduced into the atmosphere.

According to the performance displayed by WRF-H to simulate accurate discharge and precipitation, this model is suited for discharge predictions in Ouémé-river, and should be a good model for flood forecasting over West-Africa, and could also be implemented over other basins.

5.2 Limitation of the study

- In this study the performance of the CORDEX dataset driven by the RCA4 to simulate precipitation and evapotranspiration have been evaluated, and despite the good correlation of the model in respect to the observed datasets that can be deduced from the analysis, the models present some misjudgments of the input variables, which can affect the resultant indices.
- They have many uncertainties related to the prediction of drought and flood both for the historical and the future projections using climate indices, because of the fairly performance of the model regarding the observed dataset.
- Another limitation is mainly related to the potential flooding and drought projections using the climate indices. This is because, as in case of the historical period, the principal component (PC) method accompanied the EOF to explain the temporal location of the potential drought or flood events; the RCA4 models do not experience GWLs at the same period as shown in Table 4.1, which means that ensemble-mean could not be displayed in function of time. In that case, it is impossible to reveal when (period) in future the flood or drought will occur.
- Regarding the practical experiment using WRF-Hydro the major limitation is about the availability of the in-situ variables such as precipitation and streamflow gauge data.

For instance, in the case of the present study, the in-situ available precipitation and streamflow data over Ouémé catchments from 2011-2017 present either a lot of spike data or are not well transcripted, containing many missing values; a reason why the simulations of the WRF-H are limited to 2010 and not up to 2017.

5.3 Recommendations

The impacts of climate change and variability on the extreme climate events in West Africa have been successfully investigated by many studies using climate indices (Diasso and Abiodun, 2015; Oguntunde et al., 2017). The present work added credit to previous works and investigated also on the trend of the extreme events based on potential global warming levels documented. The study might want to clarify the potential future period where each event will be noticed, but this was not possible because of the generation of the ensemble-mean, which provided idea about the trend of the ensemble. Future works might focus on the way to fix this issue, I mean to explain the temporal trend of the ensemble-mean despite the exhibition of a particular GWL in different periods.

The experimental flood forecasting work was implemented on annual and seasonal scales. Since the simulation of such a model is very high, computational cost and time consumption; future works could find the way to adapt the WRF-H for flood forecasting at 10-day lead using 10-day forecasting data (e.g. from ECMWF forecasting data). Also, this 10-day lead forecasting will be more practical in case of early warning.

REFERENCES

Abatzoglou, J. T., Rupp, D. E. and Mote, P. W. (2014). Seasonal climate variability and change in the pacific northwest of the united states. Journal of Climate, 27(5), 2125–2142. https://doi.org/10.1175/JCLI-D-13-00218.1

Abiodun, B. J., Makhanya, N., Petja, B., Abatan, A. A. and Oguntunde, P. G. (2018). Future projection of droughts over major river basins in Southern Africa at specific global warming levels. Theoretical and Applied Climatology. https://doi.org/https://doi.org/10.1007/s00704-018-2693-0

Abiodun, B. J., Pal, J. S., Afiesimama, E. A., Gutowski, W. J. and Adedoyin, A. (2008). Simulation of West African monsoon using RegCM3 Part II: Impacts of deforestation and desertification. Theoretical and Applied Climatology, 93(3–4), 245–261. https://doi.org/10.1007/s00704-007-0333-1

Abramowitz, M. and Stegun, I. ren. A. (1964). Handbook of mathematical functions: with formulas, graphs, and mathematical tables (ninth Dove, Vol. Vol. 55 .). New York: Dover.

Afiesimama, E. A., Pal, J. S., Abiodun, B. J., Jr, W. J. G. and Adedoyin, A. (2006). Simulation of West African monsoon using the RegCM3 . Part I : Model validation and interannual variability, 37, 23–37. https://doi.org/10.1007/s00704-005-0202-8

Afouda, A. A. (1980). Analysis of the Rainfall-Runoff Transformation Process, National University Of Benin. 234-257.

Allen, P. M., Harmel, R. D., Dunbar, J. A. and Arnold, J. G. (2011). Upland contribution of sediment and runoff during extreme drought : A study of the 1947 – 1956 drought in the Blackland Prairie , Texas. Journal of Hydrology, 407(1–4), 1–11. https://doi.org/10.1016/j.jhydrol.2011.04.039

Arnault, Joël, Rummler, T., Baur, F., Lerch, S., Wagner, S., Fersch, B., Zhang, Z., Kerandi, N., Keil, C. and Kunstmann, H. (2018). Precipitation Sensitivity to the Uncertainty of Terrestrial Water Flow in WRF-Hydro: An Ensemble Analysis for Central Europe. Journal of Hydrometeorology, 19(6), 1007–1025. https://doi.org/10.1175/JHM-D-17-0042.1

Arnault, Joel, Wagner, S., Rummler, T., Fersch, B., Bliefernicht, J., Andresen, S. and Kunstmann, H. (2016). Role of Runoff–Infiltration Partitioning and Resolved Overland Flow on Land–Atmosphere Feedbacks: A Case Study with the WRF-Hydro Coupled Modeling System for West Africa. Journal of Hydrometeorology, 17(5), 1489–1516. https://doi.org/10.1175/JHM-D-15-0089.1

Aspliden, C. I., Tourre, Y. and John B. Sabine. (1976). Some climatological aspect of West African disturbance lines during GATE. Departement of Environmental Sciences, University of Virginia, Charlottesville 22903.

Avahounlin, R. F., Lawin, A. E., Alamou, A. E., Chabi, A. and Afouda, A. (2013). Analyse Fréquentielle des Séries de Pluies et Débits Maximaux de L ' Ouémé et Estimation des Débits de Pointe. European Journal of Scientific Research, 107(3), 355–369. Retrieved from http://www.europeanjournalofscientificresearch.com

Baldassarre, G Di, Viglione, A., Carr, G., Kuil, L., Salinas, J. L. and Bl, G. (2013). Socio-hydrology : conceptualising human-flood interactions. Hydrol. Earth Syst. Sci., 17(2013), 3295–3303. https://doi.org/10.5194/hess-17-3295-2013

Baldassarre, Giuliano Di, Schumann, G. and Bates, P. D. (2009). A technique for the calibration of hydraulic models using uncertain satellite observations of flood extent. Journal of Hydrology, 367, 276–282. https://doi.org/10.1016/j.jhydrol.2009.01.020

Barber, V. A., Juday, G. P. and Finney, B. P. (2000). Reduced growth of Alaskan white spruce in the twentieth century from temperature-induced drought stress. Nature, 405(6787), 668–673. https://doi.org/10.1038/35015049

Barron, J., Rockström, J., Gichuki, F. and Hatibu, N. (2003). Dry spell analysis and maize yields for two semi-arid locations in east Africa, 117, 23–37. https://doi.org/10.1016/S0168-1923(03)00037-6

Beaufort, L., Lancelot, Y., Camberlin, P., Cayre, O., Vincent, E., Bassinot, F. and Labeyrie, L. (1997). Insolation Cycles as a Major Control of Equatorial Indian Ocean Primary Insolation Cycles as a Major Control of Equatorial Indian Ocean Primary Production. Science, 278. https://doi.org/10.1126/science.278.5342.1451

Berner, J., Fossell, K. R., Ha, S.-Y., Hacker, J. P. and Snyder, C. (2015). Increasing the Skill of Probabilistic Forecasts: Understanding Performance Improvements from Model-Error Representations. Monthly Weather Review, 143(4), 1295–1320. https://doi.org/10.1175/MWR-D-14-00091.1

Berner, J., Shutts, G. J., Leutbecher, M. and Palmer, T. N. (2009). A Spectral Stochastic Kinetic Energy Backscatter Scheme and Its Impact on Flow-Dependent Predictability in the ECMWF Ensemble Prediction System. Journal of the Atmospheric Sciences, 66(3), 603–626. https://doi.org/10.1175/2008JAS2677.1

Blöschl, G., Nester, T., Komma, J., Parajka, J. and Perdigão, R. A. P. (2013). The June 2013 flood in the Upper Danube Basin , and comparisons with the 2002 , 1954 and 1899 floods. Hydrol. Earth Syst. Sci., 17(August 2002), 5197–5212. https://doi.org/10.5194/hess-17-5197-2013

Bouilloud, L., Chancibault, K., Vincendon, B., Ducrocq, V., Habets, F., Saulnier, G.-M., Anquetin, S. Martin, E. and Noilhan, J. (2010). Coupling the ISBA Land Surface Model and the TOPMODEL Hydrological Model for Mediterranean Flash-Flood Forecasting: Description, Calibration, and Validation. Journal of Hydrometeorology, 11(2), 315–333. https://doi.org/10.1175/2009JHM1163.1

Brázdil, R., Trnka, M., Dobrovolný, P., Chromá, K., Hlavinka, P. and Zcaron;alud, Z. (2009). Variability of droughts in the Czech Republic, 1881-2006. Theoretical and Applied Climatology, 97(3–4), 297–315. https://doi.org/10.1007/s00704-008-0065-x

Burke, E. J., Brown, S. J. and Christidis, N. (2006). Modeling the Recent Evolution of Global Drought and Projections for the Twenty-First Century with the Hadley Centre Climate Model. Journal of Hydrometeorology, 7(1990), 1113–1125.

Cadro, S., Zurovec, J. And Cherni-Cadro, S. (2017). Severity, Magnitude and Duration of Droughts in Bosnia and Herzegovina Using Standardized Precipitation Evapotranspiration Index (Spei). The Journal "Agriculture and Forestry," 63(3), 199–206. https://doi.org/10.17707/AgricultForest.63.3.20

Camberlin, P., Janicot, S. and Poccard, I. (2001). Seasonality and atmospheric dynamics of the teleconnection between african rainfall and tropical sea-surface temperature : atlantic vs . ENSO. International Journal of Climatology, 1005, 973–1005.

Cancelliere, A., Mauro, G. Di, Bonaccorso, B. and Rossi, G. (2007). Drought forecasting using the standardized precipitation index. Water Resources Management, 21(5), 801–819. https://doi.org/10.1007/s11269-006-9062-y

Chawla, I., Osuri, K. K., Mujumdar, P. P. and Niyogi, D. (2018). Assessment of the Weather Research and Forecasting (WRF) model for simulation of extreme rainfall events in the upper Ganga Basin, 1095–1117.

Chen, F. and Dudhia, J. (2001). Coupling an Advanced Land Surface–Hydrology Model with the Penn State–NCAR MM5 Modeling System. Part I: Model Implementation and Sensitivity, 569–585.

Chong, M. and Hauser, D. (1988). A tropical squall line observed during the COPT 81 experiment in West Africa: Part II: Water budget. Monthly Weather Review, 117, 728–744.

Cloke, H. L. and Pappenberger, F. (2009). Ensemble flood forecasting : A review. Journal of Hydrology, 375(3–4), 613–626. https://doi.org/10.1016/j.jhydrol.2009.06.005

Cook, K. H. (1999). Generation of the African easterly jet and its role in determining West African precipitation. Journal of Climate, 12(5 I), 1165–1184. https://doi.org/10.1175/1520-0442(1999)012<1165:GOTAEJ>2.0.CO;2

Dai, A. (2011). Drought under global warming: A review. Wiley Interdisciplinary Reviews: Climate Change. https://doi.org/10.1002/wcc.81

Dai, A., Trenberth, K. E. and Qian, T. (2004). A Global Dataset of Palmer Drought Severity Index for 1870 – 2002 : Relationship with Soil Moisture and Effects of Surface Warming, 1117–1130.

De Luis, M., González-Hidalgo, J. C., Brunetti, M. and Longares, L. A. (2011). Precipitation concentration changes in Spain 1946-2005. Natural Hazards and Earth System Science, 11(5), 1259–1265. https://doi.org/10.5194/nhess-11-1259-2011

Delestre, O. (2011). Simulation du ruissellement d ' eau de pluie sur des surfaces agricoles To cite this version : HAL Id : tel-00587197. Université d'Orléans.

Déqué, M., Calmanti, S., Bøssing, O., Dell, A., Fox, C., Haensler, A., … Teichmann, C. (2017). A multi-model climate response over tropical Africa at + 2 ° C, 7, 87–95. https://doi.org/10.1016/j.cliser.2016.06.002

Descroix, L., Genthon, P., Amogu, O., Rajot, J. L., Sighomnou, D. and Vauclin, M. (2012). Change in Sahelian Rivers hydrograph: The case of recent red floods of the Niger River in the Niamey region. Global and Planetary Change, 98–99, 18–30. https://doi.org/10.1016/j.gloplacha.2012.07.009

Diallo, I., Sylla, M. B., Giorgi, F., Gaye, A. T. and Camara, M. (2012). Multimodel GCM-RCM Ensemble-Based Projections of Temperature and Precipitation over West Africa for the Early 21st Century. International Journal OfGeophysics. https://doi.org/10.1155/2012/972896

Diasso, U. and Abiodun, B. J. (2015). Drought modes in West Africa and how well CORDEX RCMs simulate them. Theoretical and Applied Climatology, 128(1–2). https://doi.org/10.1007/s00704-015-1705-6

Diedhiou, A., Janicot, S. and Viltard, A. (2001). Composite patterns of easterly disturbances over West Africa and the tropical Atlantic : a climatology from the 1979 - 95 NCEP / NCAR reanalyses. Climate Dynamics, 18, 241–253.

Donat, M. G., Lowry, A. L., Alexander, L. V, Gorman, P. A. O. and Maher, N. (2016). More extreme precipitation in the world ' s dry and wet regions, 6(May). https://doi.org/10.1038/NCLIMATE2941

Druyan, M. L. and Fulakeza, B. M. (2000). Regional model simulations of African wave disturbances. Journal of Geophysical Research, 105, 7231–7255. https://doi.org/http://dx.doi.org/10.1029/2000JD900017

Duan, K. and Mei, Y. (2014). Comparison of Meteorological , Hydrological and Agricultural Drought Responses to Climate Change and Uncertainty Assessment. Water Resour Manage. https://doi.org/10.1007/s11269-014-0789-6

Dudhia, J. (1989). Numerical Study of convection observed during the winter monsoon experiment using a mesoscale two-Dimensional Model. https://doi.org/10.1175/1520-0469(1989)046<3077:NSOCOD>2.0.CO;2

Edwards DC, McKee TB. 1997. Characteristics of 20th century drought in the United States at multiple time scales. Atmospheric Science Paper No. 634, Climatology Report 97–2, Department of Atmospheric Science, Colorado State University, Fort Collins, Colorado, 155 pp

Eldridge, R. H. (1957). A synoptic study of West African Disturbance Lines. 551.515.8 : 551.557.3 : 551.589.1, 303–314.

Eltahir, E. A. B. and Gong, C. (1995). Dynamics of wet and dry year in West Africa. Journal of Climate, 9, 1030–1042.

Ezenwaji, E. E., Nzoiwu, C. P. and Chima, G. N. (2017). Analysis of Precipitation Concentration Index (PCI) for Awka Urban Area ,. Hydrol Current Res, 8(4), 4–9. https://doi.org/10.4172/2157-7587.1000287

FAO, IFAD and WFP. (2015). The State of Food Insecurity in the World 2015. Meeting the 2015 international hunger targets: taking stock of uneven progress. (FAO, Ed.). Rome.

Fiala, T., Ouarda, T. B. M. J. and Hladný, J. (2010). Evolution of low flows in the Czech Republic. Journal of Hydrology, 393(3–4), 206–218. https://doi.org/10.1016/j.jhydrol.2010.08.018

Fink, A. H. and Reiner, A. (2003). Spatiotemporal variability of the relation between African Easterly Waves and West African Squall Lines in 1998 and 1999. Journal of Geophysical Research, 108(2), 1–17. https://doi.org/10.1029/2002JD002816

Fiori, E., Comellas, A., Molini, L., Rebora, N., Siccardi, F., Gochis, D. J., Tanelli, S. and Parodi, A. (2014). Analysis and hindcast simulations of an extreme rainfall event in the Mediterranean area: The Genoa 2011 case. Atmospheric Research, 138, 13–29. https://doi.org/10.1016/j.atmosres.2013.10.007

Fleig, A. K., Tallaksen, L. M., Hisdal, H., Demuth, S., Fleig, A. K., Tallaksen, L. M., Hisdal, H. and Demuth, S. A. (2006). A global evaluation of streamflow drought characteristics To cite this version : HAL Id : hal-00305008 Sciences A global evaluation of streamflow drought characteristics.

Flesch, T. K. and Reuter, G. W. (2012). WRF Model Simulation of Two Alberta Flooding Events and the Impact of Topography, 695–708. https://doi.org/10.1175/JHM-D-11-035.1

Fontaine, B. and Janicot, S. (1996). Sea surface temperature fields associated with West African rainfall anomaly types. Journal of Climate, 9, 2935–2940.

Frich, P., Alexander, L. V, Gleason, B., Haylock, M., Tank, A. M. G. K. and Peterson, T. (2002). Observed coherent changes in climatic extremes during the second half of the twentieth century, 19, 193–212.

Friedl, M. A., McIver, D. K., Hodges, J. C. F., Zhang, X. Y., Muchoney, D., Strahler, A. H., Woodcock, C. E., Gopal, S., Schneider, A., Cooper, A., Baccini, A., Gao, F. and Schaaf, C. (2002). Global land cover mapping from MODIS: Algorithms and early results. Remote Sensing of Environment, 83(1–2), 287–302. https://doi.org/10.1016/S0034-4257(02)00078-0

Funk, C., Peterson, P., Landsfeld, M., Pedreros, D., Verdin, J., Shukla, S., Husak, G., Rowland, J., Harrison, L., Hoell, A. and Michaelsen, J. (2015). The climate hazards infrared precipitation with stations — a new environmental record for monitoring extremes, 1–21. https://doi.org/10.1038/sdata.2015.66

García-Valdecasas Ojeda, M., Gámiz-Fortis, S. R., Castro-Díez, Y. and Esteban-Parra, M. J. (2017). Evaluation of WRF capability to detect dry and wet periods in Spain using drought indices. Journal of Geophysical Research, 122(3), 1569–1594. https://doi.org/10.1002/2016JD025683

Garner, G., Van Loon, A. F., Prudhomme, C. and Hannah, D. M. (2015). Hydroclimatology of extreme river flows. Freshwater Biology, 60(12), 2461–2476. https://doi.org/10.1111/fwb.12667

Giorgi, F. (2014). Introduction to the special issue : the phase I CORDEX RegCM4 hyper-matrix (CREMA) experiment. Climate Change, Springer. https://doi.org/10.1007/s10584-014-1166-4

Givati, A., Gochis, D., Rummler, T. and Kunstmann, H. (2016). Comparing One-Way and Two-Way Coupled Hydrometeorological Forecasting Systems for Flood Forecasting in the Mediterranean Region. https://doi.org/10.3390/hydrology3020019

Givati, A., Lynn, B., Liu, Y. and Rimmer, A. (2012). Using the WRF model in an Operational Streamflow Forecast System for the Jordan River. Journal of Applied Meteorology and Climatology, 51(2), 285–299. https://doi.org/10.1175/JAMC-D-11-082.1

Gobena, A. K. and Gan, T. Y. (2013). Assessment of Trends and Possible Climate Change Impacts on Summer Moisture Availability in Western Canada based on Metrics of the Palmer Drought Severity Index. Journal of Climate, 26(1948), 4583–4595. https://doi.org/10.1175/JCLI-D-12-00421.1

Gochis, D., Mccreight, J., Yu, W., Dugger, A., Sampson, K., Yates, D., Wood A., Clark M., Rasmussen R., Yu, W., Yates, D., Sampson, K., Dugger, A., Mccreight, J., Barlage, M., Zhang, Y., Tewari, M., Rasmussen, R., Wood, A., Chen, F. and Clark, M. (2015). Multi-scale water cycle predictions using the community WRF-Hydro modeling system.

Gochis, D.J., Barlage, M., Dugger, A., FitzGerald, K., Karsten, L., McAllister, M., McCreight, J., Mills, J., RafieeiNasab, A., Read, L., Sampson, K., Yates, D. and Yu W. (2018). The WRF-Hydro modeling system technical description, (Version 5.0). NCAR Technical Note. 107 pages. Available online at: https://ral.ucar.edu/sites/default/files/public/WRFHydroV5TechnicalDescription.pdf.

Gochis, David J. and Chen, F. (2003). Hydrological Enhancements to the Community Noah Land Surface Model. NCAR Scientific Technical Report. University Corporation for Atmospheric Research, 77.

Godonou, J. L. (2010). Évaluation des risques environnementaux des inondations de 2010 au Bénin : cas des communes de Lalo, Dogbo, Lokossa. Association Ouest Africaine Pour l'Évaluation Environnementale Bénin, 12.

Grist, J. P., Nicholson, S. E. and Barcilon, A. I. (2001). Easterly Waves over Africa. Part II: Observed and Modeled Contrasts between Wet and Dry Years. Monthly Weather Review, 130(2), 212–225. https://doi.org/10.1175/1520-0493(2002)130<0212:EWOAPI>2.0.CO;2

Grodsky, S. A., Carton, J. A. and Nigam, S. (2003). Near surface westerly wind jet in the Atlantic ITCZ. Geophysical Research Letters, 30(19), 3–6. https://doi.org/10.1029/2003GL017867

Gurrapu, S., Chipanshi, A., Sauchyn, D. and Allan, H. (2014). Comparison of the SPI and SPEI on predicting drought conditions and streamflow in the Canadian Prairies.

Harris, I., Jones, P. D., Osborn, T. J. and Lister, D. H. (2014). Updated high-resolution grids of monthly climatic observations - the CRU TS3.10 Dataset. International Journal of Climatology, 34(3). https://doi.org/10.1002/joc.3711

Hasselmann, K. (1990). How can we predict the climate crisis. ISSN 0937—1060, (57), 35.

Heerden, J. V. A. N., Terblanche, D. E. and Schulze, G. C. (1988). The southern oscillation and south african summer, 8, 577–597.

Heine, R. A. and Pinter, N. (2011). Levee effects upon fl ood levels : an empirical assessment. Hydrological Processes. https://doi.org/10.1002/hyp

Hogg, E. H. and Hurdle, P. A. (1995). The Aspen parkland in Western Canada: a dry-climate analogue for the future boreal forest? Water, Air and Soil Pollution, (82), 391–400.

Homdee, T., Pongput, K. and Kanae, S. (2016). A comparative performance analysis of three standardized climatic drought indices in the Chi River basin, Thailand. Agriculture and Natural Resources. https://doi.org/10.1016/j.anres.2016.02.002

Hong, S.-Y., Dudhia, J. and Chen, S.-H. (2004). A Revised Approach to Ice Microphysical Processes for the Bulk Parameterization of Clouds and Precipitation. Monthly Weather Review, 132(1), 103–120. https://doi.org/10.1175/1520-0493(2004)132<0103:ARATIM>2.0.CO;2

Hounkpè, J., Diekkrüger, B., Badou, D. and Afouda, A. (2015). Non-Stationary Flood Frequency Analysis in the Ouémé River Basin, Benin Republic. Hydrology, 2(4), 210–229. https://doi.org/10.3390/hydrology2040210

Huffman, G. J., Adler, R. F., Bolvin, D. T., Gu, G., Nelkin, E. J., Bowman, K. P., Hong, Y., Stocker, E. F. and Wolff, D. B. (2007). The TRMM Multisatellite Precipitation Analysis (TMPA): Quasi-Global , Multiyear , Combined-Sensor Precipitation Estimates at Fine Scales, 38–55. https://doi.org/10.1175/JHM560.1

Huijgevoort, M. H. J. Van, Lanen, H. A. J. Van, Teuling, A. J. and Uijlenhoet, R. (2014). Identification of changes in hydrological drought characteristics from a multi-GCM driven ensemble constrained by observed discharge. Journal of Hydrology, 512, 421–434. https://doi.org/10.1016/j.jhydrol.2014.02.060

Hulme, M., Doherty, R., Ngara, T., New, M. and Lister, D. (2001). African climate change: 1900–2100, 17, 145–168. https://doi.org/10.1002/jbmr.347

Ionita, M., Lohmann, G., Rimbu, N., Chelcea, S. and Dima, M. (2012). Interannual to decadal summer drought variability over Europe and its relationship to global sea surface temperature. Climate Dynamics, 38(1–2), 363–377. https://doi.org/10.1007/s00382-011-1028-y

IPCC. (2012). Managing the Risks of Extreme Events and Disasters to Advance Climate Change Adaptation. A Special Report of Working Groups I and II of the Intergovernmental Panel on Climate Change [Field, C.B., V. Barros, T.F. Stocker, D. Qin, D.J. Dokken, K.L. Ebi, M.D.

IPCC. (2014). Climate Change 2014: Synthesis Report. Contribution of Working Groups I, II and III to the Fifth Assessment Report of the Intergovernmental Panel on Climate Change [Core Writing Team, R.K. Pachauri and L.A. Meyer (eds.)]. In IPCC (p. 151). Geneva, Switzerland.

Jasper, K., Gurtz, J. and Lang, H. (2002). Advanced flood forecasting in Alpine watersheds by coupling meteorological observations and forecasts with a distributed hydrological model. Journal of Hydrology, 267(1–2), 40–52. https://doi.org/10.1016/S0022-1694(02)00138-5

Ji, L. and Peters, A. J. (2003). Assessing vegetation response to drought in the northern Great Plains using vegetation and drought indices. Remote Sensing OfEnvironment, 87, 85–98. https://doi.org/10.1016/S0034-4257(03)00174-3

Jiang, P., Gautam, M. R., Zhu, J. and Yu, Z. (2013). How well do the GCMs/RCMs capture the multi-scale temporal variability of precipitation in the Southwestern United States? Journal of Hydrology, 479, 75–85. https://doi.org/10.1016/j.jhydrol.2012.11.041

Joetzjer, E., Douville, H., Delire, C., Ciais, P., Decharme, B. and Tyteca, S. (2013). Hydrologic benchmarking of meteorological drought indices at interannual to climate change timescales: A case study over the Amazon and Mississippi river basins. Hydrology and Earth System Sciences, 17(12), 4885–4895. https://doi.org/10.5194/hess-17-4885-2013

Judt, F. and Chen, S. S. (2016). Predictability and Dynamics of Tropical Cyclone Rapid Intensification Deduced from High-Resolution Stochastic Ensembles. Monthly Weather Review, 144(11), 4395–4420. https://doi.org/10.1175/MWR-D-15-0413.1

Kasei, R., Diekkrüger, B. and Leemhuis, C. (2010). Drought frequency in the Volta Basin of West Africa. Sustainability Science, 5(1), 89–97. https://doi.org/10.1007/s11625-009-0101-5

Kerandi, N., Arnault, J., Laux, P., Wagner, S., Kitheka, J. and Kunstmann, H. (2017). Joint atmospheric-terrestrial water balances for East Africa : a WRF-Hydro case study for the upper Tana River basin, 1337–1355. https://doi.org/10.1007/s00704-017-2050-8

Kerandi, N., Arnault, J., Laux, P., Wagner, S., Kitheka, J. and Kunstmann, H. (2018). Joint atmospheric-terrestrial water balances for East Africa: a WRF-Hydro case study for the upper Tana River basin. Theoretical and Applied Climatology, 131(3–4), 1337–1355. https://doi.org/10.1007/s00704-017-2050-8

Kerandi, N. M. (2017). Joint Atmospheric-Terrestrial Water Balance for the Tana River Basin of Kenya , East Africa by Coupled Atmospheric- Hydrological Modeling. Universität Augsburg.

Klein, C., Heinzeller, D., Bliefernicht, J. and Kunstmann, H. (2015). Variability of West African monsoon patterns generated by a WRF multi-physics ensemble. Climate Dynamics, 45(9–10), 2733–2755. https://doi.org/10.1007/s00382-015-2505-5

Klutse, N. A. B., Ajayi, V., Gbobaniyi, E. O., Egbebiyi, T. S., Kouadio, K., Nkrumah, F., Quagraine, K. A., Olusegun, C., Diasso, U., Abiodun, B. J., Lawal, K., Nikulin, G., Lennard, C. and Dosio, A. (2018). Potential impact of 1.5°C and 2°C global warming on consecutive dry and wet days over West Africa. Environmental Research Letters. https://doi.org/10.1088/1748-9326/aab37b

Klutse, N. A. B., Sylla, M. B., Diallo, I., Sarr, A., Dosio, A., Diedhiou, A., Kamga, A., Lamptey, B., Ali, A., Gbobaniyi, E. O., Owusu, K., Lennard, C., Hewitson, B., Nikulin, G., Panitz, H-J. and Büchner, M. (2015). Daily characteristics of West African summer monsoon precipitation in CORDEX simulations. Theoretical and Applied Climatology, 123(1–2), 369–386. https://doi.org/10.1007/s00704-014-1352-3

Kumar, M. N., Murthy, C. S., Sesha, M. V. R. and Roy, P. S. (2009). On the use of Standardized Precipitation Index (SPI) for drought intensity assessment, 389(April), 381–389. https://doi.org/10.1002/met

Kumar, R., Musuuza, J. L., Van Loon, A. F., Teuling, A. J., Barthel, R., Ten Broek, J., Mai, J., Samaniego, L. and Attinger, S. (2016). Multiscale evaluation of the Standardized Precipitation Index as a groundwater drought indicator. Hydrology and Earth System Sciences, 20(3), 1117–1131. https://doi.org/10.5194/hess-20-1117-2016

Kumi, N. and Abiodun, B. J. (2018). Potential impacts of 1.5 °c and 2 °c global warming on rainfall onset, cessation and length of rainy season in West Africa. Environmental Research Letters, 13(5), 12–13. https://doi.org/10.1088/1748-9326/aab89e

Kundzewicz, Z. W. (1997). Water resources for sustainable development. Taylor & Francis, 42(4), 467–480. https://doi.org/10.1080/02626669709492047

L'Hôte, Y., Mahé, G., Somé, B. and Triboulet, J.-P. (2002). Analysis of a Sahelian annual rainfall index from 1896 to 2000; the drought continues. Hydrological Sciences Journal, 47(4), 563–572. https://doi.org/10.1080/02626660209492960

Laing, A. G., Carbone, R. and Tuttle, J. (2008). The propagation and diurnal cycles of deep convection in northern tropical Africa, 109, 93–109. https://doi.org/10.1002/qj

Laprise, R., Hernandez-Dıaz, L., Tete, K., Sushama, L., Separovic, L., Martynov, A., Winger, K. and Valin, M. (2013). Climate projections over CORDEX Africa domain using the fifth-generation Canadian Regional Climate Model (CRCM5). https://doi.org/10.1007/s00382-012-1651-2

Le Barbé, L., Lebel, T. and Tapsoba, D. (2002). Rainfall variability in West Africa during the years 1950-90. Journal of Climate, 15(2), 187–202. https://doi.org/10.1175/1520-0442(2002)015<0187:RVIWAD>2.0.CO;2

Le Barbé Luc, Alé G., Millet Bertrand, Texier H., Borel Yves, G. R. (1993). Les ressources en eaux superficielles de la République du Bénin.

Lebel, T. and Ali, A. (2009). Recent trends in the Central and Western Sahel rainfall regime (1990-2007). Journal of Hydrology, 375(1–2), 52–64. https://doi.org/10.1016/j.jhydrol.2008.11.030

Lebel, T., Cappelaere, B., Galle, S., Hanan, N., Kergoat, L., Levis, S., Vieux, B., Descroix, L., Gosset, M., Mougin, E., Peugeot, C. and Seguis, L. (2009). AMMA-CATCH studies in the Sahelian region of West-Africa: An overview. Journal of Hydrology, 375(1–2), 3–13. https://doi.org/10.1016/j.jhydrol.2009.03.020

Lehner, B., Verdin, K. and Jarvis, A. (2008). New global hydrography derived from spaceborne elevation data. Eos, 89(10), 93–94. https://doi.org/10.1029/2008EO100001

Leutbecher, M., Lock, S.-J., Ollinaho, P., Simon T. K., L., Balsamo, G., Bechtold, P., Bonavita M., Christensen, H. M., Diamantakis ,M., Dutra, E., English, S., Fisher, M., Forbes, R. M., Goddard, J., Haiden, T., Hogan, R. J., Juricke, S., Lawrence, H., MacLeod, D.,Magnusson, L., Malardel, S., Massart, S., Sandu, I., Smolarkiewicz. P. K., Subramanian, A., Vitart, F., Nils, W. and Antje, W. (2017). Stochastic representations of model uncertainties at ECMWF: State of the art and future vision. Virchows Archiv Für Pathologische Anatomie Und Physiologie Und Für Klinische Medizin, 270(1), 267–275. https://doi.org/10.1002/qj.3094

Li, X., Jiang, F., Li, L. and Wang, G. (2011). Spatial and temporal variability of precipitation concentration index, concentration degree and concentration period Xinjiang, China. International Journal of Climatology, 31(11), 1679–1693. https://doi.org/10.1002/joc.2181

Lindesay, J. A. (1988). South african rainfall, the southern oscillation and a southern hemisphere semi-annual cycle. Journal of Climatology, 30, 17–30.

Lobell, D. B. (2014). Climate change adaptation in crop production : Beware of illusions. Global Food Security, 1–5. https://doi.org/10.1016/j.gfs.2014.05.002

Lorenzo-lacruz, J., Vicente-serrano, S. M., López-moreno, J. I., Beguería, S. and García-ruiz, J. M. (2010). The impact of droughts and water management on various hydrological systems in the headwaters of the Tagus River (central Spain). Journal of Hydrology, 386(1–4), 13–26. https://doi.org/10.1016/j.jhydrol.2010.01.001

Maraun, D., Wetterhall, F., Ireson, A. M., Chandler, R. E., Kendon, E. J., Widmann, M., Brienen, S., Rust, H. W., Sauter, T., Themeßl, M., Venema, V. K. C., Chun, K. P., Goodess, C. M., Jones, R. G., Onof, C., Vrac, M. and Thiele-Eich, I. (2010). Precipitation downscaling under climate change : recent developments to bridge the gap between dynamical models and the end user, (2009), 1–34. https://doi.org/10.1029/2009RG000314.1

Marty, R., Zin, I. and Obled, C. (2013). Sensitivity of hydrological ensemble forecasts to different sources and temporal resolutions of probabilistic quantitative precipitation forecasts: Flash flood case studies in the C??vennes-Vivarais region (Southern France). Hydrological Processes, 27(1), 33–44. https://doi.org/10.1002/hyp.9543

Masih, I., Maskey, S., Mussá, F. E. F. and Trambauer, P. (2014). A review of droughts on the African continent: A geospatial and long-term perspective. Hydrology and Earth System Sciences. https://doi.org/10.5194/hess-18-3635-2014

Mathon, V., Laurent, H. and Lebel, T. (2002). Mesoscale Convective System Rainfall in the Sahel. American Meteorological Society, 41, 1081–1092.

Maúre, G., Pinto, I., Ndebele-Murisa, M., Muthige, M., Lennard, C., Nikulin, G., Dosio A. and Meque A. (2018). The southern African climate under 1.5 °C and 2 °C of global warming as simulated by CORDEX regional climate models. Environmental Research Letters, 13(6), 065002. https://doi.org/10.1088/1748-9326/aab190

Maussion, F., Scherer, D., Finkelnburg, R., Richters, J., Yang, W. and Yao, T. (2011). Sciences WRF simulation of a precipitation event over the Tibetan Plateau , China – an assessment using remote sensing and ground observations, 1372, 1795–1817. https://doi.org/10.5194/hess-15-1795-2011

Mba, W. P., Longandjo, G.-N., Moufouma-Okia, W., Bell, J. P., James, R., Vondou, D. A., Haensler, A., Fotso-Nguemo, T. C., Guenang, G. M., Tchotchou, A. L. D., Kamsu-Tamo, P. H., Takong, R. R., Nikulin, G., Lennard, C. and Dosio, A. (2018). Consequences of 1.5° C and 2° C global warming levels for temperature and precipitation changes over Central Africa. Environmental Research Letters. Retrieved from http://iopscience.iop.org/article/10.1088/1748-9326/aab048/meta

McKee, T. B., Doesken, N. J. and Kleist, J. (1993). The relationship of drought frequency and duration to time scales. Eighth Conference on Applied Climatology, 17-22 January 1993, Anaheim, California, 26(2). https://doi.org/10.1088/1755-1315/5

Meque, A. and Abiodun, B. J. (2015). Simulating the link between ENSO and summer drought in Southern Africa using regional climate models. Climate Dynamics, 44(7–8), 1881–1900. https://doi.org/10.1007/s00382-014-2143-3

Miguez-Macho, G., Fan, Y., Weaver, C. P., Walko, R. and Robock, A. (2007). Incorporating water table dynamics in climate modeling: 2. Formulation, validation, and soil moisture simulation. Journal of Geophysical Research Atmospheres, 112(13), 1–16. https://doi.org/10.1029/2006JD008112

Milly, P. C. D., Wetherald, R. T., Dunne, K. A. and Delworth, T. L. (2002). Increasing risk of great floods in a changing climate. Nature, 415(6871), 514–517. https://doi.org/10.1038/415514a

Mishra, A. K. and Singh, V. P. (2010). A review of drought concepts. Journal of Hydrology, 391(1–2), 202–216. https://doi.org/10.1016/j.jhydrol.2010.07.012

Mlawer, E. J., Taubman, S. J., Brown, P. D., Iacono, M. J. and Clough, S. A. (1997). Radiative transfer for inhomogeneous atmospheres: RRTM, a validated correlated-k model for the longwave. Journal of Geophysical Research: Atmospheres, 102(D14), 16663–16682. https://doi.org/10.1029/97JD00237

Moreno, H. A., Vivoni, E. R. and Gochis, D. J. (2013). Limits to Flood Forecasting in the Colorado Front Range for Two Summer Convection Periods Using Radar Nowcasting and a Distributed Hydrologic Model. Journal of Hydrometeorology, 14(4), 1075–1097. https://doi.org/10.1175/JHM-D-12-0129.1

Moriasi, D. N., Arnold, J. G., Liew, M. W. Van, Bingner, R. L., Harmel, R. D. and Veith, T. L. (2007). Model evaluation guidelines for systematic quantification of accuracy in watershed simulations, 50(3), 885–900.

Moss, R., Mustafa, B., Sarah, B. and Eduardo, C. (2008). Towards New Scenarios for Analysis of Emissions, Climate Change, Impacts, and Response Strategies. IPCC Expert meeting report. Noordwijkerhout, The Netherlands.

Naabil, E., Lamptey, B. L., Arnault, J., Kunstmann, H. and Olufayo, A. (2017). Water resources management using the WRF-Hydro modelling system: Case-study of the Tono dam in West Africa. Journal of Hydrology: Regional Studies, 12(May), 196–209. https://doi.org/10.1016/j.ejrh.2017.05.010

Nash, J. E. and Sutcliffe, J. V. (1970). River flow forecasting through conceptual models part I—A discussion of principles. Journal of Hydrology, 10(3), 282–290.

Ngailo, T. J., Shaban, N., Reuder, J., Mesquita, M. D. S., Rutalebwa, E., Mugume, I. and Sangalungembe, C. (2018). Assessing Weather Research and Forecasting (WRF) Model Parameterization Schemes Skill to Simulate Extreme Rainfall Events over Dar es Salaam on 21 December 2011, 36–54. https://doi.org/10.4236/gep.2018.61003

Nicholson, S. (2005). On the question of the “recovery” of the rains in the West African Sahel. Journal of Arid Environments, 63(3), 615–641. https://doi.org/10.1016/j.jaridenv.2005.03.004

Nicholson, S E and Grist, J. P. (2001). A conceptual model for understanding rainfall variability in the west african sahel on interannual and interdecadal timescales, 1757, 1733–1757.

Nicholson, S E and Selato, J. C. (2000). The influence of la nina on african rainfall. International Journal of Climatology, 1776, 1761–1776.

Nicholson, Sharon E. (2013). The West African Sahel : A Review of Recent Studies on the Rainfall Regime and Its Interannual Variability. Hindawi Publishing Corporation : ISRN Meteorology, 2013. https://doi.org/http://dx.doi.org/10.1155/2013/453521

Nikulin, G., Jones, C., Giorgi, F., Asrar, G., Büchner, M., Cerezo-Mota, R., Christensen, O. B., Déqué, M., Fernandez, J., Hänsler, A., van Meijgaard, E., Samuelsson, P., Sylla, M. B. and Sushama, L. (2012). Precipitation climatology in an ensemble of CORDEX-Africa regional climate simulations. Journal of Climate, 25(18), 6057–6078. https://doi.org/10.1175/JCLI-D-11-00375.1

Nikulin, G., Lennard, C., Dosio, A., Kjellström, E., Chen, Y., Hansler, A., Kupiainen, M., Laprise, R., Mariotti, L., Maule, C. F., Van Meijgaard, E., Panitz, H. J., Scinocca, J. F. and Somot, S. (2018). The effects of 1.5 and 2 degrees of global warming on Africa in the CORDEX ensemble. Environmental Research Letters, 13(6). https://doi.org/10.1088/1748-9326/aab1b1

Nouaceur, Z., Laignel, B. and Turki, I. (2013). Changements climatiques au Maghreb : vers des conditions plus humides et plus chaudes sur le littoral algérien? Physio-Géo- Géographie Physique et Environnement, 7(January). https://doi.org/10.4000/physio-geo.3686

Ogilvie, A., Mahé, G., Ward, J., Serpantié, G., Lemoalle, J., Morand, P., Barbier, B., Diop, A. T., Caron, A., Namarra, R., Kaczan, D., Lukasiewicz, A., Paturel, J. E., Liénou, G. and Clanet, J. C. (2010). Water, agriculture and poverty in the niger river basin. Water International, 35(5), 594–622. https://doi.org/10.1080/02508060.2010.515545

Oguntunde, P. G., Abiodun, B. J. and Lischeid, G. (2017). Impacts of climate change on hydro-meteorological drought over the Volta Basin, West Africa. Global and Planetary Change, 155(March), 121–132. https://doi.org/10.1016/j.gloplacha.2017.07.003

Oguntunde, P. G., Lischeid, G. and Abiodun, B. J. (2017). Impacts of climate variability and change on drought characteristics in the Niger River Basin, West Africa. Stochastic Environmental Research and Risk Assessment. https://doi.org/10.1007/s00477-017-1484-y

Oliver, J. E. (1980). Monthly precipitation distribution: A comparative index. Professional Geographer, 32(3), 300–309. https://doi.org/10.1111/j.0033-0124.1980.00300.x

Omotosho, J. B. (1985). The separate contributions of line squalls, thunderstorms and the monsoon to the total rainfall in Nigeria, 5, 543–552.

Önen, A. (2013). Analyses Of Flood Events Using Regional. Middle East Technical University.

Orlowsky, B. and Seneviratne, S. I. (2012). Global changes in extreme events : regional and seasonal dimension, 669–696. https://doi.org/10.1007/s10584-011-0122-9

Palmer, W. C. (1965). Meterological drought. Research Paper No. 45. US Department of Commerce. Weather Bureau, Washington, DC.

Panthou, G., Vischel, T. and Lebel, T. (2014). Recent trends in the regime of extreme rainfall in the Central Sahel. International Journal of Climatology, 34(15), 3998–4006. https://doi.org/10.1002/joc.3984

Pasho, E., Camarero, J. J., Luis, M. De and Vicente-serrano, S. M. (2011). Agricultural and Forest Meteorology Impacts of drought at different time scales on forest growth across a wide climatic gradient in north-eastern Spain. Agricultural and Forest Meteorology, 151(12), 1800–1811. https://doi.org/10.1016/j.agrformet.2011.07.018

Paturel, J. E., Servat, E., Delattre, M. O. and Lubes-niel, H. (1998). Analyse de séries pluviométriques de longue durée en Afrique de l'Ouest et Centrale non sahélienne dans un contexte de variabilité climatique. Hydrological Sciences Journal, 43(6), 937–946. https://doi.org/10.1080/02626669809492188

Petrow, T. and Merz, B. (2009). Trends in flood magnitude, frequency and seasonality in Germany in the period 1951-2002. Journal of Hydrology, 371(1–4), 129–141. https://doi.org/10.1016/j.jhydrol.2009.03.024

Pleim, J. E. (2007). A Combined Local and Nonlocal Closure Model for the Atmospheric Boundary Layer. Part I: Model Description and Testing. Journal of Applied Meteorology and Climatology, 46(9), 1383–1395. https://doi.org/10.1175/JAM2539.1

Pu, B. and Cook, K. H. (2010). Dynamics of the West African Westerly Jet. American Meteorological Society, 23, 6263–6276. https://doi.org/10.1175/2010JCLI3648.1

Ratnayake, U., Sachindra, D. A. and Nandalal, K. D. W. (2010). Rainfall Forecasting for Flood Prediction in the Nilwala Basin, (December), 13–14.

Rebeteza, M., Mayerb, H., Dupontc, O., Schindlerb, D., Gartnerd, K., Kroppe, J. P. and Menzel, A. (2006). Heat and drought 2003 in Europe : a climate synthesis, 63, 569–577.

Redmond, K. T. . (2002). The depiction of drought: A commentary. American Meteorological Society, 1143–1148.

Reed, R. J., Klinker, E. and Hollingsworth, A. (1988). Structure and Characteristics of African Easterly Wave Disturbances as Determined from the ECMWF Operational Analysis / Forecast System. Meteorol. Atmos. Phys, 38, 22–33.

Richard R. Heim Jr. (2002). A Review of Twentieth-Century Drought Indices Used in the United States. Bull Am Meteorol Soc 83, (August), 1149–1165.

Rogelj, J., den Elzen, M., Höhne, N., Fransen, T., Fekete, H., Winkler, H., Schaeffer, R., Sha, F., Riahi, K. and Meinshausen, M. (2016). Paris Agreement climate proposals need a boost to keep warming well below 2 °C. Nature, 534, 631. Retrieved from https://doi.org/10.1038/nature18307

Rosegrant, M., Cai, X., Cline, S. and Nakagawa, N. (2002). The Role of Rainfed Agriculture in the Future of Global Food Production. Environment and Production Technology Division Discussion Paper. International Food Policy Research Institute, (90), 127.

Roux, F. (1987). The West African Squall line observed on 23 june 1981 during COPT81: Kinematics and Thermodynamics of the convective region. Journal of the Atmospheric Sciences, 45(3), 406–426.

Saba, A., Gerrard, M. B., Lobell, D. B., Saba, A., Biasutti, M., Gerrard, M. B. and Lobell, D. B. (2013). Getting Ahead of the Curve : Supporting Adaptation to Long-term Climate Change and Short-term Climate Variability Alike. CCLR, 7. Retrieved from https://scholarship.law.columbia.edu/faculty_scholarship/563

Schrier, G. VAN DER, Briffa, K. R., P.D.Jones and Osborn, T. J. (2006). Summer Moisture Variability across Europe. Journal of Climate, (Alley 1984), 2818–2834.

Senatore, A., Mendicino, G., Gochis, D. J., Yu, W., Yates, D. N. and Kunstmann, H. (2015). Fully coupled atmosphere-hydrology simulations for the central Mediterranean: Impact of enhanced hydrological parameterization for short and long time scales. Journal of Advances in Modeling Earth Systems, 7(4), 1693–1715. https://doi.org/10.1002/2015MS000510

Seneviratne, S. I., Nicholls, N., Easterling, D., Goodess, C. M., Kanae, S., Kossin, J., Luo, Y., Marengo, J., McInnes, K., Rahimi, M., Reichstein, M., Sorteberg, A., Vera, C. and Zhang, X. (2012). Changes in Climate Extremes and their Impacts on the Natural Physical Environmentt. In: Managing the Risks of Extreme Events and Disasters to Advance Climate Change Adaptation [Field, C.B., V. Barros, T.F. Stocker, D. Qin, D.J. Dokken, K.L. Ebi, M.D. Mast.

Seuffert, G., Gross, P., Simmer, C. and Wood, E. F. (2002). The Influence of Hydrologic Modeling on the Predicted Local Weather: Two-Way Coupling of a Mesoscale Weather Prediction Model and a Land Surface Hydrologic Model. Zeitschrift Fur Gastroenterologie, 53(8), 782–788. https://doi.org/10.1055/s-0035-1553476

Shelton, M. L. (2009). Hydroclimatology: perspectives and applications. Cambridge University Press.

Shi, P., Wu, M., Qu, S., Jiang, P., Qiao, X., Chen, X., Zhou, M. and Zhang, Z. (2015). Spatial Distribution and Temporal Trends in Precipitation Concentration Indices for the Southwest China. Water Resources Management, 29(11), 3941–3955. https://doi.org/10.1007/s11269-015-1038-3

Shih, D. S., Chen, C. H. and Yeh, G. T. (2014). Improving our understanding of flood forecasting using earlier hydro-meteorological intelligence. Journal of Hydrology, 512, 470–481. https://doi.org/10.1016/j.jhydrol.2014.02.059

Shutts, G. (2005). A kinetic energy backscatter algorithm for use in ensemble prediction systems. Quarterly Journal of the Royal Meteorological Society, 131(612), 3079–3102. https://doi.org/10.1256/qj.04.106

Sivakumar, M. V. K., Motha, R. P., Wilhite, D. A. and Wood, D. A. (Eds. . (2011). Agricultural Drought Indices. Proceedings of the WMO/UNISDR Expert Group Meeting on Agricultural Drought Indices , 2-4 June 2010, Murcia, Spain: Geneva, Switzerland: World Meteorological Organization. AGM-11, WMO/TD No. 1572; WAOB-2011, 219.

Sivapalan, M., Savenije, H. H. G. and Blöschl, G. (2011). Socio-hydrology : A new science of people and water. Hydrological Processes, (November).

https://doi.org/10.1002/hyp.8426

Skamarock, W. C., Klemp, J. B., Dudhia, J., Gill, D. O., Barker, D. M., Wang, W. and Powers, J. G. (2007). A Description of the Advanced Research WRF Version 2, (January).

Sossou-agbo, A. L. (2013). Université de Grenoble (France) et l'Université d'Abomey-Calavi (Bénin).

Sousa, P. M., Trigo, R. M., Aizpurua, P., Nieto, R., Gimeno, L. and Garcia-Herrera, R. (2011). Trends and extremes of drought indices throughout the 20th century in the Mediterranean. Natural Hazards and Earth System Science, 11(1), 33–51. https://doi.org/10.5194/nhess-11-33-2011

Stensrud, D. J., Xue, M., Wicker, L. J., Kelleher, K. E., Foster, M. P., Schaefer, J. T., Schneider, R. S., Benjamin, S. G., Stephen S. W., Ferrée J. T. and Tuell, J. P. (2009). Convective-scale warn-on-forecast system a Vision for 2020. American Meteorological Society, 1487–1499.

Stocker, T. F., Allen, S. K., Bex, V. and Midgley, P. M. (2013). Climate Change 2013 The Physical Science Basis Working Group I Contribution to the Fifth Assessment Report of the Intergovernmental Panel on Climate Change Edited by.

Sultan, B. and Gaetani, M. (2016). Agriculture in West Africa in the Twenty-First Century: Climate Change and Impacts Scenarios, and Potential for Adaptation. Frontiers in Plant Science, 7(August), 1–20. https://doi.org/10.3389/fpls.2016.01262

Sung, J. H. and Chung, E. S. (2014). Development of streamflow drought severity–duration–frequency curves using the threshold level method. Hydrology and Earth System Sciences, 18(9), 3341–3351. https://doi.org/10.5194/hess-18-3341-2014

Szinell, C. S., Bussay, A. and Szentimrey, T. (1998). Drought tendencies in hungary. International Journal of Climatology, 1491, 1479–1491.

Tallaksen, L. M. and Stahl, K. (2014). Spatial and temporal patterns of large-scale

droughts in Europe: Model dispersion and performance. Geophysical Research Letters, 47, 429–434. https://doi.org/10.1002/2013GL058573.Received

Teuling, A. J., Van Loon, A. F., Seneviratne, S. I., Lehner, I., Aubinet, M., Heinesch, B., Bernhofer, C., Grünwald, T., Prasse, H. and Spank, U. (2013). Evapotranspiration amplifies European summer drought. Geophysical Research Letters, 40(10), 2071–2075. https://doi.org/10.1002/grl.50495

Thorncroft, C. and Hodges, K. (2000). African Easterly Wave Variability and Its Relationship to Atlantic Tropical Cyclone Activity. Journal of Climate, 14, 1166–1179.

Trambauer, P., Dutra, E., Maskey, S., Werner, M., Pappenberger, F., Van Beek, L. P. H. and Uhlenbrook, S. (2014). Comparison of different evaporation estimates over the African continent. Hydrology and Earth System Sciences, 18(1), 193–212. https://doi.org/10.5194/hess-18-193-2014

Tsakiris, G. and Vangelis, H. (2004). Towards a Drought Watch System based on spatial SPI. Water Resources Management, 18(1), 1–12. https://doi.org/10.1023/B:WARM.0000015410.47014.a4

Tschakert, P., Sagoe, R., Samuel, G. O. and Codjoe, N. (2010). Floods in the Sahel : an analysis of anomalies , memory , and anticipatory learning, 471–502. https://doi.org/10.1007/s10584-009-9776-y

UNHCR, 2010 : https://www.lemonde.fr/afrique/article/2010/10/22/680-000-personnes-touchees-par-les-inondations-au-benin_1429957_3212.html (accessed on 13 December 2018)

Van De Giesen, N., Liebe, J. and Jung, G. (2010). Special section: climate change and water resources Adapting to climate change in the Volta Basin, West Africa. Current Science, 98(8). Retrieved from www.glowa-volta.de

Van Loon, A. F., Huijgevoort, M. H. J. Van and Lanen, H. A. J. Van. (2012). Evaluation of drought propagation in an ensemble mean of large-scale hydrological models. Hydrology and Earth System Sciences, 4057–4078. https://doi.org/10.5194/hess-16-4057-2012

Van Loon, A. F. and Lanen, H. A. J. Van. (2012). Sciences A process-based typology of hydrological drought. Hydrology and Earth System Sciences, 1915–1946. https://doi.org/10.5194/hess-16-1915-2012

Van Vuuren, D. P., Edmonds, J., Kainuma, M., Riahi, K., Nakicenovic, N., Smith, S. J. and Rose, S. K. (2011). The representative concentration pathways : an overview, 5–31. https://doi.org/10.1007/s10584-011-0148-z

Vicente-serrano, S. M. (2007). Evaluating the Impact of Drought Using Remote Sensing in a Mediterranean , Semi-arid Region, 173–208. https://doi.org/10.1007/s11069-006-0009-7

Vicente-Serrano, S. M. and López-Moreno, J. I. (2005). Hydrological response to different time scales of climatological drought : an evaluation of the Standardized Precipitation Index in a mountainous Mediterranean basin. Hydrology and Earth System Sciences, 9, 523–533.

Vicente-Serrano, Sergio M., Beguería, S. and López-Moreno, J. I. (2010). A multiscalar drought index sensitive to global warming: The standardized precipitation evapotranspiration index. Journal of Climate, 23(7), 1696–1718. https://doi.org/10.1175/2009JCLI2909.1

Vicente-Serrano, Sergio M., Beguería, S., Lorenzo-Lacruz, J., Camarero, J. J., López-Moreno, J. I., Azorin-Molina, C., Revuelto, J., Morán-Tejeda, E. and Sanchez-Lorenzo, A. (2012). Performance of drought indices for ecological, agricultural, and hydrological applications. Earth Interactions, 16(10). https://doi.org/10.1175/2012EI000434.1

Wagner, S., Fersch, B., Yuan, F., Yu, Z. and Kunstmann, H. (2016). Fully coupled atmospheric-hydrological modeling at regional and long-term scales: Development, application, and analysis of WRF-HMS. Water Resources Research, 1–24. https://doi.org/10.1002/2016WR018704.

Wallez, Lucie. (2010). Inondations dans les villes d'Afrique de l'Ouest: Diagnostic et éléments de renforcement des capacités d'adaptation dans le Grand Cotonou. Diplôme de maîtrise en environnement et master en Ingénierie et

Management de l'Environnement et du Développement Durable, Centre Universitaire de Formation en Environnement de l'Université de Sherbrooke, Québec, Canada, 76p.

Wang, L., Koike, T., Wang, M., Liu, J., Sun, J., Lu, H., Tsutsui, H., Tamagawa, K. and Xu, X. (2012). Use of Integrated Observations to Improve 0-36 h Flood Forecasting: Development and Application of a Coupled Atmosphere-Hydrology System in the Nanpan River Basin, China. Journal of the Meteorological Society of Japan. Ser. II, 90C(0), 131–144. https://doi.org/10.2151/jmsj.2012-C09

White, D., Collins, D. and Howden, M. (1993). Drought in Australia : Prediction , Monitoring , Management , and Policy.

Wiebe, K., Sulser, T. B., Croz, D. M. and Rosegrant, M. W. (2017). The Effects of Climate Change on Agriculture and Food Security in Africa, 5–21.

Wigmosta, M. S. and Lettenmaier, P. (1999). A comparison of simplified methods for routing topographically driven subsurface flow, 35(1), 255–264.

Wigmosta, M. S., Vail, L. W. and Lettenmaier, D. P. (1994). A distributed hydrology-vegetation model for complex terrain, 30(6).

Wilby, R. L. and Dessai, S. (2010). Robust adaptation to climate change. Royal Meterological Society, 2010. https://doi.org/10.1002/wea.504

Wilhite, D. A. and Glantz, M. H. (1985). Understanding : the Drought Phenomenon : The Role of Definitions. Water International, 10(August 2013), 111–120.

Younis, J., Anquetin, S., Thielen, J., Younis, J., Anquetin, S. and The, J. T. (2008). The benefit of high-resolution operational weather forecasts for flash flood warning To cite this version : HAL Id : hal-00330816 The benefit of high-resolution operational weather forecasts for flash flood warning.

Yucel, I., Onen, A., Yilmaz, K. K. and Gochis, D. J. (2015). Calibration and evaluation of a flood forecasting system: Utility of numerical weather prediction model, data assimilation and satellite-based rainfall. Journal of Hydrology, 523, 49–66. https://doi.org/10.1016/j.jhydrol.2015.01.042

Yucel, Ismail and Keskin, F. (2011). Assessment of flash flood events using remote sensing and atmospheric model-derived precipitation in a hydrological model. Hydro-Climatology: Variability and Change, 344(July), 245–251. Retrieved from http://apps.webofknowledge.com/full_record.do?product=UA&search_mode=GeneralSearch&qid=1&SID=X2MCdoaXnNeEr3zGkOI&page=4&doc=155

Yukiko, H., Shinjiro, K., Seita, E. and Taikan, O. (2010). Global projections of changing risks of floods and droughts in a changing climate Global projections of changing risks of floods and droughts in a changing climate, 6667. https://doi.org/10.1623/hysj.53.4.754

Zabel, F. and Mauser, W. (2013). 2-way coupling the hydrological land surface model PROMET with the regional climate model MM5. Hydrology and Earth System Sciences, 17(5), 1705–1714. https://doi.org/10.5194/hess-17-1705-2013

Zhai, J., Su, B., Krysanova, V., Vetter, T., Gao, C. and Jiang, T. (2010). Spatial variation and trends in PDSI and SPI indices and their relation to streamflow in 10 large regions of china. Journal of Climate, 23(3), 649–663. https://doi.org/10.1175/2009JCLI2968.1

Zhang, L. and Qian, Y. (2003). Annual distribution features of precipitation in china and their interannual variations. Acta Meteorologica Sinica.

Zhao, L., Xia, J., Sobkowiak, L., Wang, Z. and Guo, F. (2012). Spatial Pattern Characterization and Multivariate Hydrological Frequency Analysis of Extreme Precipitation in the Pearl River Basin, China. Water Resources Management, 26(12), 3619–3637. https://doi.org/10.1007/s11269-012-0094-1